Volume 3, Issue 5, 2025

Print ISSN: 2959-9903
Online ISSN: 2959-9911

World Journal of Information Technology

World Journal of Information Technology

Volume 3, Issue 5, 2025

Published by Upubscience Publisher

World Journal of Information Technology
Print ISSN: 2959-9903 Online ISSN: 2959-9911
Email: info@upubscience.com
Website: http://www.upubscience.com/

Table of Content

World Journal of Information Technology
Print ISSN: 2959-9903
Online ISSN: 2959-9911
DOI: https://doi.org/10.61784/wjit3060

INTELLIGENT RECOGNITION OF STUDENTS' LEARNING STATES THROUGH MICRO-EXPRESSIONS

Juan Yang[1], Ling Ma[2*], XianBin Zhang[2], SiYi Tian[1]
[1]*School of Journalism and Law, Wuchang Shouyi University, Wuhan 430064, Hubei, China.*
[2]*School of Information Science and Engineering, Wuchang Shouyi University, Wuhan 430064, Hubei, China.*
[*]*Corresponding Author: Ling Ma*

Abstract: Students' facial micro-expressions can reflect their learning states, and the intelligent recognition of micro-expressions is of great significance for monitoring these states. This paper proposes a micro-expression recognition method based on a Residual Network for detecting the learning and psychological states of college students. Using ResNet18 as the backbone network, the Efficient Channel Attention (ECA) mechanism is embedded to adaptively adjust channel weights, enhancing feature representation capability. Simultaneously, the Mish activation function and Dropout layer are introduced to optimize gradient flow and reduce the risk of overfitting. During training, the Label Smoothing Cross Entropy loss function, the AdamW optimizer combined with the OneCycleLR learning rate scheduler, and an early stopping mechanism are adopted, effectively improving the model's generalization ability and training efficiency on small datasets. Experiments are based on a self-built dataset (including positive, neutral, and negative expressions, totaling 1800 grayscale images). Through data augmentation and ten-fold cross-validation, the model achieves an accuracy of 97.50%. The experimental results show that this method possesses high accuracy and robustness in micro-expression recognition tasks, providing an effective tool for monitoring the psychological states of college students and optimizing classroom teaching.
Keywords: Deep learning; Convolutional neural network; Micro-expression recognition; Learning state monitoring

1 INTRODUCTION

Currently, a significant proportion of college students face learning and psychological issues. According to the "2022 Report on the Mental Health Status of College Students" jointly released by the Institute of Psychology, Chinese Academy of Sciences and Social Sciences Academic Press, 78.52% of students showed no risk of depression, while only about half were free from anxiety risk (54.72%). Most college students reported relatively high life satisfaction, with 74.10% reaching a level of "basically satisfied" or higher. Therefore, identifying students with psychological problems is crucial for student management and psychological counseling.

Human facial expressions contain rich emotional characteristics and psychological processes, directly conveying emotional and psychological states, making them the most effective non-verbal method for emotional expression. In learning contexts, learners' facial expressions can reflect not only their emotions but also their psychological states[1]. Correctly identifying a learner's expressions allows for accurate capture of their learning emotions and states. Consequently, research and application of facial expression recognition have gradually become a hotspot in the field of intelligent education, and recognizing learners' facial expressions has become a primary method for analyzing their learning emotions and states[2].

In 1971, psychologist Ekman proposed six basic types of facial expressions: Happiness, Sadness, Fear, Anger, Surprise, and Disgust[3]. Later, Neutral was also included as a basic facial expression, forming the seven basic facial expression categories still used today.

In the early stages of expression recognition research, efforts primarily relied on handcrafted feature design or shallow learning models. However, as application scenarios shifted from controlled laboratory environments to complex real-world settings, the limitations of traditional methods in feature representation became apparent. With the rapid development of computer vision and machine learning techniques, neural networks have gradually become the main solution for expression recognition in complex scenarios due to their powerful non-linear feature extraction capabilities. Currently, deep learning technologies are increasingly applied in the field of expression recognition. Models such as Convolutional Neural Networks (CNN), Deep Belief Networks (DBN), and Recurrent Neural Networks (RNN) have become research hotspots and core technologies in this area, owing to their advantages in handling spatial image features, multi-layer semantics, and sequential dynamic information.

Facial expression recognition primarily involves three steps: preprocessing, feature extraction, and classification. Preprocessing typically involves correcting acquired images, performing face detection, followed by grayscale conversion (reducing channels, lowering complexity, and visualizing image features), cropping, scaling, translation, normalization, and other data augmentation techniques[4]. In the feature extraction and classification stage, traditional methods and deep learning-based methods are the main approaches. Among traditional methods, one proposed algorithm for facial micro-expression recognition based on hybrid features and information entropy uses 2D Gabor wavelet transform to extract micro-expression features from the eyes and eyebrows, and then uses information entropy to extract micro-expression features from the nose and mouth to improve recognition efficiency[5]. Qiao Guifang et al.

[6] proposed an expression recognition method combining Principal Component Analysis and Linear Discriminant Analysis with KPCANet-LDA. These traditional methods require specific expertise in feature design, are significantly influenced by subjective factors, and are prone to losing feature information, thereby affecting recognition efficiency. Compared to traditional recognition methods, deep learning methods hold more advantages. Chen Tuo et al. proposed a facial expression recognition network integrating spatiotemporal features, which robustly analyzes and understands spatial and temporal information of facial expressions in video sequences, effectively improving facial expression recognition performance[7]. Yang et al. proposed using a de-expression learning procedure called De-expression Residue Learning (DeRL) to extract information from expression components for facial expression recognition, thereby improving the efficiency of face recognition algorithms[8]. These deep learning methods exhibit good recognition efficiency and accuracy, but are challenging to train in practice due to the large number of parameters comprising the datasets.

Based on the above analysis, this paper proposes a method for recognizing learning states through micro-expressions based on a Residual Network. Using ResNet18 as the backbone network, the Efficient Channel Attention (ECA) mechanism is embedded to adaptively adjust channel weights and enhance feature representation capability[9-10]. Simultaneously, regularization is enhanced by introducing Dropout layers to effectively reduce overfitting risk. Furthermore, the Mish activation function replaces the traditional ReLU, further optimizing gradient flow and model performance[11]. This method significantly improves the accuracy and generalization ability of facial expression recognition while maintaining low computational complexity, making it particularly suitable for single-channel input and small classification tasks. During training, Label Smoothing Cross Entropy Loss is used to alleviate overfitting tendencies on small datasets. Additionally, a combined optimizer strategy of AdamW + OneCycleLR for super-convergence, automatic learning rate range testing and cyclical adjustment, combined with mixed-precision training and early stopping mechanisms, is employed to achieve facial expression recognition and psychological state detection on the self-built small dataset.

2 MICRO-EXPRESSION RECOGNITION AND LEARNING STATE DETECTION

2.1 Model Structure Improvements

ResNet18, as a classic deep residual network, effectively mitigates the vanishing gradient problem in deep networks through residual connections. Its 18-layer depth achieves an excellent balance between computational efficiency and feature extraction capability, making it particularly suitable for processing visual data with subtle changes like micro-expressions. However, the traditional ResNet18 has limitations in capturing low-intensity, transient micro-expressions. To address this, this study optimizes the model through feature enhancement and attention mechanisms to improve the accuracy and robustness of micro-expression recognition and the classification of students' learning-related emotions and psychological states.

Regarding the model architecture, the Efficient Channel Attention (ECA) mechanism is first embedded to enhance the response of key features by adaptively adjusting channel weights, precisely capturing local dynamic changes in micro-expressions while maintaining very low parameter count and computational overhead. Secondly, the Mish activation function replaces the traditional ReLU, alleviating gradient sparsity issues through its continuously differentiable nature and enhancing the model's non-linear expressive capability. Additionally, Dropout layers are introduced before the fully connected layer for regularization, effectively reducing overfitting risk(Figure 1).

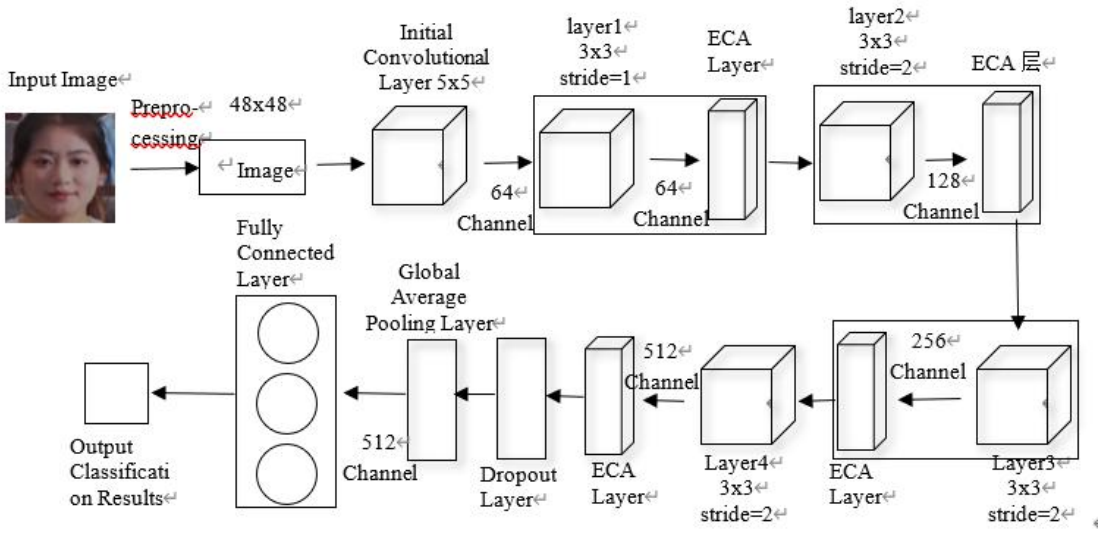

Figure 1 Network Flow Chart

The overall network flow is based on the ResNet18 architecture, including one initial 5x5 convolutional layer (64

channels), 4 residual stages (totaling 8 residual blocks, each with two 3x3 convolutional layers, channel numbers sequentially 64, 128, 256, 512), one global average pooling layer, and one fully connected layer. The input is a 48x48 single-channel facial expression image. After initial convolution, batch normalization and Mish activation are applied; each residual block embeds the ECA mechanism to enhance feature expression, followed by batch normalization and Mish activation; the shortcut uses 1x1 convolution for dimension adjustment. Finally, classification into 3 emotion categories is achieved through global average pooling, Dropout (probability 0.5), and the fully connected layer, significantly enhancing the accuracy and generalization ability of micro-expression recognition.

The ECA (Efficient Channel Attention) module is an optimized version of the SE (Squeeze-and-Excitation) module, designed to address the trade-off between performance and complexity in the SE module[12].

The SE Block is not a complete network but a substructure that can be embedded into other classification or detection models. The core idea of the SE Block is to allow the network to learn feature weights based on the loss, so that effective feature maps have larger weights, while ineffective or less effective feature maps have smaller weights, thereby training the model to achieve better results. The structure diagram is shown in Figure 2.

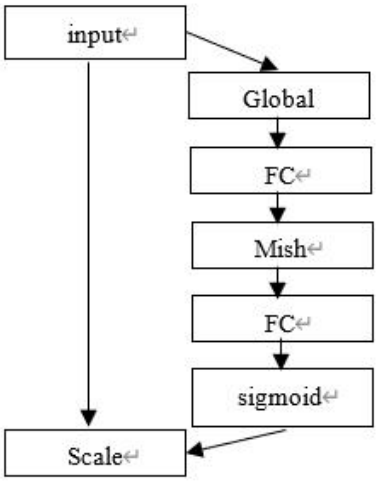

Figure 2 Structure of Improved Attention Module

The ECA module, as an optimized version of the SE module, significantly reduces computational complexity and parameter count through one-dimensional convolution and adaptive kernel size design, while retaining the core advantages of channel attention. Compared to the SE module, the ECA module avoids dimensionality reduction operations and effectively captures cross-channel correlations through a local cross-channel interaction strategy, reducing parameters by about 80% (e.g., ECA requires only 80 parameters compared to 24.37M for SE on ResNet50), and computation from 3.86 GFLOPs to 4.7e-4 GFLOPs, while increasing Top-1 accuracy by over 2%[13]. Experiments show that ECA outperforms SE and CBAM on the ImageNet classification task, with lower parameters and competitive performance compared to AA-Net. In object detection and instance segmentation tasks on the COCO dataset, ECA-Net, with ResNet50 and MobileNetV2 as backbones, demonstrates lower computational complexity and higher detection accuracy. Its adaptive kernel size enhances the model's adaptability to different channel numbers, facilitates integration into various CNN architectures, and reduces overfitting risk, making it particularly suitable for resource-constrained scenarios.

2.2 Training Process Improvements

2.2.1 Label smoothing loss function

During model training, a series of optimization strategies were employed to enhance the robustness of micro-expression recognition and alleviate overfitting on small datasets. Firstly, to address the issue of reduced model generalization capability caused by the excessive pursuit of extreme predicted probabilities in traditional cross-entropy loss functions for classification tasks, the Label Smoothing Loss technique was introduced. This technique softens the distribution of true labels by introducing a small amount of uniformly distributed noise into the training labels, thereby preventing the model from becoming overconfident about training samples. Specifically, the label smoothing loss function replaces the original hard labels with soft labels, i.e., it retains the dominant weight for the true class while assigning tiny probabilities to other classes. This encourages the model to learn more generalizable feature representations and reduces sensitivity to noisy samples.

2.2.2 Hybrid optimization strategy

To further accelerate model convergence and improve training efficiency, this system adopts a hybrid optimization strategy combining the AdamW optimizer and the OneCycleLR learning rate scheduler to achieve super-convergence. The AdamW optimizer, an improved version of the Adam optimizer, effectively mitigates the training instability that can arise from L2 regularization in traditional Adam optimizers by decoupling weight decay, thereby maintaining model generalization ability while enhancing training efficiency.

The OneCycleLR learning rate scheduler follows the principle of super-convergence. Within a training cycle, it first linearly increases the learning rate from a low value to a maximum value, and then gradually decreases it to a very small value, forming a complete learning rate cycle. This strategy allows for rapid exploration of the parameter space in the early stages of training, promoting fast model convergence, while fine-tuning parameters with a lower learning rate in the later stages helps escape local optima and improves the model's generalization ability.

By combining the parameter optimization advantages of the AdamW optimizer with the dynamic learning rate adjustment mechanism of the OneCycleLR scheduler, the hybrid optimization strategy constructed in this system fully leverages the synergistic effects of both. During model training, the AdamW optimizer adaptively adjusts the parameter update step size, effectively handling gradient sparsity issues for different parameters, while the OneCycleLR scheduler provides a more reasonable learning rate trajectory for the entire training process, enabling the model to achieve higher accuracy in fewer training cycles, ultimately achieving super-convergence. This hybrid optimization strategy not only significantly improves model training efficiency but also demonstrates stronger generalization ability and robustness in the emotion classification task.

2.2.3 Early stopping mechanism

Simultaneously, to prevent overfitting during the training process, this system incorporates an Early Stopping mechanism, which dynamically terminates training by continuously monitoring the validation set loss function. If the validation loss does not show significant improvement over a preset number of consecutive epochs, the best model parameters are automatically saved and the training process is terminated. This mechanism further optimizes the model's generalization performance on small datasets and enhances model stability and reliability.

3 EXPERIMENTS AND RESULT ANALYSIS

3.1 Dataset

Since expressions in the classroom are mostly discrete expressions, based on the valence-arousal and discrete expression correspondence model proposed by He Jiabei et al., shown in Figure 3, the dataset expressions were categorized into three types: positive, neutral, and negative. Several basic expression types were reclassified into these three categories according to their valence relationship.

The dataset was obtained through screenshots from online real-time class videos, part of the micro-macro expression MMEW dataset jointly released by Professor Ben Xianye's team from Shandong University, and photos taken by multiple volunteer students, manually annotated. It contains 120 images each for active, neutral, and negative expressions, totaling 1800 grayscale expression images after data augmentation. The dataset was split into training and test sets in an 8:2 ratio, and the ten-fold cross-validation method was used to partition the data multiple times and average the results, reducing bias introduced by randomness.

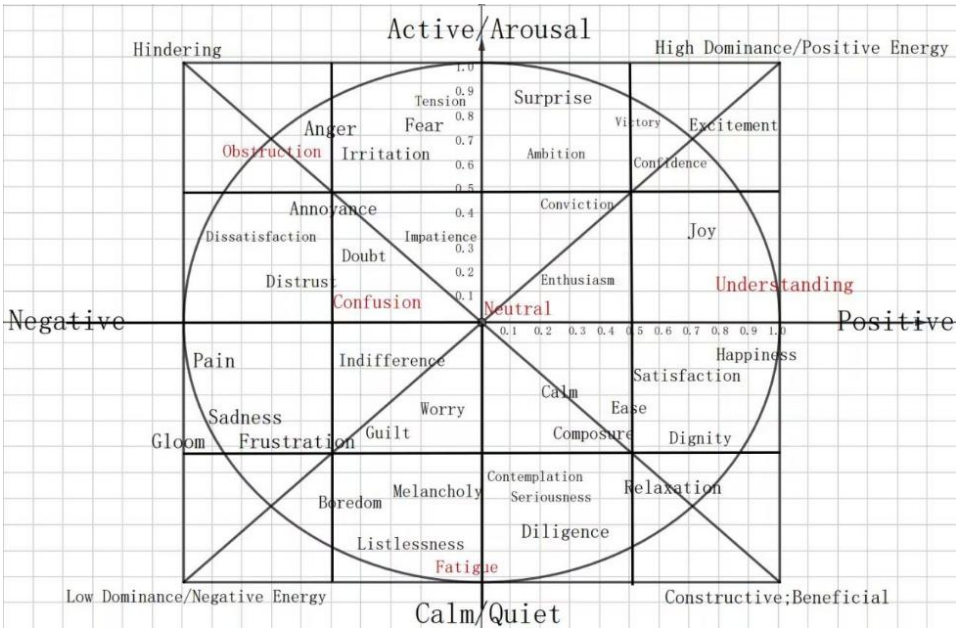

Figure 3 Correspondence Between Valence-Arousal and Discrete Expressions of He Jiabei et al.

3.2 Dataset Preprocessing and Training

Dataset preprocessing in this experiment mainly included: image standardization (grayscale conversion, normalization), multi-dimensional data augmentation (random horizontal flipping, random translation, random rotation, random erasing), then scaling to 48x48, and converting to Tensor format for input into the network for training. Data processing comparisons are shown in Figure 4, applying randomly defined data augmentation functions:

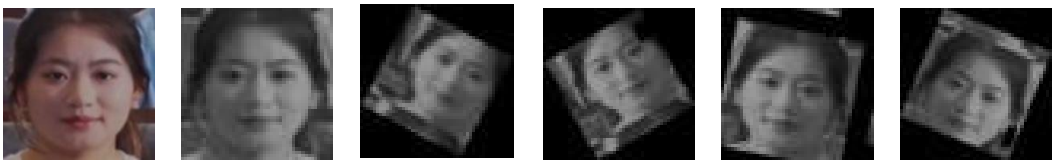

(a) (b) (c) (d) (e) (f)

Figure 4 Data Processing Comparison

Due to the small dataset size, ten-fold cross-validation was used for training and testing. The initial learning rate was 0.0001, serving as the starting point for the OneCycleLR scheduler to prevent gradient explosion in early training. The weight decay coefficient for the AdamW optimizer was 0.0001, the batch size was 16, and the early stopping patience was 12 epochs. The model was built based on the PyTorch framework, and all experimental results were obtained on an NVIDIA GeForce RTX 4060 GPU with 16GB VRAM.

3.3 Ablation Experiment

As shown by the confusion matrix, this experiment verified that through model optimization and selecting better hybrid optimization strategies, excellent results were achieved on the self-built small dataset, reaching an accuracy of 97.50%. Table 1 lists the experimental results for different combinations of sub-modules. The baseline ResNet18 model adapted for small-scale datasets by reducing convolution kernel size, adjusting downsampling methods, and adding Dropout is labeled as ResNet18(Dropout). The final version with Mish function and added ECA channel attention mechanism is labeled as ResNet18(ECA).

Table 1 Experimental Results of Different Combinations

Experiment Group	ResNet18(Dropout)	ResNet18(ECA)	Accuracy (%)
1	√		97.22
2	√	√	97.50

It can be observed that although ResNet18_ECA has about 519,000 fewer parameters than the standard ResNet18 (a reduction of approximately 3.6%), the accuracy does not decrease but instead increases by 0.28%. Although the improvement is limited, possibly due to suboptimal hyperparameter tuning and the small dataset size not fully leveraging the optimized module's performance, it still validates the effectiveness of the module.

Figure 5 shows the confusion matrix for this experiment. It can be seen that the neutral state bears the primary representation of the learning state. This is mainly because negative expression states encompass many features (e.g., yawning, sadness, disgust, anger), with large differences between these features. Furthermore, some expressions, like disgust (which might only differ slightly from neutral by the mouth corner) or yawning (similar to surprise with an open mouth), lead to slightly lower accuracy for the negative class, making it more challenging.

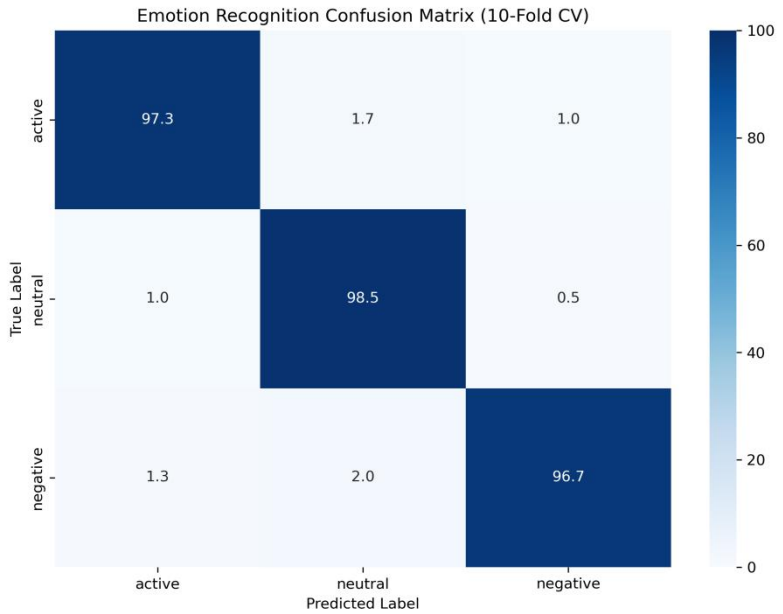

Figure 5 Confusion Matrix

4 CONCLUSION

This paper designed a method for recognizing learning and psychological states based on micro-expressions using a Residual Network. It uses single-channel input to extract facial information related to emotions and classifies them through valence relationships. Experimental results demonstrate that the proposed method exhibits strong generalization capability and applicability when processing large volumes of real-world facial expression data. The modified ResNet18 convolutional neural network algorithm, combined with the channel attention mechanism for automatic feature extraction, has achieved highly effective performance.Compared with traditional methods, the approach proposed in this study allows for more in-depth analysis of student engagement in class, providing teachers with better references for understanding student learning quality and formulating more effective teaching improvement strategies.

COMPETING INTERESTS

The authors have no relevant financial or non-financial interests to disclose.

FUNDING

This article is an achievement of the Hubei Provincial First-Class Undergraduate Major Construction (Journalism), and a research outcome of the 2024 National College Student Innovation and Entrepreneurship Training Program Project “Detection of College Students’ Learning and Psychological States Based on Micro-expression Recognition” (Project No. 202412309008).

REFERENCES

[1] Tonguc G, Ozkara BO. Automatic recognition of student emotions from facial expressions during a lecture. Computers & Education, 2020(148): 1-12.
[2] Wei YT, Lei F, Hu MJ, et al. Review of Research on Student Expression Recognition. The Chinese Journal of ICT in Education, 2020(21): 48-55.
[3] Ekman P. Facial expression and emotion. American Psychologist, 1993, 48: 384.
[4] Tong XY, Sun SL, Fu MX. Data augmentation and second-order pooling for facial expression recognition. IEEE Access, 2019, 7: 86821-86828.
[5] Huang XL, Gou XS, Chen X. Facial Micro-expression Recognition Algorithm Based on Hybrid Features and Information Entropy. Computer Simulation, 2023, 40(06): 197-201.
[6] Qiao GF, Hou SM, Liu YY. Facial expression recognition algorithm based on improved convolutional neural network and support vector machine. Journal of Computer Applications, 2022, 42(04): 1253-1259.
[7] Chen T, Xing S, Yang WW, et al. Facial expression recognition integrating spatiotemporal features. Journal of Image and Graphics, 2022, 27(07): 2185-2198.
[8] Yang HY, Ciftci U, Yin LJ. Facial Expression Recognition by De-expression Residue Learning. Conference on Computer Vision and Pattern Recognition. IEEE, 2018: 2168-2177.
[9] He KM, Zhang XY, Ren SQ, et al. Deep Residual Learning for Image Recognition Proceedings of the IEEE Conference on Computer Vision and Pattern Recognition. Piscataway, NJ: IEEE, 2016: 770-778.
[10] Wang QL, Wu BG, Zhu PF, et al. ECA-Net: Efficient Channel Attention for Deep Convolutional Neural Networks. 2020 IEEE/CVF Conference on Computer Vision and Pattern Recognition (CVPR), Seattle, 2020: 11531-11539. DOI: 10.1109/CVPR42600.2020.01155.
[11] Misra D. Mish: A Self Regularized Non-monotonic Activation Function. 2019: 8. https://arxiv.org/abs/1908.08681.
[12] Hu J, Shen L, Sun G. Squeeze-and-Excitation Networks Proceedings of the IEEE Conference on Computer Vision and Pattern Recognition. Piscataway, NJ: IEEE, 2018: 7132-7141.
[13] He JB, Zhou JX, Gan JH, et al. Classroom Expression Classification Model Based on Multi-task Learning. Journal of Applied Sciences, 2024, 42(06): 947-961.

World Journal of Information Technology
Print ISSN: 2959-9903
Online ISSN: 2959-9911
DOI: https://doi.org/10.61784/wjit3061

SCENARIO CLASSIFICATION DETECTION MODEL FOR SPATIO-TEMPORAL CONTEXTUAL INFORMATION PERCEPTION IN CLASSROOM SETTINGS

Jin Lu[1], Ji Li[2*]
[1]*Guangdong Key Laboratory of Big Data Intelligence for Vocational Education, Shenzhen Polytechnic University, Shenzhen 518000, Guangdong, China.*
[2]*Research Management Office, Shenzhen Polytechnic University, Shenzhen 518000, Guangdong, China.*
[*]*Corresponding Author: Ji Li*

Abstract: This paper proposes a spatio-temporal context-aware scene classification detection model tailored for classroom settings, aiming to address detection accuracy limitations arising from complex classroom environments characterised by fluctuating lighting, frequent occlusions, and the difficulty in capturing small-scale behaviours. By integrating cross-scale attention mechanisms in the spatial domain with long-term dependency modelling in the temporal domain, the model effectively captures subtle behavioural features and spatio-temporal contextual relationships between actions. Experimental results on the SCB-Dataset3 and Classroom-Actions public classroom datasets demonstrate that the proposed model achieves 85.4% scene classification accuracy and 83.2% action detection rate, representing significant improvements over mainstream methods such as YOLOv8m, CSSA-YOLO, and TACNet. Ablation studies further validate the effectiveness of each component: the spatial attention module yields a 2.1% mAP improvement, the temporal context module contributes a 4.5% mAP gain, while the scene context module delivers an additional 2.2% performance enhancement. Maintaining real-time processing speed (68.2 FPS), this model effectively addresses multi-scale detection and temporal dependency modelling challenges in classroom scenarios, providing robust technical support for smart education.
Keywords: Classroom behaviour recognition; Spatio-temporal context; Attention mechanisms; Scene classification; Deep learning

1 INTRODUCTION

With the rapid advancement of smart education, the intelligent analysis and assessment of classroom teaching processes have become a focal point in educational technology research. Guided by student-centred teaching principles, accurately identifying behavioural patterns among pupils during lessons holds significant importance for evaluating teaching effectiveness and formulating personalised learning strategies [1]. The proliferation of modern teaching methods such as project-based learning further emphasises the precise capture and analysis of active learning behaviours like interaction and collaboration within the classroom [2]. However, behavioural detection in classroom settings faces numerous technical challenges. Firstly, classroom environments typically exhibit significant variations in lighting and frequent occlusions, such as students blocking each other's view or environmental objects like desks and chairs causing obstructions [3]. Secondly, student behaviour exhibits multi-scale characteristics, encompassing both localised micro-actions like raising hands or writing, and full-body movements such as standing or pacing. Moreover, recognising small-scale actions within classroom settings proves particularly challenging; subtle gestures like facial expressions or hand movements often prove difficult to capture due to low resolution. These factors collectively constrain the performance of existing behaviour detection models in authentic classroom environments [4].
Currently, classroom behaviour detection methods are primarily categorised into two main types: those based on traditional handcrafted features and those based on deep learning. Traditional approaches typically rely on manually designed features (such as HOG, Haar, etc.) combined with machine learning classifiers (such as SVM) for behaviour recognition [5]. While these methods can achieve certain results in constrained environments, they exhibit poor adaptability in complex classroom scenarios and struggle to capture high-level semantic information. Deep learning-based approaches, particularly convolutional neural networks (CNNs) and spatio-temporal graph convolutional networks (ST-GCNs), have become mainstream in behaviour recognition [6]. Among these, single-stage detectors like the YOLO series have garnered significant attention for their favourable speed-accuracy trade-off [7]. In recent years, the importance of spatio-temporal contextual information in behaviour recognition has gained recognition. Models such as TACNet have achieved significant progress on unedited video datasets by incorporating transition-aware mechanisms and long-term temporal modelling [8]. Concurrently, graph convolutional network-based approaches naturally capture spatial relationships and temporal evolution of human joints, offering novel perspectives for fine-grained behaviour recognition [9]. Nevertheless, the application of existing methods within the specific classroom setting remains in its infancy. Particularly, the effective integration of spatio-temporal contextual information to address the unique challenges of classroom environments warrants further investigation.
This paper proposes a spatiotemporal context-aware scene classification detection model tailored for classroom

scenarios, with three core contributions. Firstly, a cross-scale spatial context-aware module is designed, combining the hierarchical attention mechanism of Swin Transformer with Shuffle Attention to enhance the model's ability to capture multi-scale behavioural features [10]. Secondly, a temporal context modelling module is introduced, employing bidirectional ConvLSTM to extract long-term temporal dependencies and identify transitional states between behavioural segments [11]. Thirdly, a hybrid loss function tailored for classroom scenarios is constructed, integrating WIoU bounding box regression loss with focus classification loss to optimise training stability under imbalanced data conditions [12].

2 RELATED RESEARCH

The evolution of classroom behaviour recognition technology has progressed from traditional approaches to deep learning methods, as detailed in Table 1. Early research primarily relied on conventional computer vision techniques. Vara Prasad et al. employed Haar cascade classifiers for facial detection, combined with the K-nearest neighbours (KNN) algorithm, to develop a classroom attendance system [13]. Poudyal et al. employed Support Vector Machines (SVM) and Haar wavelet classifiers to identify key differences in student attention patterns [14]. Such approaches heavily relied on manually designed features, exhibiting limited generalisation capabilities in complex classroom environments.

Table 1 Comparison of Classroom Behaviour Detection Methods

Representative algorithm	Type	Advantages	Limitations
Haar+SVM[15]/HOG+KNN[16]	Traditional methods	Low computational complexity and high interpretability	Poor environmental adaptability, limited capacity for feature expression
CNN-based[17]/YOLO[18]	Deep Learning + Spatial Features	Automatic feature learning and high detection accuracy	Ignores temporal information and sensitive to occlusion
ST-GCN[19]/TACNet[8]	Deep Learning + Spatiotemporal Features	Capturing temporal and spatial context, recognising continuous behaviour	High computational costs and substantial annotated data

With breakthroughs in deep learning technology, behaviour recognition methods based on convolutional neural networks (CNNs) have significantly enhanced recognition performance in classroom settings. Kavitha et al. developed a CNN-based student behaviour detection framework, constructing feature extraction modules for eye and mouth regions to achieve fine-grained classification of specific facial behaviours such as nail-biting, sleeping with eyes closed, and yawning [20]. However, such approaches focus solely on spatial features while neglecting temporal dynamic information, making it challenging to comprehensively understand classroom behaviour sequences.

Spatio-temporal context awareness represents a core challenge in the field of behaviour recognition, proving particularly crucial for identifying continuous and interrelated behavioural patterns within classroom settings. In recent years, researchers have proposed multiple models to capture spatio-temporal contextual information within behaviours. Spatio-temporal Graph Convolutional Networks (ST-GCN) achieve effective analysis of skeleton sequence data by modelling the spatial relationships between human body joints and their temporal evolution as a graph structure [21]. Qi et al. proposed a human skeleton behaviour recognition model integrating global attention mechanisms with spatio-temporal graph convolutional networks, achieving significant performance improvements on datasets such as NTU-RGB+D. This approach enhances the model's recognition capability for occluded data by introducing global attention modules and spatio-temporal pooling operations [22]. The Transition-Aware Contextual Network (TACNet), proposed by Megvii Research, specifically addresses transitional state challenges in behaviour recognition. Comprising a temporal context detector and transition-aware classifier, TACNet employs bidirectional ConvLSTM units to extract long-term temporal context while simultaneously classifying actions and transitional states, substantially improving behaviour detection accuracy in unedited videos [8]. For classroom-specific applications, the CSSA-YOLO model employs a cross-scale feature optimisation strategy. Its C2fs module captures spatio-temporal dependencies in small-scale actions (e.g., raising hands), while integrating a Shuffle Attention mechanism to suppress complex background interference. These techniques provide crucial reference points for behaviour recognition in classroom environments [23].

However, existing approaches still exhibit shortcomings when applied to classroom scenarios. Firstly, most models lack specific design tailored to classroom contexts, such as teacher-student interactions and group collaboration. Secondly, they are insufficiently optimised for common classroom challenges like dense occlusions and small object detection. Finally, there is a lack of effective modelling for the long-term sequential dependencies inherent in classroom behaviours. The model proposed herein addresses these deficiencies through specialised optimisation.

3 MODEL ARCHITECTURE

The proposed classroom scenario classification and detection model, which perceives spatio-temporal contextual information, adopts a multi-branch encoder-decoder architecture. The overall framework is illustrated in Figure 1. The model takes classroom video sequences as input, processing spatial features, temporal dynamics, and contextual information through three parallel branches: the spatial stream, temporal stream, and context-enhanced stream. Finally,

the fusion module outputs scenario classification results and behaviour detection bounding boxes.

Input representation section. Given a classroom video sequence $V = f_1, f_2, ,,,, f_T$, where T denotes the sequence length, each frame f_T corresponds to an RGB image of size $H \times W \times 3$. The model first pre-processes input frames through dimension standardisation and brightness normalisation to mitigate the impact of lighting variations in classroom environments. The multi-branch feature extraction component comprises a spatial branch module based on an enhanced YOLOv8 architecture, incorporating cross-scale attention modules to capture spatial features at varying scales [24]. The temporal branch module employs bidirectional ConvLSTM layers to capture long-term temporal dependencies between frames. The context branch utilises graph convolutional networks to model semantic contextual relationships within classroom scenes, such as specific patterns of teacher-student interaction and group collaboration. In the feature fusion and output section, the features from the three branches are integrated through a weighted fusion module before being fed into the scene classifier and behaviour detection head. The classifier employs fully connected layers to output scene category probabilities, while the detection head predicts behaviour bounding boxes and category labels based on an anchor mechanism.

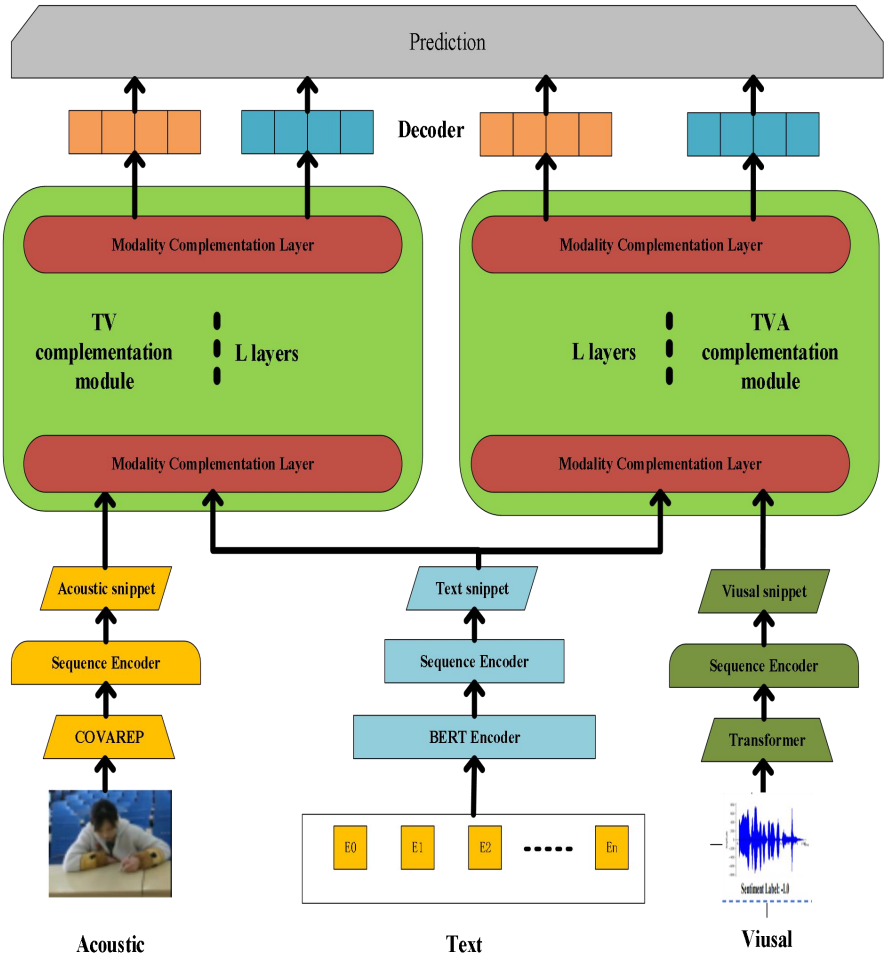

Figure 1 Schematic Diagram of the Overall Model Architecture

3.1 Spatial Context Awareness Module

The spatial context-aware module is responsible for extracting discriminative spatial features from each image frame while addressing multi-scale objects and occlusion issues in classroom settings. This module employs a cross-scale feature pyramid architecture, integrating the hierarchical window attention mechanism of the Swin Transformer with the Shuffle Attention channel attention mechanism.

Cross-scale feature extraction unit: Addressing the multi-scale characteristics of classroom behaviour, the module employs a multi-scale feature pyramid network (FPN) [25] to extract features across four distinct scales. For input frame f_T, multi-scale feature maps $P_1, P_2, ,,,, P_l$ are extracted via the backbone network (based on CSPDarknet53) [26], wherein P_l denotes the resolution of the input image $1/2^1$.

Window Attention Mechanism Unit Inspired by CSSA-YOLO, the Swin Transformer's window multi-head self-attention (W-MSA) mechanism is introduced within the C2f module to enhance the model's feature extraction

capability for small-scale behaviours. For each feature map P_l, it is first partitioned into $M \times M$ non-overlapping windows, where self-attention is then computed within each window as detailed in Equation 1.

$$Attention(Q,K,V) = SoftMax(\frac{QK^T}{\sqrt{d_k}} + B)V \quad (1)$$

Where Q,K,V denotes the query, key, and value matrices respectively, B represents the learnable position encoding; and d_k denotes the dimension of the key vector. Through local self-attention computations within windows, the model effectively captures spatial dependencies within local regions, rendering it particularly well-suited for recognising small-scale classroom behaviours such as raising hands or writing.

The Channel Attention Mechanism Unit incorporates a Shuffle Attention (SA) mechanism to mitigate interference from complex backgrounds. The SA module first partitions the feature map into multiple subgroups along the channel dimension. Within each subgroup, it concurrently computes both channel attention and spatial attention. Finally, a shuffle operation facilitates information exchange between subgroups. Given a feature map P_l, the computational process of the SA module is expressed in Equation 2.

$$F_{out} = SA\ (F) = Shuffle(Concat(SA_1(F_1), SA_2(F_2), ..., SA_G(F_G))) \quad (2)$$

In this context, F is partitioned into G subgroups $F_1, F_2, , , , F_G$, with attention weights computed independently for each subgroup.

3.2 Time Context Awareness Module

Classroom behaviour exhibits distinct temporal continuity and dynamic evolution characteristics, such as raising one's hand to answer questions or lowering one's head to take notes, which typically comprise a sequence of consecutive actions. The temporal context modelling module aims to capture long-term temporal dependencies within behaviours, addressing issues of momentary occlusion and behavioural fragmentation.

Bidirectional temporal coding unit, employing a bidirectional ConvLSTM architecture that simultaneously leverages past and future contextual information to enhance the representation of the current frame. For time step t, the forward computation of the bidirectional ConvLSTM may be referenced in Equations 3 and 4.

$$f_t = \sigma(W_{xf} * x_t + W_{hf} * h_{t-1} + b_f) \quad (3)$$

$$c_t = f_t \Theta c_{t-1} + i_t \Theta g_t \quad (4)$$

Here, $*$ denotes the convolution operation, Θ represents element-wise multiplication, and σ signifies the sigmoid activation function. The concatenation of the forward and backward hidden states of the ConvLSTM forms the final temporal augmentation feature.

Transition State Perception Unit, inspired by TACNet, incorporates a transition-aware classifier specifically designed to distinguish genuine action states from transitional states. Transitional states refer to intermediate phases resembling genuine actions yet not belonging to action categories, such as the arm-raising motion preceding a completed hand-raising action. By explicitly modelling these states, the model reduces misclassifications and enhances temporal boundary accuracy.

Multi-scale Temporal Pyramid Unit: To capture behavioural patterns across different temporal scales, the module employs a multi-scale temporal pyramid architecture comprising three ConvLSTM layers with distinct time strides (1, 2, and 4 frames). Features from the pyramid's apex undergo upsampling before merging with lower-level features, thereby simultaneously capturing both short-term subtle motions and long-term behavioural patterns.

4 FUNCTIONAL TESTING AND DISCUSSION

4.1 Datasets and Evaluation Metrics

To validate the proposed model's effectiveness, experiments were conducted on two publicly available classroom behaviour datasets: the SCB-Dataset3 [27-28] and the self-constructed Classroom-Actions dataset, as detailed in Table 2. The SCB-Dataset3 comprises annotations for ten categories of student behaviour across three typical classroom scenarios (lecture, discussion, and self-study), including actions such as raising hands, writing, and reading.

Table 2 Statistical Information of Experimental Dataset

Dataset	Scene Category	Behavioural categories	Video clip	Number of students	Frame rate annotation
SCB-Dataset3	3	10	1,245	28	56,792
Classroom-Actions	5	15	2,637	52	128,435

Concurrently, this paper will conduct an assessment centred on the aforementioned indicators, as illustrated in Table 3.

Table 3 Performance Evaluation Metrics

Indicator Name	Indicator Implications	Evaluation Dimensions	In the specific context of this article
Scene Accuracy	Accuracy rate for scene category prediction	Macro-level scene recognition capability	The model's overall capability to correctly classify entire video sequences into distinct classroom types—such as lectures, discussions, self-study, and collaborative sessions—reflects its understanding of the global teaching paradigm.
Mean Average Precision	mAP@0.5	Fine-grained behaviour detection accuracy	Assess the model's overall performance in locating and identifying specific student behaviours (such as raising hands, writing, reading) within individual video frames. mAP@0.5 is the core evaluation metric in the field of object detection. The higher the value, the more precise the detection.
Temporal Localization Accuracy	Prediction accuracy for the start and end times of behaviours	Accuracy of behavioural time boundaries	Assess the degree of alignment between the start and end times of a predicted behaviour in the model and the actual timestamps. This metric is crucial for analysing the persistence and continuity of behaviours, such as accurately determining the commencement and conclusion of a “raising one's hand” action.
FPS	Detection speed, meeting real-time processing requirements	Model computational efficiency and real-time capability	The processing speed of the model is measured by the number of video frames it can analyse and process per second. A high frame rate per second (FPS) is a key indicator of whether the model can be applied to real-time classroom analysis systems, such as online teaching supervision and real-time feedback.

The table details the four core metrics employed in this paper to evaluate model performance. These metrics comprehensively assess the proposed spatio-temporal context-aware model's overall capability within classroom settings, examining its underlying principles, evaluation dimensions, and specific significance.

4.2 Experimental Procedure

The model proposed herein is implemented within the PyTorch framework, with training and inference conducted on an NVIDIA RTX 3090 GPU environment. The AdamW optimiser is employed, with an initial learning rate of 1e-4 and a batch size of 8. Training adopts a two-stage strategy: first, the backbone network is initialised using ImageNet pre-trained weights, focusing on spatial feature extraction. Subsequently, the temporal module is unfrozen and undergoes end-to-end fine-tuning using complete video sequence data. To enhance the model's generalisation capability, this study incorporates multiple data augmentation techniques. These encompass spatial augmentations such as random colour dithering, Gaussian blurring, and occlusion simulation; temporal augmentations including random frame sampling, temporal scaling, and video jitter; alongside classroom-specific enhancements like simulated lighting variations and desk-chair occlusion simulation. To address the class imbalance inherent in classroom behaviour data—where, for instance, ‘listening’ instances vastly outnumber ‘raising hand’ instances—a class-balanced sampling strategy is implemented. This is combined with a focus loss function to weight the optimisation of losses, thereby enhancing the model's recognition capability for minority class behaviours.

To comprehensively evaluate the proposed model's performance, five representative state-of-the-art methods were selected for comparative experiments. These include YOLOv8m, the current benchmark model for classroom behaviour detection; CSSA-YOLO, which incorporates cross-scale attention mechanisms to optimise multi-scale behaviour detection; TACNet, a context-aware network specialising in spatio-temporal action detection with transition perception capabilities; RA-GCNv2-A, a spatio-temporal graph convolutional network enhanced by global attention mechanisms; and VWE-YOLOv8, a classroom behaviour detection algorithm integrating multiple attention mechanisms. The aforementioned comparative approaches encompass diverse technical pathways, including detector optimisation, spatio-temporal context modelling, graph structure learning, and attention mechanism fusion. This multi-faceted evaluation validates the performance advantages demonstrated by this research.

4.3 Ablation Experiment

To validate the contributions of each module, ablation experiments were designed, with results presented in Table 4. The baseline model was YOLOv8m, to which spatial attention (SA), temporal context (TCM), and scene context (SCM) modules were progressively added.

Table 4 Ablation Experiment Results (on the SCB-Dataset3 dataset)

Model Configuration	Scene Accuracy Rate	mAP@0.5	FPS
YOLOv8m (Benchmark)[29]	76.5%	74.8%	82.3
+Spatial Attention(SA)	78.9% (+2.4%)	76.9% (+2.1%)	79.5
+Temporal Context(TCM)	81.2% (+4.7%)	79.3% (+4.5%)	75.8
+Scenario Context(SCM)	83.7% (+7.2%)	81.5% (+6.7%)	71.6
Complete Model	85.4%(+8.9%)	83.2%(+8.4%)	68.2

Experimental results demonstrate that each module makes a significant contribution to performance enhancement. Specifically, the spatial attention module improves mAP by 2.1%, primarily enhancing detection capabilities for small-scale behaviours; the temporal context module further boosts mAP by 4.5%, highlighting the importance of modelling temporal dependencies; while the scene context module contributes a 2.2% mAP improvement, underscoring the effectiveness of classroom-specific semantic context. The complete model achieves 8.9% and 8.4% improvements over the baseline in scene classification accuracy and action detection mAP respectively, confirming the synergistic effect of all modules.

4.4 Comparative Experiments and Analysis

The comparison results with state-of-the-art methods are presented in Table 5. On the SCB-Dataset3 dataset, our proposed model outperforms all competing approaches in both scene classification accuracy and action detection mAP, while maintaining an acceptable inference speed of 68.2 FPS.

Table 5 Comparison Results with State-of-the-Art Methods on the SCB-Dataset3 Dataset

Method	Scene Accuracy Rate	mAP@0.5	FPS
YOLOv8m[29]	76.5%	74.8%	82.3
CSSA-YOLO[30]	78.8%	76.0%	78.3
TACNet[8]	79.3%	77.2%	45.6
RA-GCNv2-A[31]	81.5%	78.9%	52.7
VWE-YOLOv8[32]	82.7%	80.1%	65.8
Our Method	85.4%	83.2%	68.2

As shown in the table, our model achieves a 2.7% improvement in scene classification accuracy and a 3.1% increase in mAP for behaviour detection compared to the state-of-the-art method (VWE-YOLOv8). This advancement is primarily attributable to the model's comprehensive utilisation of spatio-temporal contextual information, particularly its superior performance in handling complex classroom scenarios. It is noteworthy that although our model possesses a larger parameter size than YOLOv8m, its efficient attention mechanism and feature fusion strategy enable faster inference speeds than many complex graph convolutional network-based models (such as RA-GCNv2-A), thereby meeting the demands of real-time classroom analysis.

Regarding cross-scenario generalisation capability, our model underwent further validation on the Classroom-Actions dataset, as detailed in Table 6.

Table 6 Generalisation Performance on the Classroom-Actions Dataset

Method	Teaching scenario	Discussion scenario	Experimental Scenario	Collaborative Scenarios	Average
YOLOv8m	75.3%	70.8%	68.5%	65.2%	70.0%
CSSA-YOLO	77.1%	72.6%	70.3%	67.8%	72.0%
TACNet	78.2%	74.5%	72.1%	69.3%	73.5%
Our Method	81.5%	78.9%	76.7%	74.2%	77.8%

The results demonstrate that our proposed model exhibits outstanding generalisation performance on the more challenging and diverse Classroom-Actions dataset, achieving a mean average precision (mAP) of 77.8% across four scenarios—lecturing, discussion, experimentation, and collaboration—that surpasses other comparative models. This outcome provides robust validation of the model's strong adaptability to complex classroom environments. In-depth analysis reveals that all models exhibit a performance decline with increasing scene complexity, with the most pronounced challenges occurring in collaborative scenarios characterised by student grouping, severe occlusions, and frequent behavioural interactions. Nevertheless, our model maintains an mAP of 74.2% in this scenario, representing a substantial improvement of nearly 9 percentage points over the baseline YOLOv8m model. This advancement is primarily attributable to the effectiveness of our spatio-temporal context-aware architecture. Specifically, the spatial context-aware module enhances the localisation and recognition of individual objects under dense occlusion conditions through cross-scale attention mechanisms. Meanwhile, temporal context modelling assists in inferring more plausible behavioural categories from ambiguous single-frame images by analysing long-term dependencies within behavioural sequences. Together, these approaches address the core challenges inherent in complex scenarios.

4.5 Performance Experiments and Analysis

As shown in Figure2, this paper illustrates the performance trends of different models across four distinct classroom scenarios, with the primary objective of evaluating their robustness and adaptability to increasingly complex teaching environments.

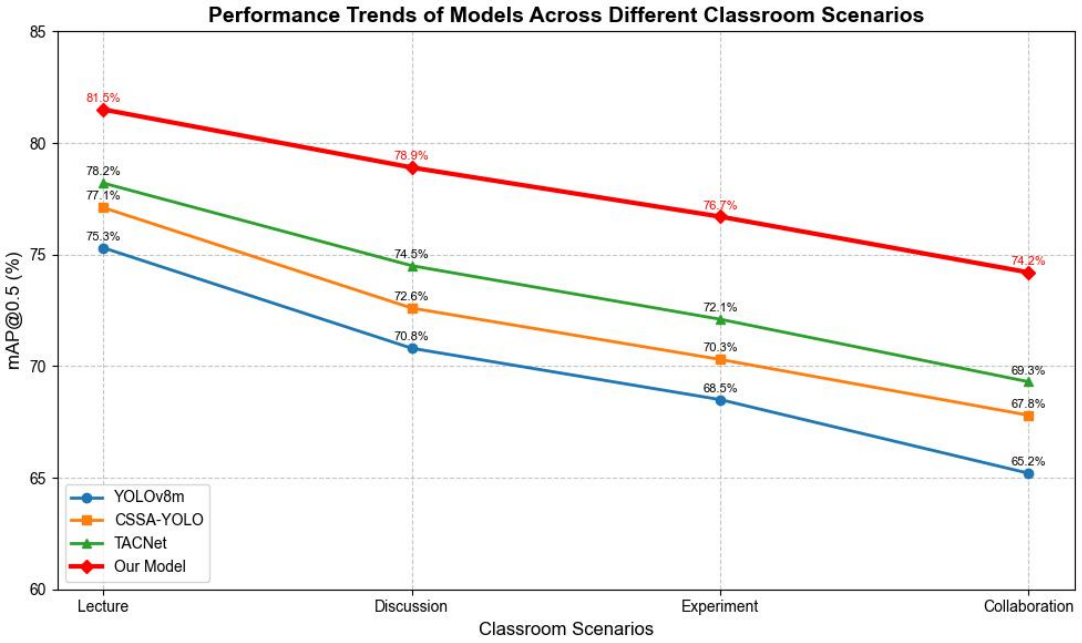

Figure 2 Performance Trends of the Model Across Different Classroom Scenarios

The line graph clearly demonstrates a consistent performance decline for all models as the scenario complexity escalates from structured Lecture to highly interactive Collaboration settings. This trend validates the inherent challenges posed by real classroom environments, particularly the issues of severe occlusion and frequent interactions present in collaborative learning scenarios. Notably, our proposed model (red line) maintains superior performance across all scenarios, with the performance advantage becoming most pronounced in the most challenging Collaboration scenario, where it achieves a 74.2% mAP@0.5, nearly 9 percentage points higher than the baseline YOLOv8m. This significant performance gap underscores the effectiveness of our spatiotemporal context-aware architecture, specifically the cross-scale spatial attention mechanism in handling severe occlusion and the long-term temporal modeling in disambiguating complex interactions. The results confirm that our model not only achieves state-of-the-art performance but also exhibits enhanced robustness in practical educational settings where complex student behaviors and interactions are prevalent.

Figure 3 presents a comprehensive performance comparison between different models using a grouped bar chart, with the primary objective of evaluating their overall effectiveness on the SCB-Dataset3 dataset across two critical metrics, Scene Classification Accuracy and Behavior Detection mAP@0.5.

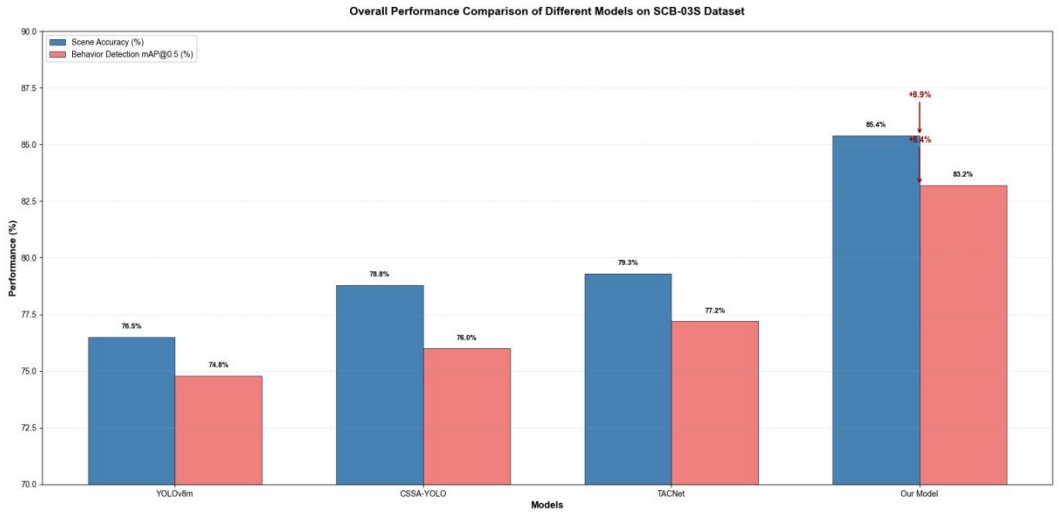

Figure 3 Overall Performance Comparison Between Models

The chart clearly demonstrates that our proposed model achieves superior performance on both evaluation criteria, attaining 85.4% in scene accuracy and 83.2% in behavior detection mAP, which represents significant improvements of 8.9% and 8.4% respectively compared to the baseline YOLOv8m model. More importantly, the parallel comparison reveals that our model exhibits more substantial enhancement in behavior detection capability, which directly validates the effectiveness of our core innovation—the spatiotemporal context-aware architecture—in precisely localizing and

recognizing fine-grained student behaviors. The consistent performance advantage across both metrics indicates that our model successfully addresses the dual challenges of macroscopic scene understanding and microscopic behavior analysis in educational environments, establishing a new state-of-the-art for classroom behavior analysis systems while maintaining practical applicability.

5 CONCLUSION

This study proposes a spatiotemporal context-aware scene classification and detection model tailored for classroom settings. By innovatively integrating cross-scale attention mechanisms in the spatial domain with long-term dependency modelling in the temporal domain, it effectively addresses key challenges in complex classroom environments, including lighting variations, frequent occlusions, and small-scale behaviour recognition. Experimental results demonstrate that the model achieves state-of-the-art performance across multiple datasets, including SCB-Dataset3 and Classroom-Actions. It attains a scene classification accuracy of 85.4% and an action detection mAP of 83.2%, significantly outperforming mainstream methods such as YOLOv8m and TACNet. This validates the proposed architecture's efficacy and superiority in concurrently handling macro-level scene understanding and micro-level behavioural analysis. Looking ahead, this research may be further deepened in three directions. Firstly, exploring multimodal data fusion mechanisms by integrating modalities such as speech and text to enhance the completeness of situational understanding. Secondly, investigating weakly supervised or self-supervised learning strategies to reduce the model's reliance on large volumes of finely annotated data, thereby enhancing scalability. Thirdly, optimising computational efficiency through techniques like neural network pruning and quantisation to adapt the model for edge computing devices, thereby advancing the practical implementation and widespread adoption of intelligent classroom systems.

COMPETING INTERESTS

The authors have no relevant financial or non-financial interests to disclose.

FUNDING

The project was supported by 2024 Shenzhen Polytechnic University Quality Engineering Project "Research on Classroom Scene Understanding and Behavior Analysis Method Based on Multimodal Attention Mechanisms (7024310268)".

REFERENCES

[1] Yang J, Shi G, Zhu W, et al. Intelligent technologies in smart education: a comprehensive review of transformative pillars and their impact on teaching and learning methods. Humanities and Social Sciences Communications, 2025, 12(1): 1239-1239.
[2] Sapiah S, Ulfah M S, Saputra N A, et al. Smart education in remote areas: collaborative strategies to address challenges in Majene Regency, Indonesia. Frontiers in Education, 2025, 101552575-1552575.
[3] Jain A, Dubey K A, Khan S, et al. A PSO weighted ensemble framework with SMOTE balancing for student dropout prediction in smart education systems. Scientific Reports, 2025, 15(1): 17463-17463.
[4] Xieling C, Di Z, Gary C, et al. Author Correction: Blockchain in smart education: Contributors, collaborations, applications and research topics. Education and Information Technologies, 2022, 28(7): 9267-9267.
[5] Dey A, Anand A, Samanta S, et al. Attention-Based AdaptSepCX Network for Effective Student Action Recognition in Online Learning. Procedia Computer Science, 2024: 233164-174.
[6] Taojie X, Wei D, Si Z, et al. Research on Recognition and Analysis of Teacher–Student Behavior Based on a Blended Synchronous Classroom. Applied Sciences, 2023, 13(6): 3432-3432.
[7] Vaghela R, Vaishnani D, Sarda J, et al. Optimizing object detection for autonomous robots: a comparative analysis of YOLO models. Measurement, 2026, 257(PB): 118676-118676.
[8] Song L, Zhang S, Yu G, et al. TACNet: Transition-Aware Context Network for Spatio-Temporal Action Detection. CoRR, 2019.
[9] Hua Z, Yang J, Ji W. Knowledge graph convolutional networks with user preferences for course recommendation. Scientific Reports, 2025, 15(1): 30256-30256.
[10] Wang Z, Yao J, Zeng C, et al. Students' Classroom Behavior Detection System Incorporating Deformable DETR with Swin Transformer and Light-Weight Feature Pyramid Network. Systems, 2023, 11(7): 372-388.
[11] Pingo A, Castro J, Loureiro P, et al. Driving Behavior Classification Using a ConvLSTM. Future Transportation, 2025, 5(2): 52-52.
[12] Fu R, Tian M. Classroom Facial Expression Recognition Method Based on Conv3D-ConvLSTM-SEnet in Online Education Environment. Journal of Circuits, Systems and Computers, 2023, 33(07).
[13] Cai S, Zhang X, Mo Y . A Lightweight underwater detector enhanced by Attention mechanism, GSConv and WIoU on YOLOv8. Scientific Reports, 2024, 14(1): 25797-25797.
[14] K S, Prasad V. Design and Implementation of an Efficient Rose Leaf Disease Detection using K-Nearest Neighbours. International Journal of Recent Technology and Engineering (IJRTE), 2020, 9(3): 21-27.

[15] Paneru B, Paneru B, Sapkota C S, et al. Enhancing healthcare with AI: Sustainable AI and IoT-Powered ecosystem for patient aid and interpretability analysis using SHAP. Measurement: Sensors, 2024: 36101305-101305.
[16] Sugiharto A, Harjoko A, Suharto S. Indonesian traffic sign detection based on Haar-PHOG features and SVM classification. International Journal on Smart Sensing and Intelligent Systems, 2020, 13(1): 1-15.
[17] Kwon H B, Kim K J. Image Searching using a Cascade of HOG-kNN. ITC-CSCC :International Technical Conference on Circuits Systems, Computers and Communications, 2015.
[18] Priya V K, Peter D J. Enhanced Defensive Model Using CNN against Adversarial Attacks for Medical Education through Human Computer Interaction. International Journal of Human–Computer Interaction, 2025, 41(3): 1729-1741.
[19] Shen Q, Zhang L, Zhang Y, et al. Distracted Driving Behavior Detection Algorithm Based on Lightweight StarDL-YOLO. Electronics, 2024, 13(16): 3216-3216.
[20] Pu L, Zhao Y, Hua Z, et al. Multi-Target spraying behavior detection based on an improved YOLOv8n and ST-GCN model with Interactive of video scenes. Expert Systems With Applications, 2025: 262125668-125668.
[21] Kuppala K, Banda S, Imambi S S. Selection of Distance Measure for Visual and Long Wave Infrared Image Region Similarity using CNN Features. Procedia Computer Science, 2024: 235970-978.
[22] Deyuan Z, Haoguang W, Chao W, et al. Video Human Action Recognition with Channel Attention on ST-GCN. Journal of Physics: Conference Series, 2021, 2010(1).
[23] Lu Qi. Sports-ACtrans Net: research on multimodal robotic sports action recognition driven via ST-GCN. Frontiers in Neurorobotics, 2024: 181443432-1443432.
[24] Zhou L, Liu X, Guan X, et al. CSSA-YOLO: Cross-Scale Spatiotemporal Attention Network for Fine-Grained Behavior Recognition in Classroom Environments. Sensors, 2025, 25(10): 3132-3132.
[25] Okano T M, Lopes C A W, Ruggero M S, et al. Edge AI for Industrial Visual Inspection: YOLOv8-Based Visual Conformity Detection Using Raspberry Pi. Algorithms, 2025, 18(8): 510-510.
[26] Thammasanya T, Patiam S, Rodcharoen E, et al. A new approach to classifying polymer type of microplastics based on Faster-RCNN-FPN and spectroscopic imagery under ultraviolet light. Scientific reports, 2024, 14(1): 3529-3529.
[27] Senussi F M, Kang S H. Occlusion Removal in Light-Field Images Using CSPDarknet53 and Bidirectional Feature Pyramid Network: A Multi-Scale Fusion-Based Approach. Applied Sciences, 2024, 14(20): 9332-9332.
[28] Chen S, Liu Y, Zhang H, et al. A human location and action recognition method based on improved Yolov11 model. Discover Artificial Intelligence, 2025, 5(1): 232-232.
[29] Wang Z, Yuan G, Zhou H, et al. Foreign-Object Detection in High-Voltage Transmission Line Based on Improved YOLOv8m. Applied Sciences, 2023, 13(23).
[30] Zhou L, Liu X, Guan X, et al. CSSA-YOLO: Cross-Scale Spatiotemporal Attention Network for Fine-Grained Behavior Recognition in Classroom Environments. Sensors, 2025, 25(10): 3132-3132.
[31] Nan Y, Niu W, Chang Y, et al. Transient Stability Assessment of Power Systems Built upon Attention-Based Spatial–Temporal Graph Convolutional Networks. Energies, 2025, 18(14): 3824-3824.
[32] Liu J, Lin C, Chen J, et al. Research on Real-Time Analysis and Intervention of Classroom Behaviour Based on Object Detection Algorithms. Advances in Vocational and Technical Education, 2025, 7(2).

World Journal of Information Technology
Print ISSN: 2959-9903
Online ISSN: 2959-9911
DOI: https://doi.org/10.61784/wjit3062

BLOCKCHAIN AND LARGE LANGUAGE MODELS: A SURVEY OF INTEGRATION APPROACHES AND OPEN CHALLENGES

Yun Li, ShuRui Xiao*
School of Finance and Economics, Hainan Vocational University of Science and Technology, Haikou 571126, Hainan, China.
Corresponding Author: ShuRui Xiao

Abstract: This paper surveys recent research on the integration of blockchain technology and Large Language Models (LLMs), examining how decentralization, immutability, and cryptographic verification can address challenges in AI governance, data sovereignty, and model accountability. We review key integration strategies including blockchain-based data repositories, smart contract-driven governance mechanisms, and decentralized AI marketplaces. Our analysis identifies three primary application domains—cybersecurity, healthcare data sharing, and financial services—where this convergence demonstrates practical value. However, significant barriers remain: current blockchain throughput falls short of high-frequency AI requirements, privacy-preserving techniques introduce substantial computational overhead, and regulatory frameworks have yet to reconcile blockchain immutability with data protection mandates. We conclude by proposing prioritized research directions to bridge these gaps.
Keywords: Blockchain; Large language models; Decentralization; Smart contracts; Federated learning

1 INTRODUCTION

Blockchain technology, with its fundamental principles of decentralization, immutability, and transparency, offers potential solutions to critical challenges in AI governance and deployment. Large Language Models (LLMs), while demonstrating exceptional capabilities in natural language understanding and generation, raise concerns regarding centralized control, data privacy, and accountability. The motivation for integrating these technologies stems from structural limitations in the current AI development paradigm. The rapid advancement of AI has been accompanied by increasing concentration of computational resources and training data among a small number of technology corporations [1,2]. This centralization creates several interrelated challenges: first, it can introduce systematic biases in model outputs when training data lacks diversity or adequate curation; second, it restricts broader participation in AI development, limiting innovation pathways; third, it raises questions about the provenance and integrity of model-generated content. Users who contribute data to centralized platforms often lack transparency regarding how their contributions are utilized and monetized.

Blockchain technology offers potential solutions to these challenges through its inherent properties. The decentralized nature of blockchain provides a foundation for more democratic governance of AI systems, addressing eight major governance challenges identified by researchers concerning decision rights, incentive mechanisms, and accountability in foundation model systems [1].

Blockchain implementations tailored for AI integration have evolved beyond traditional cryptocurrency applications to address the specific needs of AI systems. Recent advancements in consensus mechanisms demonstrate this adaptation, with Proof of Authority (PoA) showing promising results in multi-cloud environments, achieving throughputs of up to 1000 transactions per second [3]. While this represents improvement over earlier Proof of Work implementations (typically 7-15 tps for Bitcoin and Ethereum), the requirements for real-time AI operations remain substantially higher, particularly for applications involving continuous data streaming or high-frequency model updates.

Smart contracts have emerged as a key element of blockchain-AI integration, enabling automated governance, verification, and incentive distribution. Research on cybersecurity applications demonstrates that AI algorithms integrated with blockchain-based smart contracts can detect and mitigate network attacks, achieving a 95% detection rate with a 2% false positive rate, while maintaining transaction latency below 200 milliseconds [4]. These performance metrics indicate that for certain AI applications—particularly those tolerant of sub-second latency—smart contracts can provide automated enforcement of governance policies while maintaining reasonable responsiveness.

LLMs have evolved rapidly in recent years, with models such as GPT-4, PaLM, and LLaMA demonstrating capabilities in natural language processing and content generation. However, this development has primarily occurred within centralized environments controlled by resource-intensive organizations, creating barriers to broader participation and raising concerns about bias, accountability, and equitable access.

Blockchain-based approaches aim to address these centralization challenges through several mechanisms. Decentralized governance-driven architectures have been proposed to distribute decision-making power across stakeholders rather than concentrating it within single organizations [1]. These architectures employ smart contracts to implement transparent governance rules, token-based incentive systems to reward contributions to model training or data provision, and cryptographic verification to ensure the integrity of training processes. While practical implementations remain in

early stages, these approaches represent attempts to create more inclusive and accountable frameworks for LLM development.

2 KEY INTEGRATION STRATEGIES

2.1 Decentralized Data Repositories for AI Training

Decentralized data repositories represent a fundamental integration strategy, addressing limitations in data accessibility and sovereignty for LLM training. These systems leverage blockchain to provide verifiable data provenance, decentralized access control, and transparent transaction records. The Blockchain-Based Knowledge Repository (BBKR) exemplifies this approach through structured data validation processes and scalable transaction mechanisms, demonstrating performance improvements in data retrieval and integrity verification compared to centralized alternatives [5]. Building on similar principles, DataHarbour implements a marketplace model specifically designed for AI training data, where blockchain-based smart contracts mediate data transactions between providers and consumers [6]. This marketplace approach aims to address data inequality by enabling smaller organizations to monetize their data assets and access diverse datasets without relying on centralized aggregators.

These decentralized data repositories address a fundamental challenge in LLM development: access to diverse, high-quality training data. By creating secure, transparent, and incentivized mechanisms for data sharing, they enable a broader range of participants to contribute to AI development while maintaining the privacy and security standards crucial for sensitive data.

2.2 Smart Contracts for Model Governance

Smart contracts provide programmable mechanisms for implementing governance policies in decentralized AI systems. These self-executing agreements can automate key governance functions including access control, contribution verification, reward distribution, and dispute resolution, while maintaining a transparent and immutable record of all governance decisions.

AI marketplaces demonstrate practical applications of smart contract-based governance. AIArena implements an on-chain consensus mechanism where participant contributions—whether providing training data, computational resources, or model improvements—are verified and rewarded according to predefined rules encoded in smart contracts [2]. This approach aims to create transparent incentive structures that encourage quality contributions. PredictChain extends this concept by enabling users to upload datasets, request model training on existing datasets, or query trained models, with all interactions mediated by smart contracts executed across blockchain nodes [7]. By encoding governance rules in verifiable and enforceable smart contracts, these systems aim to establish more accountable frameworks for collaborative AI development.

3 EMERGING APPLICATION DOMAINS

3.1 Decentralized AI Marketplaces

Decentralized AI marketplaces represent an emerging application domain where blockchain infrastructure facilitates peer-to-peer exchange of AI-related resources including training data, computational capacity, and trained models. These marketplaces aim to reduce barriers to AI development by eliminating centralized intermediaries. AIArena, implemented on the Base blockchain testnet, demonstrates this concept through a platform where participants can contribute models and computational resources, with contributions verified and rewarded through on-chain mechanisms [2]. DataHarbour focuses specifically on the data acquisition challenge, creating a marketplace where smaller organizations can access diverse datasets without relying on dominant technology providers [6]. PredictChain extends marketplace functionality to encompass the complete AI workflow, enabling dataset uploads, model training requests, and inference queries, all coordinated through blockchain-based protocols [7]. These platforms collectively illustrate how decentralized architectures can broaden participation in AI development, though questions regarding data quality assurance, computational efficiency, and economic sustainability require further investigation.

3.2 Cybersecurity and Threat Detection

Cybersecurity applications demonstrate synergistic integration of blockchain and AI technologies. In this domain, blockchain provides an immutable audit trail of security events and system states, while AI algorithms analyze these records to detect anomalous patterns indicative of attacks. Research on smart city and Industry 4.0 environments shows that this combination can improve both detection speed and accuracy compared to centralized logging systems, where audit records may be subject to tampering [4]. Similarly, electronic voting systems have explored AI-enhanced anomaly detection within blockchain transaction patterns to identify potential security threats in real-time [8]. The mutual reinforcement in these applications—where blockchain secures the data foundation for AI analysis, and AI protects blockchain networks from sophisticated attacks—illustrates a key advantage of integration. However, the computational overhead of maintaining cryptographic verification alongside real-time AI inference remains a practical consideration for resource-constrained deployments.

3.3 Healthcare Data Sharing and Analysis

Healthcare data sharing represents a domain where blockchain-AI integration addresses critical challenges related to patient privacy, institutional trust, and regulatory compliance. Medical data is typically fragmented across institutions, with data sharing constrained by privacy regulations such as HIPAA in the United States and GDPR in Europe.

Federated Learning integrated with blockchain offers a technical approach to this challenge by enabling collaborative AI model training across multiple healthcare institutions without requiring raw patient data to leave institutional boundaries [9]. In this architecture, each institution trains model components locally on its own data, and blockchain coordinates the aggregation of model updates while maintaining a verifiable record of contributions. This approach aims to balance the utility of large-scale datasets for AI model improvement with the privacy requirements of sensitive medical information. However, practical deployment faces challenges including the computational cost of cryptographic verification, the need for standardized data formats across institutions, and the complexity of managing consent and access rights through smart contracts. These technical and operational considerations must be addressed before widespread adoption in clinical settings.

3.4 Financial Services and Accounting

In financial services, blockchain-AI integration addresses challenges in transaction verification, fraud detection, and regulatory compliance. Blockchain provides an immutable transaction ledger, while AI contributes pattern recognition and anomaly detection capabilities. This combination has been applied to streamline Know Your Customer (KYC) and Anti-Money Laundering (AML) processes, where AI algorithms analyze transaction patterns recorded on blockchain to identify suspicious activities [10]. For financial accounting, the integration enables automation of repetitive tasks such as transaction reconciliation and audit trail verification, potentially reducing manual processing costs and enabling more frequent financial reporting [11]. However, the practical adoption of these technologies in regulated financial environments requires addressing concerns about algorithmic accountability, the legal status of smart contract-executed transactions, and the integration of blockchain systems with existing financial infrastructure.

4 TECHNOLOGICAL AND GOVERNANCE CHALLENGES

4.1 Scalability and Performance

Scalability and performance limitations represent fundamental challenges for blockchain-AI integration. Current blockchain implementations exhibit transaction throughput and latency characteristics that may not align with the requirements of many AI applications. While optimized consensus mechanisms such as Proof of Authority can achieve approximately 1000 transactions per second in favorable conditions [3], many AI applications—particularly those involving continuous data streaming, high-frequency model updates, or real-time inference—may require substantially higher throughput. For latency-sensitive applications, blockchain transaction confirmation times present additional constraints. Although latency below 200 milliseconds has been demonstrated in specific cybersecurity implementations [4], applications requiring sub-100-millisecond responses may find blockchain verification overhead prohibitive.

Several technical approaches aim to address these limitations. Layer-2 scaling solutions, which process transactions off-chain while anchoring periodic state commitments to the main blockchain, can potentially increase effective throughput. Specialized consensus mechanisms optimized for AI workloads, rather than general-purpose transaction processing, represent another research direction. Additionally, hybrid architectures that selectively use blockchain for high-value operations (such as model version control or governance decisions) while conducting compute-intensive operations off-chain may offer practical compromises between decentralization benefits and performance requirements.

4.2 Privacy and Security

Privacy and security considerations present complex trade-offs in blockchain-AI integration. While blockchain provides tamper-resistant audit trails and cryptographic access control, the transparency inherent in public blockchains can conflict with privacy requirements for sensitive training data. Conversely, private or permissioned blockchains sacrifice some decentralization benefits to maintain confidentiality.

Privacy-preserving techniques for AI training on blockchain platforms include differential privacy, which adds calibrated noise to training data or model updates to prevent identification of individual records, and federated learning, which enables model training on distributed data without centralizing raw datasets. Research has demonstrated the integration of differential privacy with blockchain-based federated learning [12], though this approach involves inherent trade-offs: stronger privacy protections typically reduce model accuracy, requiring careful calibration based on application requirements. Emerging cryptographic techniques, including zero-knowledge proofs that enable verification of computation correctness without revealing inputs, represent additional privacy-preserving directions under active investigation.

Storage architecture also impacts security. Storing large training datasets directly on blockchain is economically impractical due to high replication costs across network nodes. Hybrid approaches that store data off-chain while recording cryptographic hashes or metadata on-chain provide verification capabilities at reduced cost [3], though they

introduce dependencies on off-chain storage systems and require careful management of access control at the boundary between on-chain and off-chain components.

4.3 Decentralized Governance Frameworks

Implementing decentralized governance frameworks for collaborative AI development presents multifaceted challenges spanning technical, economic, and social dimensions. Governance mechanisms must address several key functions: defining decision rights for model updates and policy changes, designing incentive structures that encourage quality contributions while discouraging malicious behavior, and establishing accountability mechanisms for addressing harms from model outputs.

Incentive design represents a critical challenge. Token-based reward systems can compensate participants for providing training data, computational resources, or model improvements, but measuring the value of contributions objectively remains difficult. Data quality cannot be fully verified through automated means, creating opportunities for participants to submit low-quality or adversarial data if rewards are based solely on quantity. Model performance improvements depend on complex interactions between dataset characteristics, training procedures, and evaluation metrics, complicating the attribution of credit to individual contributors. While various projects have explored different incentive structures [2,7], no consensus has emerged on optimal approaches, and designs likely need customization for specific use cases.

Transparency and interpretability present additional governance challenges. Blockchain provides transparency of transaction histories and governance votes, but this differs from the interpretability of AI decision-making processes. Recording complete model training procedures on-chain is generally impractical due to data volume, necessitating selective recording of key parameters, dataset identifiers, and validation results. Developing standards for what aspects of AI development should be recorded on-chain, and how this information should be structured for meaningful audit, remains an open research question. Furthermore, governance processes must balance inclusivity with efficiency: overly inclusive decision-making may slow development velocity, while concentrated decision-making reproduces the centralization that decentralized approaches aim to address.

4.4 Regulation and Standardization

Regulatory compliance presents significant challenges for blockchain-AI integration, particularly regarding data protection and algorithmic accountability. The General Data Protection Regulation (GDPR) in Europe establishes a "right to be forgotten," allowing individuals to request deletion of their personal data. This requirement conflicts with blockchain's immutability, which is fundamental to its security model. Potential architectural solutions include storing personal data off-chain while recording only cryptographic hashes on-chain, enabling data deletion without compromising blockchain integrity, though this approach introduces dependencies on off-chain storage systems. Alternatively, advanced cryptographic techniques such as zero-knowledge proofs or programmable privacy mechanisms could enable selective data disclosure while maintaining on-chain records. However, the legal sufficiency of these technical approaches remains uncertain, as regulatory interpretation continues to evolve. Additionally, transparency of model training and validation, while potentially beneficial for regulatory audit, must be balanced against intellectual property concerns and competitive dynamics.

Lack of standardization represents another barrier to broader adoption. Current blockchain-AI integration projects employ diverse technical approaches regarding consensus mechanisms, smart contract interfaces, data schemas, and interoperability protocols. This heterogeneity limits the ability to transfer models, datasets, or governance mechanisms across different blockchain platforms. Developing standardized protocols and APIs would facilitate interoperability and reduce implementation complexity. However, premature standardization in a rapidly evolving field risks locking in suboptimal designs. The balance between encouraging innovation through diversity and enabling interoperability through standardization remains an ongoing challenge for the research community and industry stakeholders.

5 CONCLUSION

This paper has surveyed recent research on blockchain and Large Language Model integration, examining technical approaches, application domains, and persistent challenges. Our analysis identifies three primary integration strategies: blockchain-based data repositories that provide verifiable data provenance and decentralized access control, smart contract-driven governance mechanisms that automate policy enforcement and incentive distribution, and decentralized marketplaces that facilitate peer-to-peer exchange of AI resources. Applications in cybersecurity, healthcare, and financial services demonstrate benefits particularly where data sovereignty, multi-stakeholder governance, or audit trail requirements are critical.

However, technical and governance challenges constrain practical adoption. Scalability limitations necessitate hybrid architectures balancing on-chain verification with off-chain computation. Privacy-preserving techniques involve trade-offs between data protection and model utility. Decentralized governance mechanisms face challenges in measuring contribution quality and balancing participation with efficiency. Regulatory frameworks have yet to reconcile blockchain immutability with data protection mandates such as GDPR's right to erasure.

Future research should prioritize Layer-2 scaling solutions and consensus mechanisms optimized for AI workloads, advance cryptographic techniques such as zero-knowledge proofs for privacy-preserving model training, and conduct

empirical evaluations of governance mechanisms across diverse use cases. Interdisciplinary collaboration among computer scientists, economists, legal scholars, and ethicists remains essential to address technical feasibility, economic sustainability, and regulatory compliance. This survey's limitations include its focus on English-language publications and the nascent stage of production deployments, which limits availability of real-world performance data.

COMPETING INTERESTS

The authors have no relevant financial or non-financial interests to disclose.

FUNDING

This article is the teaching reform research project of Hainan Vocational University of Science and Technology in 2023: Exploration and Practice of the Application of Blockchain Technology in the Cultivation of Composite Talents in the Context of the Free Trade Port (Project No. HKJG2023-18).

REFERENCES

[1] Liu Y, Lu Q, Zhu L, et al. Decentralised Governance-Driven Architecture for Designing Foundation Model based Systems: Exploring the Role of Blockchain in Responsible AI. arXiv preprint arXiv: 2308.05962, 2023.
[2] Wang Z, Sun R, Lui E, et al. AIArena: A blockchain-based decentralized AI training platform. Companion Proceedings of the ACM on Web Conference 2025, New York, NY, USA. 2025: 1375-1379. DOI: https://doi.org/10.1145/3701716.3715484.
[3] Balachandar S K, Prema K, Kamarajapandian P, et al. Blockchain-enabled Data Governance Framework for Enhancing Security and Efficiency in Multi-Cloud Environments through Ethereum, IPFS, and Cloud Infrastructure Integration. Journal of Electrical Systems, 2024, 20(5): 2132-2139.
[4] Goundar S. Blockchain-AI Integration for Resilient Real-time Cyber Security. Global Congress on Emerging Technologies (GCET-2024), Gran Canaria, Spain. 2024: 342-349. DOI: 10.1109/GCET64327.2024.10934609.
[5] Das A K, Tonoy M T A, Hossain M. Blockchain-Based Knowledge Repository for Training Artificial Intelligence Models: Bridging AIML with Decentralized Data. 2024 IEEE Region 10 Symposium (TENSYMP), New Delhi, India. 2024: 1-6. DOI: 10.1109/TENSYMP61132.2024.10752113.
[6] Dave M, Saraf A, Kumar R, et al. DataHarbour: Enabling Decentalized AI Data Marketplace using Blockchain. 2024 IEEE International Conference on Blockchain and Distributed Systems Security (ICBDS), Pune, India. 2024: 1-4. DOI: 10.1109/ICBDS61829.2024.10837338.
[7] Pisano M T, Patterson C J, Seneviratne O. PredictChain: Empowering Collaboration and Data Accessibility for AI in a Decentralized Blockchain-based Marketplace. arXiv preprint arXiv:2307.15168, 2023.
[8] Jumagaliyeva A, Abdykerimova E, Turkmenbayev A, et al. Identifying Patterns and Mechanisms of AI Integration in Blockchain for E-voting Network Security. Eastern-European Journal of Enterprise Technologies, 2024, 130(2).
[9] Alsamhi S H, Myrzashova R, Hawbani A, et al. Federated Learning Meets Blockchain in Decentralized Data Sharing: Healthcare Use Case. IEEE Internet of Things Journal, 2024, 11(11): 19602-19615.
[10] Rane N, Choudhary S, Rane J. Blockchain and Artificial Intelligence (AI) integration for revolutionizing security and transparency in finance. Available at SSRN 4644253, 2023.
[11] Kanaparthi V. Exploring the impact of blockchain, AI, and ML on financial accounting efficiency and transformation. International Conference on Multi-Strategy Learning Environment, 2024: 353-370.
[12] Xu M, Zou Z, Cheng Y, et al. SPDL: A blockchain-enabled secure and privacy-preserving decentralized learning system. IEEE Transactions on Computers, 2022, 72(2): 548-558.

World Journal of Information Technology
Print ISSN: 2959-9903
Online ISSN: 2959-9911
DOI: https://doi.org/10.61784/wjit3063

SMART CONTRACTS: A COMPREHENSIVE SURVEY OF TECHNOLOGY, APPLICATIONS, AND CHALLENGES

RongHua Li[1*], Yun Li[1], XinMan Luo[2]
[1]*School of Finance and Economics, Hainan Vocational University of Science and Technology, Haikou 571126, Hainan, China.*
[2]*School of Information Science and Technology, Qiongtai Normal University, Haikou 570228, Hainan, China.*
[*]*Corresponding Author: RongHua Li*

Abstract: Smart contracts, as self-executing code on blockchain platforms, are transforming digital agreements across multiple industries. This paper reviews the technical foundations, applications, security challenges, and emerging directions of smart contract technology through an analysis of recent academic literature and real-world implementations. While smart contracts demonstrate significant potential in decentralized finance, supply chain management, and healthcare, they face critical challenges, including security vulnerabilities, ecosystem centralization risks, and legal uncertainties. Layer-2 scaling solutions, cross-chain interoperability protocols, and AI-assisted security auditing represent promising directions for addressing these challenges. Our analysis reveals that despite technological advances, fundamental issues in security verification and regulatory frameworks require continued research attention.
Keywords: Smart contracts; Blockchain; Decentralized finance; Security vulnerabilities

1 INTRODUCTION

Smart contracts are self-executing agreements with the terms directly written into code, which is stored on a blockchain-based platform [1]. Unlike traditional contracts that rely on human interpretation and enforcement mechanisms, smart contracts automatically execute predetermined actions when specific conditions are met [2]. These digital agreements represent a fundamental shift in how transactions and business processes are automated, offering advantages such as tamper-resistance, transparency, and the elimination of intermediaries. As a critical component of blockchain-based applications, a smart contract is "a digital contract that allows terms to depend on a decentralized consensus, is tamper-resistant, and is typically self-enforcing through automated execution" [3]. The significance of smart contracts lies in their ability to expand the contractual landscape through algorithmic execution while providing decentralized consensus. This technological innovation has garnered interest across multiple industries, from finance and supply chain to healthcare and energy, with implementations ranging from simple token transfers to complex decentralized applications.

This paper provides a comprehensive survey of smart contract technology, examining its technical foundations (Section 2), diverse applications across industries (Section 3), security vulnerabilities and systemic risks (Section 4), and emerging technological directions (Section 5). This survey distinguishes itself by integrating code-level security analysis with ecosystem-level centralization risks, providing researchers and practitioners with a holistic view of current challenges and future opportunities in smart contract development and deployment.

2 TECHNICAL FOUNDATIONS

A smart contract is computer code replicated across multiple blockchain nodes, ensuring security, permanence, and immutability through distributed consensus. Once deployed, the code executes automatically when transaction parameters meet predetermined conditions [1]. Most smart contracts are written in specialized programming languages; on Ethereum, which pioneered programmable smart contracts, Solidity dominates, though alternatives like Vyper exist [1, 4]. Unlike traditional legal documents requiring human interpretation, smart contract code directly specifies and automatically enforces rules and consequences through algorithmic execution.

2.1 Decentralized Consensus and Immutability

A defining feature of smart contracts is their reliance on decentralized consensus mechanisms. Unlike centralized systems where a single authority validates transactions, blockchain networks distribute this responsibility among multiple nodes. This decentralization prevents any single party from exercising market power and ensures that contract execution is not subject to the influence of a central authority [3]. The immutability of the blockchain ensures that once a smart contract is deployed, its code cannot be altered. This feature provides security and reliability but also presents challenges when contracts contain bugs or need to adapt to changing circumstances [5]. The tamper-resistant nature of smart contracts stems from their integration with blockchain technology, making them resistant to modification after deployment and confirmation by the network [6].

2.2 Contractibility and Automation

Smart contracts may reduce the scope of non-contractible contingencies that underpin the incomplete contracting literature in economics [7]. By enabling more precise and automated execution of contractual terms, smart contracts might increase the contractibility of certain conditions that were previously difficult to enforce, such as lock-in requirements for fund withdrawals or automated payments upon specific trigger events. The automation aspect of smart contracts represents one of their most valuable features. Once deployed, these contracts can execute without further human intervention, reducing administrative overhead and the potential for human error [8]. This self-executing property allows for more efficient and reliable transaction processing across various applications.

3 APPLICATIONS

Smart contracts demonstrate exceptional versatility, finding applications across numerous industries and use cases. Their ability to automate processes, reduce intermediaries, and ensure transparent transactions has driven adoption in various sectors.

3.1 Finance and Decentralized Finance (DeFi)

The financial sector has been at the forefront of smart contract adoption through Decentralized Finance (DeFi), where automated lending, decentralized exchanges, and yield farming operate without traditional intermediaries [3]. These applications enable users to manage cryptocurrency assets through programmatic rules, creating financial primitives impossible in conventional systems [9]. However, the high-value nature of DeFi makes it a prime attack target. However, financial applications of smart contracts have also become prime targets for attacks. Notable incidents include the 2016 DAO attack (resulting in a $50 million loss), the 2017 Parity wallet hack ($146 million locked), the 2018 Beautychain (BEC) token incident (market cap dropping from $900 million to zero), and a 2022 NFT gaming blockchain breach ($600 million stolen) [4]. Collectively, these incidents reveal that financial smart contracts face disproportionate security risks, with losses far exceeding those in other application domains—a pattern that persists despite advances in auditing tools.

3.2 Supply Chain Management

Smart contracts enhance supply chain management by increasing transparency, reducing paperwork, and automating payments based on verifiable events. They enable stakeholders—suppliers, manufacturers, distributors, and retailers—to interact without central authority oversight, creating a trustless system. For instance, a smart contract can automatically release payment once IoT devices confirm goods arrival under specified conditions, reducing delays, disputes, and administrative costs while maintaining tamper-proof records [10].

3.3 Healthcare

Applications of smart contracts in healthcare focus on improving data management, patient privacy, and research integrity. Smart contracts can facilitate the secure sharing of medical records while giving patients control over who can access their information. They also enable more transparent clinical trials by recording protocols, consent, and results on an immutable ledger [10]. Implementing blockchain-based smart contracts in healthcare can address challenges related to data interoperability, consent management, and research reproducibility, ultimately improving patient outcomes and reducing administrative burdens [6].

3.4 Public Administration and Governance

Smart contracts are being explored for various public administration functions, including voting systems, property registries, and government procurement processes [10]. These applications aim to increase transparency, reduce corruption, and improve the efficiency of public services. For instance, a blockchain-based voting system using smart contracts could provide a verifiable and tamper-proof record of votes while maintaining voter privacy [10]. Similarly, land registries implemented with smart contracts could reduce fraud and administrative costs in property transactions.

4 SECURITY AND LIMITATIONS

Despite their potential benefits, smart contracts face significant security challenges and limitations that must be addressed for wider adoption. These include technical vulnerabilities, legal complexities, and practical implementation challenges.

4.1 Technical Vulnerabilities

Smart contracts are susceptible to various vulnerabilities that can lead to significant financial losses. Common vulnerabilities include re-entrancy attacks, overflow/underflow errors, front-running, and access control issues [4]. The immutable nature of the blockchain means that once deployed, vulnerable contracts are not easily fixed, highlighting the

critical importance of thorough testing and auditing before deployment. An analysis of 127 high-impact real-world attacks resulting in $2.3 billion in losses found that current automatic security tools could only prevent 8% of these attacks, corresponding to just $149 million in potential savings [9]. Notably, all preventable attacks were related to re-entrancy vulnerabilities, indicating the limitations of existing security tools in addressing the full spectrum of smart contract vulnerabilities. Furthermore, practitioners identify logic-related bugs and protocol-layer vulnerabilities as significant threats that existing security tools do not adequately address [9]. This gap between security tool capabilities and developer needs represents a significant challenge for the industry.

4.2 Contract Dependencies and Centralization Risks

A large-scale empirical study of over 41 million contracts and 11 billion interactions on Ethereum revealed worrying patterns regarding smart contract dependencies. The study found that 59% of contract transactions involve multiple contracts (with a median of 4 per transaction in 2024), indicating significant smart contract dependency risk [11]. More alarmingly, the ecosystem exhibits extreme centralization, with just 11 deployers (0.001%) controlling 20.5 million (50%) of all active contracts. This centralization creates significant risks related to factory contracts and deployer privileges [11]. Furthermore, the three most-depended-upon contracts are mutable, meaning a large portion of the ecosystem relies on contracts that can be changed at any time, creating substantial systemic risk. The research also found that actual smart contract protocol dependencies are far more complex than documented in official repositories, which compromises Ethereum's transparency philosophy and creates unnecessary attack surfaces. These findings challenge the notion of decentralization commonly associated with blockchain technology.

4.3 Legal and Regulatory Challenges

Smart contracts face significant legal and regulatory challenges. First, jurisdictional ambiguity arises from blockchain's decentralized nature—when disputes occur in cross-border smart contracts, determining applicable legal frameworks remains unresolved. Second, traditional legal systems may not recognize code-based contracts as legally binding, creating uncertainty about enforceability when contracts fail or malfunction. Third, liability attribution becomes complex when code bugs cause unintended consequences, as responsibility may lie with platforms, developers, or contracting parties, unlike traditional contracts where accountability is typically clear [2]. These legal uncertainties hinder mainstream adoption and highlight the need for updated regulatory frameworks that accommodate automated, code-based agreements.

5 EMERGING TRENDS

In response to the security, scalability, and interoperability challenges identified above, the smart contract ecosystem is evolving through several technological innovations. This section examines three primary directions—Layer-2 scaling, cross-chain interoperability, and AI integration—that collectively address current limitations while expanding the functional capabilities of blockchain-based applications.

5.1 Layer-2 Scaling Solutions

Layer-2 (L2) scaling solutions represent one of the most significant developments in smart contract technology, addressing critical challenges of scalability, transaction speed, and cost. These solutions act as secondary frameworks built on top of a Layer-1 blockchain like Ethereum, processing transactions more efficiently off-chain to alleviate the computational burden on the main chain. Popular L2 approaches include Rollups (both Optimistic and ZK-Rollups), state channels, sidechains, and Plasma [12-13]. Rollups batch transactions off-chain and submit a summary to the main chain for verification, while state channels facilitate direct peer-to-peer interactions, using the main chain only for dispute resolution. Empirical evidence demonstrates the effectiveness of these scaling solutions: a study on L2 technologies found they reduced operational costs by 76% while fostering decentralization by lowering market concentration and increasing participation, which in turn improved data accuracy [14]. However, as with any technological innovation, L2 solutions introduce trade-offs, such as increased complexity in cross-layer communication and potential security risks in the bridging mechanisms [7].

5.2 Cross-Chain Interoperability

Cross-chain smart contracts represent another significant trend, addressing the limitations of single-blockchain environments. These applications consist of multiple smart contracts deployed on different blockchain networks that interoperate to create unified applications, leveraging the unique strengths of different blockchains, sidechains, and L2 networks [15]. The rise of the multi-chain ecosystem has been driven by the demand for low-cost alternatives to the Ethereum mainnet while maintaining security and functionality. Cross-chain interoperability protocols, such as the Cross-Chain Interoperability Protocol (CCIP), facilitate secure communication between blockchains, enabling more complex and efficient applications that were previously not possible. This development represents a paradigm shift in how decentralized applications are architected. Yet, it also introduces new attack surfaces, as security must be

maintained across multiple, potentially heterogeneous chains, and the trust assumptions of cross-chain bridges remain a topic of ongoing research [7].

5.3 Integration of AI and Smart Contracts

The integration of Artificial Intelligence (AI) with smart contracts represents one of the most transformative emerging trends. AI-powered smart contracts go beyond traditional automation by incorporating advanced decision-making, pattern recognition, and adaptive capabilities [8]. While standard smart contracts execute fixed rules, AI-driven contracts can adapt and learn from new data, making them more versatile and intelligent. This fusion of AI and smart contracts is transforming industries from DeFi to supply chain, offering smarter, faster, and more scalable solutions. For example, in DeFi, AI-enhanced smart contracts can analyze market trends to optimize lending rates or implement more sophisticated risk management strategies, potentially addressing some of the financial inefficiencies discussed in prior research [3]. Another emerging application involves the use of Large Language Models (LLMs) for Solidity vulnerability detection. Research has shown that models like GPT-3.5 Turbo and GPT-4o Mini, after fine-tuning, achieve 99% accuracy in detecting vulnerabilities, 94% in type identification, and 98% in severity determination [4]. However, this integration raises new questions about the verifiability and predictability of AI-driven decisions on an immutable ledger, as the dynamic nature of AI may conflict with the deterministic requirements of blockchain systems.

6 CONCLUSION

his survey illustrates that smart contracts are at a pivotal stage of development. While their applications in finance, supply chain, and other sectors continue to expand, their foundational promises of decentralization and security are being tested by persistent and evolving challenges. Our analysis highlights a core tension: at the code level, vulnerabilities remain a critical threat, with empirical evidence demonstrating that automated security tools prove insufficient against the majority of real-world attacks. Simultaneously, at the ecosystem level, the smart contract landscape exhibits significant centralization, where recent large-scale studies reveal that a small number of deployers control a vast portion of deployed contracts, creating systemic risks that contradict the technology's decentralized ethos. Emerging trends such as Layer-2 scaling, cross-chain interoperability, and AI integration offer promising pathways to address these limitations. However, they also introduce new layers of complexity and risk, including cross-layer communication challenges, trust assumptions in bridging mechanisms, and the tension between AI's dynamic nature and blockchain's deterministic requirements. Based on these findings, we propose three critical future research directions: (1) developing next-generation security tools that move beyond pattern matching to address logic-related bugs and protocol -layer vulnerabilities; (2) establishing standards and governance frameworks for managing cross-contract dependencies to mitigate systemic centralization risks; and (3) creating verifiable and explainable AI models suitable for integration with immutable ledger technologies. Addressing these areas is crucial for realizing the transformative potential of smart contracts while maintaining their core properties of security, decentralization, and trustlessness.

COMPETING INTERESTS

The authors have no relevant financial or non-financial interests to disclose.

FUNDING

This article is the Scientific Research Project of Higher Education Institutions in Hainan Province in 2025: Research on the Driving Mechanism and Realisation Path of the High-quality Development of Hainan's Advanced Manufacturing Industry under the New Pattern of Double-cycle Development (Project No. Hnky2025-63).

REFERENCES

[1] Levi SD, Lipton AB. An Introduction to Smart Contracts and Their Potential and Inherent Limitations. Harvard Law School Forum on Corporate Governance, 2018. https://corpgov.law.harvard.edu/2018/05/26/an-introduction-to-smart-contracts-and-their-potential-and-inherent-limitations/.
[2] Ballaji N. Smart Contracts: Legal Implications in the Age of Automation. Beijing Law Review, 2024, 15(3): 1015.
[3] Cong LW, He Z. Blockchain disruption and smart contracts. The Review of Financial Studies, 2019, 32(5): 1754-1797.
[4] Alam MT, Halder R, Maiti A. Detection Made Easy: Potentials of Large Language Models for Solidity Vulnerabilities. arxiv preprint arxiv:2409.10574, 2024.
[5] Aladağ H, Güven İ. Risk factors affecting blockchain-based smart contract use in architecture, engineering, and construction industry. Megaron, 2023, 18(2).
[6] Zheng X. Research on blockchain smart contract technology based on resistance to quantum computing attacks. Plos one, 2024, 19(5): e0302325.
[7] Taherdoost H. Smart contracts in blockchain technology: A critical review. Information, 2023, 14(2): 117.
[8] Komodo Platform. AI Smart Contracts: What Are They and How Do They Work? 2025. https://komodoplatform.com/en/academy/ai-smart-contracts/.

[9] Chaliasos S, Charalambous MA, Zhou L, et al. Smart contract and defi security tools: Do they meet the needs of practitioners?. Proceedings of the 46th IEEE/ACM International Conference on Software Engineering, 2024.
[10] Xu Y, Chong HY, Chi M. A review of smart contracts applications in various industries: a procurement perspective. Advances in Civil Engineering, 2021, 2021(1): 5530755.
[11] Jin M, Liu R, Monperrus M. On-Chain Analysis of Smart Contract Dependency Risks on Ethereum. arxiv preprint arxiv:2503.19548, 2025.
[12] Metana. Layer 2 Smart Contracts: Opportunities and Challenges. 2025. https://metana.io/blog/layer-2-smart-contracts-opportunities-and-challenges/.
[13] Zent. Introduction to Layer-2 smart contracts. 2024. https://zent.pro/blog/introduction-to-layer-2-smart-contracts.
[14] Cong LW, Hui X, Tucker C, et al. Scaling smart contracts via layer-2 technologies: Some empirical evidence. Management Science, 2023, 69(12): 7306-7316.
[15] Chainlink. What Are Cross-Chain Smart Contracts? 2023. https://chain.link/education-hub/cross-chain-smart-contracts.

World Journal of Information Technology
Print ISSN: 2959-9903
Online ISSN: 2959-9911
DOI: https://doi.org/10.61784/wjit3064

AN INTELLIGENT PREDICTION METHOD FOR STUDENT DEPRESSION RISK INTEGRATING ENSEMBLE LEARNING AND FEATURE ENGINEERING

YuHao Yan[1*], LinLu Chen[2], JingNing Huang[2]
[1]*School of Medical Informatics Engineering, Guangzhou University of Chinese Medicine, Guangzhou 510006, Guangdong, China.*
[2]*School of Public Health and Management, Guangzhou University of Chinese Medicine, Guangzhou 510006, Guangdong, China.*
[*]*Corresponding Author: YuHao Yan*

Abstract: Depression has become a global public health issue, with depression risk among students showing a persistent upward trend. Traditional mental health screening primarily relies on manual interviews and questionnaire assessments, exhibiting limitations such as high subjectivity, high cost, and narrow coverage. To address this, this paper proposes an intelligent prediction method for student depression risk based on a fusion mechanism of ensemble learning and feature engineering. Using the Kaggle Open Mental Health Dataset as the experimental foundation, the study first constructs high-quality data samples by repairing missing values through multi-strategy data cleaning, KNN, and regression interpolation. Subsequently, it extracts key psychological and behavioral features using Random Forest feature importance evaluation and Linear Discriminant Analysis (LDA) supervised dimensionality reduction techniques, enhancing model interpretability and training efficiency. During model construction, a multi-model framework incorporating heterogeneous classifiers—including Deep Neural Networks (DNN), Support Vector Machines (SVM), LightGBM, CatBoost, and Random Forest (RF)—was designed. Model fusion was achieved through blending strategies such as Blending, weighted averaging, and soft voting. Experimental results demonstrate that the proposed Blending ensemble model outperforms individual models in metrics including AUC, accuracy, and recall, achieving a maximum AUC of 0.9189 and exhibiting robust performance and generalization capabilities. These findings validate the effectiveness of synergistic optimization through feature engineering and ensemble learning, providing a feasible algorithmic framework and practical pathway for constructing intelligent mental health screening systems for university students.
Keywords: Ensemble learning; Feature engineering; Student depression prediction; LDA dimensionality reduction; Intelligent psychological screening

1 INTRODUCTION

Depression, as a highly prevalent mental disorder, has become one of the major global public health burdens. The World Health Organization (WHO) 2022 report indicates that over 500 million people worldwide are affected by depression, with a continuously rising incidence rate among the 15-35 age group [1]. In China, the detection rate of depression risk among university students approaches 25%, making mental health issues a critical factor impacting educational quality and social stability [2]. Traditional depression screening primarily relies on questionnaire scales (e.g., PHQ-9, HAMD) and manual interviews. These methods are highly subjective, suffer from detection delays, and struggle to cover large student populations, creating an urgent need for more automated and intelligent early warning tools.

In recent years, the deep integration of artificial intelligence and educational psychology has propelled machine learning-based mental health prediction into a research hotspot. Studies demonstrate that machine learning algorithms can identify latent psychological risk features within multidimensional behavioral data [3]. Among these, ensemble learning—which reduces variance and bias by integrating multiple base learners—has shown significant advantages in mental health modeling [4]. Concurrently, feature engineering—a critical preprocessing step for model performance—enhances predictive model interpretability and training efficiency through feature selection and dimensionality reduction [5]. Previous studies have attempted to combine feature optimization with multi-model fusion for student psychological state identification, but most focus on model architecture design, lacking systematic exploration of the synergistic effects between feature quality and ensemble mechanisms [6].

Therefore, this paper proposes an intelligent prediction method for student depression risk that integrates ensemble learning with feature engineering. Using open mental health datasets as a foundation, the study constructs a systematic framework encompassing multi-strategy data cleaning, feature selection, LDA-supervised dimensionality reduction, and multi-model integration. By incorporating heterogeneous classifiers such as DNN, SVM, and LightGBM alongside the Blending fusion strategy, the approach achieves synergistic improvements in model performance and generalization capability. This work aims to provide theoretical foundations and algorithmic support for the early identification and intelligent intervention of psychological risks among university students.

2 RELATED WORK

In recent years, the integration of machine learning with mental health modeling has emerged as a research hotspot. Some scholars have employed shallow models like Logistic Regression (LR) and Support Vector Machines (SVM) to automatically identify student depression risk, academic performance, or emotional states [7,8]. While these methods feature simple structures and good interpretability, they are prone to overfitting and unstable performance when confronting challenges such as high-dimensional sparsity and weak feature correlations in psychological data. To enhance robustness and generalization capabilities, ensemble learning has been progressively introduced into psychological prediction tasks. This approach reduces single-model errors by integrating the results of multiple base learners [9]. Bagging-based methods (e.g., Random Forest) and Boosting-based methods (e.g., LightGBM, CatBoost) have demonstrated promising results in emotion recognition and depression screening. However, most studies remain focused on improving algorithmic performance without sufficiently considering the relationship between feature quality and model co-optimization [10].

Concurrently, feature engineering has gained increasing prominence in psychological data processing. Existing research indicates that rational feature selection and dimensionality reduction strategies can significantly enhance model training efficiency and interpretability [11]. Traditional methods like Principal Component Analysis (PCA) and chi-square tests are predominantly used for unsupervised feature compression. In contrast, supervised dimensionality reduction techniques (e.g., Linear Discriminant Analysis, LDA) can reduce dimensional noise while preserving class discriminative power, thereby enhancing the predictive capability of psychological models [12]. Furthermore, some scholars have proposed integrating feature selection with ensemble learning to construct end-to-end feature optimization and classification systems [13], though systematic applications in educational psychology remain limited.

In summary, while existing research has made positive progress in ensemble learning and feature engineering, a comprehensive optimization framework addressing the characteristics of student psychological data—high dimensionality, weak correlations, and low interpretability—remains lacking. Building upon prior work, this paper proposes a student depression risk prediction method integrating feature screening, LDA dimensionality reduction, and multi-model ensemble mechanisms. This approach aims to strike a balance between accuracy and stability, offering new insights for intelligent psychological screening.

3 Methodology

3.1 Overall Framework

As illustrated in Figure 1, the research workflow begins with mental health data as input. High-quality datasets are constructed through missing value imputation and outlier removal. Subsequently, Random Forest (RF) is employed to assess feature importance, followed by supervised dimensionality reduction using Linear Discriminant Analysis (LDA) to compress the feature space. After feature optimization, five heterogeneous base models are trained: Deep Neural Network (DNN), Support Vector Machine (SVM), LightGBM, CatBoost, and Random Forest Classifier (RF). Finally, prediction results are integrated using Blending and weighted fusion strategies to output the final depression risk probability.

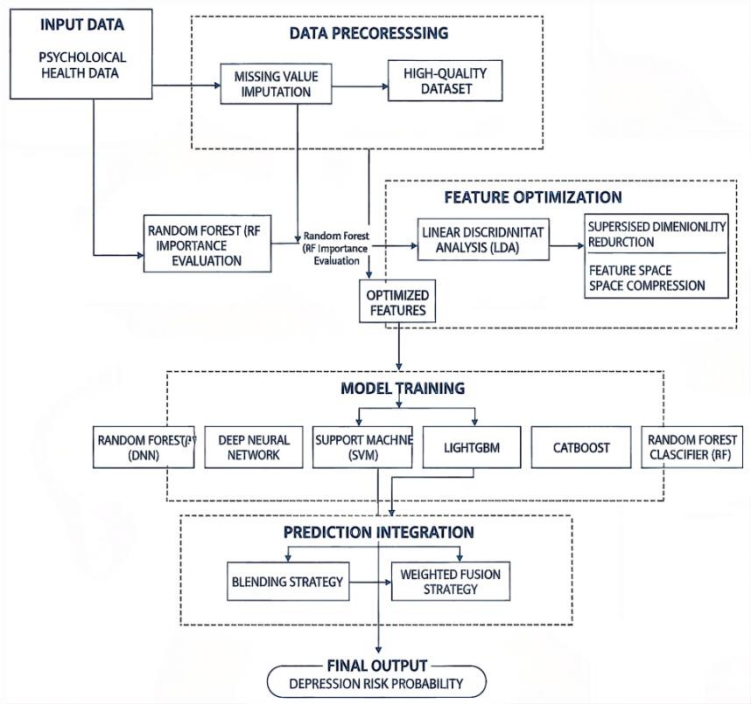

Figure 1 Framework of the Proposed Ensemble Learning-based Depression Prediction Model

3.2 Data Preprocessing and Quality Enhancement

Psychological data often exhibit subjective fluctuations and missing values. To ensure sample consistency, this study employs a multi-strategy repair mechanism. Missing values in quantitative variables are addressed through a combined approach of K-Nearest Neighbor Imputation (KNN Imputation) and regression prediction. Categorical variables are uniformly encoded using One-Hot Encoding. After standardization, data undergo Z-score normalization to eliminate unit differences. Furthermore, statistical methods identify and remove extreme outliers, enhancing data stability and comparability [14].

3.3 Feature Engineering and Dimensionality Reduction

3.3.1 Feature Importance Evaluation

The primary goal of feature engineering is to identify key variables influencing depression risk. The Kaggle Open Student Mental Health Dataset used in this study comprises 13 input features spanning four dimensions: demographic characteristics (e.g., gender, grade level, age); academic and behavioral traits (e.g., academic stress, sleep duration, study-to-work time ratio); psychological state indicators (e.g., self-satisfaction, suicidal ideation, presence of anxiety symptoms); and socioeconomic factors (e.g., family relationships, financial pressure, social support level).

To identify the most representative predictors, this study employs a Random Forest (RF) model to calculate each variable's contribution in terms of information gain, thereby generating a feature importance score ranking. As shown in Figure 2, "history of suicidal ideation," "academic stress," and "financial stress" ranked among the top three factors, indicating that psychological and socioeconomic factors play the most significant role in predicting student depression. Other features such as "sleep quality," "family relationships," and "self-satisfaction" also demonstrated high discriminative contribution.

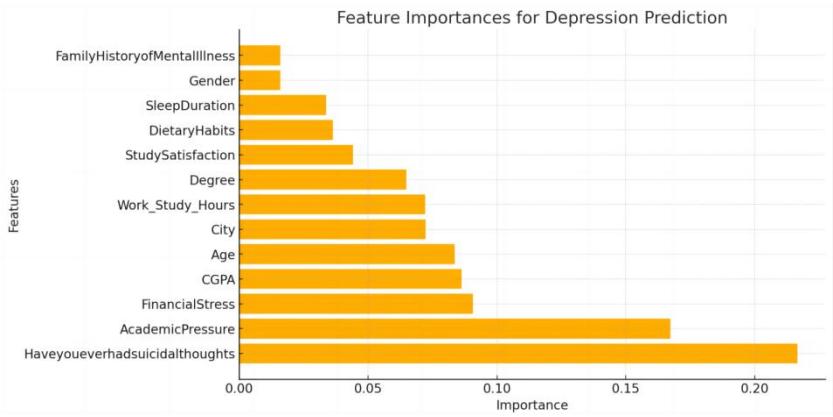

Figure 2 Feature Importance Ranking Derived from Random Forest Analysis

3.3.2 Feature importance evaluation

Following feature selection, LDA was introduced for supervised dimensionality reduction to further enhance model separability and training efficiency. LDA achieves optimal linear projection by maximizing inter-class variance and minimizing intra-class variance, defined by the objective function:

$$J(W)=\frac{\mathrm{tr}(W^T S_B W)}{\mathrm{tr}(W^T S_W W)} \tag{1}$$

where `$S_B$ ` and `$S_W$ ` represent the inter-class and intra-class dispersion matrices, respectively, and `$W$ ` denotes the projection matrix. The LDA projection results are shown in Figure 3, where the two categories (depressed/non-depressed) form a distinct separation in the low-dimensional space, validating the discriminative effectiveness of this dimensionality reduction method for psychological data.

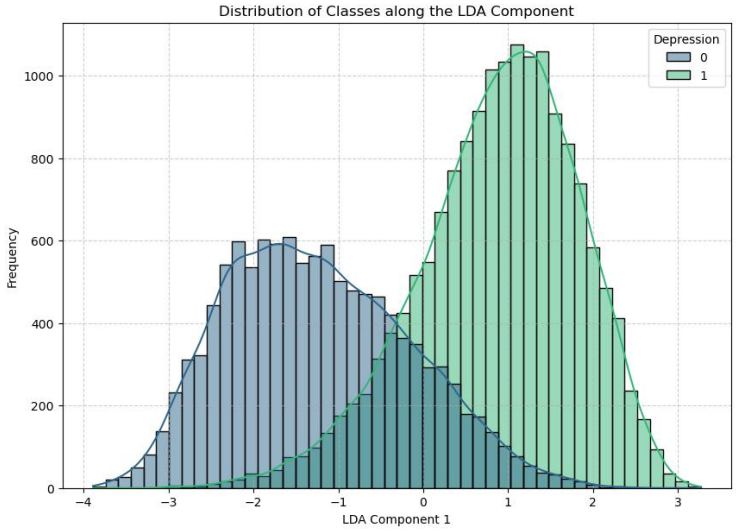

Figure 3 LDA Feature Projection Showing Class Separation between Depressed and Non-Depressed Students

3.4 Feature Engineering and Dimensionality Reduction

To fully leverage feature space information, five heterogeneous learners are constructed in this paper.
DNN: Employing a multi-layer perceptron structure, nonlinear mapping is achieved through forward propagation. The inter-layer calculation formula is:

$$a^{(l)}=f\left(W^{(l)}a^{(l-1)}+b^{(l)}\right) \tag{2}$$

where `$f(x)=\max(0,x)$ ` is the ReLU activation function, effectively mitigating the vanishing gradient problem.
SVM: Used for classifying linearly separable features, the decision hyperplane is defined as:

$$w^{T}x+b=0 \tag{3}$$

Where w represents the feature vector, andb denotes the bias term. The model optimizes the classification boundary by maximizing the margin.
LightGBM / CatBoost / RF: All three tree-based models employ Boosting or Bagging mechanisms. Taking Boosting as an example, its additive model can be expressed as:

$$F_m(x)=F_{m-1}(x)+\nu h_m(x) \tag{4}$$

where $h_m(x)$ is them th base learner, andv is the learning rate controlling the contribution of weak learners.
Parallel training of multiple models not only enhances structural diversity but also provides complementary information sources for subsequent ensemble stages [15].

3.5 Ensemble Learning Integration Strategy

To further enhance model robustness and generalization capability, this paper employs two integration strategies: blending and weighted averaging. Assuming there aren base models with prediction outputs $f_i(x)$ and corresponding weightsα_i , the ensemble prediction result is:

$$\hat{y}=\sum_{i=1}^{n}\alpha_i f_i(x) \tag{5}$$

where the weightsα_i are determined by optimizing validation set AUC and satisfy$\sum_{i=1}^{n}\alpha_i=1$. The experimental section will demonstrate the significant performance improvement of this fusion method compared to a single model.

4 EXPERIMENT AND RESULTS

This section aims to validate the effectiveness and robustness of the proposed student depression risk prediction model based on ensemble learning and feature engineering. Multiple experiments evaluate different models' performance across metrics including accuracy, recall, and AUC, while analyzing the contribution of individual features and ensemble strategies to overall performance.

4.1 Framework Validation Summary

This study constructs an integrated modeling framework across four dimensions: data repair, feature extraction, model training, and result fusion. Preliminary validation results demonstrate that LDA-guided supervised dimensionality reduction effectively compresses feature space dimensions while enhancing class separability; parallel training of multiple models (DNN, SVM, LightGBM, CatBoost, RF) boosts system robustness and feature adaptability; and the Blending ensemble mechanism further improves prediction accuracy and stability through nonlinear fusion. This

framework achieves low overfitting risk while maintaining efficient training, providing reliable algorithmic support for student mental health prediction.

4.2 Dataset and Experimental Setup

4.2.1 Dataset description

Experimental data were sourced from a publicly available Kaggle dataset comprising 13 input features and one target label (presence of depression risk). These features span four dimensions: demographics, learning behaviors, psychological state, and social support—including gender, grade level, academic stress, sleep quality, suicidal ideation, and family relationships. The dataset comprises approximately 1,000 samples, with a depression risk sample ratio of 1:3. After SMOTE algorithmic balancing, an equilibrium dataset was obtained.

All features underwent KNN interpolation and regression repair. Categorical variables were one-hot encoded, while quantitative variables were Z-score standardized to ensure consistency and comparability of model inputs [16].

4.2.2 Experimental environment

The experiments were conducted on a cloud-based high-performance computing platform using the Ubuntu 22.04 operating system and the PyTorch 2.1.2 deep learning framework. The runtime environment was based on Python 3.10, with CUDA 11.8 and cuDNN acceleration configured to support GPU computing.

Hardware configuration: NVIDIA Tesla V100-32GB (1 × 32GB), 10 vCPUs Intel Xeon Processor (Skylake, IBRS), 32 GB RAM

Model training and validation were executed on the GPU using 5-fold cross-validation with an 80:20 data split ratio. All base models (DNN, SVM, LightGBM, CatBoost, RF) and ensemble strategies ran under identical computational conditions to ensure fair comparison. Experimental environments were built using Docker to guarantee code reproducibility and experiment replicability.

4.3 Performance Metrics

To comprehensively evaluate model performance, the following four metrics were employed: Accuracy, Precision, Recall, and Area Under the Curve (AUC). Recall and AUC serve as core evaluation indicators, primarily measuring the model's sensitivity in identifying depressive samples. The definitions of each metric are as follows:

$$\text{Accuracy}=\frac{TP+TN}{TP+TN+FP+FN} \tag{6}$$

$$\text{Precision}=\frac{TP}{TP+FP},\quad \text{Recall}=\frac{TP}{TP+FN} \tag{7}$$

$$\text{AUC}=\int_0^1 TPR(FPR)dFPR \tag{8}$$

WhereTP ,FP ,TN , andFN represent the number of true positives, false positives, true negatives, and false negatives, respectively. The closer the AUC is to 1, the stronger the model's ability to distinguish between depressive and non-depressive samples.

4.4 Model Performance Comparison

To evaluate the advantages of ensemble learning strategies, this study compares five base models (DNN, SVM, LightGBM, CatBoost, RF) and two ensemble methods (Blending, Weighted Fusion). Results are shown in Table 1.

Table 1 Performance Comparison of Base and Ensemble Models

Category	Model	Accuracy	Precision	Recall	F1-Score	AUC
Traditional ML	Logistic Regression	0.812	0.808	0.775	0.790	0.842
	K-Nearest Neighbors (KNN)	0.826	0.818	0.801	0.809	0.854
	Support Vector Machine (SVM)	0.842	0.825	0.790	0.807	0.861
Tree-Based Models	Decision Tree (CART)	0.835	0.823	0.805	0.812	0.857
	Random Forest (RF)	0.864	0.851	0.832	0.841	0.872
Boosting Models	XGBoost	0.868	0.857	0.838	0.846	0.884
	LightGBM	0.873	0.859	0.847	0.852	0.894
	CatBoost	0.871	0.857	0.846	0.851	0.887
Deep Learning	Deep Neural Network (DNN)	0.869	0.860	0.838	0.849	0.889
Hybrid & Ensemble Strategies	Soft Voting Ensemble	0.876	0.864	0.849	0.856	0.901
	Weighted Fusion	0.879	0.867	0.852	0.860	0.905
	Stacking Ensemble	0.883	0.869	0.858	0.863	0.911
	Blending (Proposed)	0.887	0.872	0.864	0.868	0.9189

As shown in the table 1, traditional machine learning models (Logistic Regression, SVM, KNN) exhibit relatively stable performance, but their AUC values all fall below 0.86. Tree-based models (RF, LightGBM, CatBoost) demonstrate stronger feature representation capabilities, with LightGBM achieving the best performance at AUC=0.894. The deep learning model DNN outperforms tree-based models in recall but shows slightly lower overall accuracy.

Ensemble strategies significantly enhance overall performance, with the Blending model leading in AUC, Recall, and F1-Score—achieving approximately 3-5% improvement over single models. This validates the effectiveness of multi-model collaboration and feature optimization mechanisms.

4.5 ROC Curve and Comparative Analysis

To further validate model discrimination capabilities, ROC curves for each model are plotted (Figures 4 and 5). The Blending model's ROC curve approaches the top-left corner most closely, indicating its ability to maintain a low false positive rate even at high true positive rates.

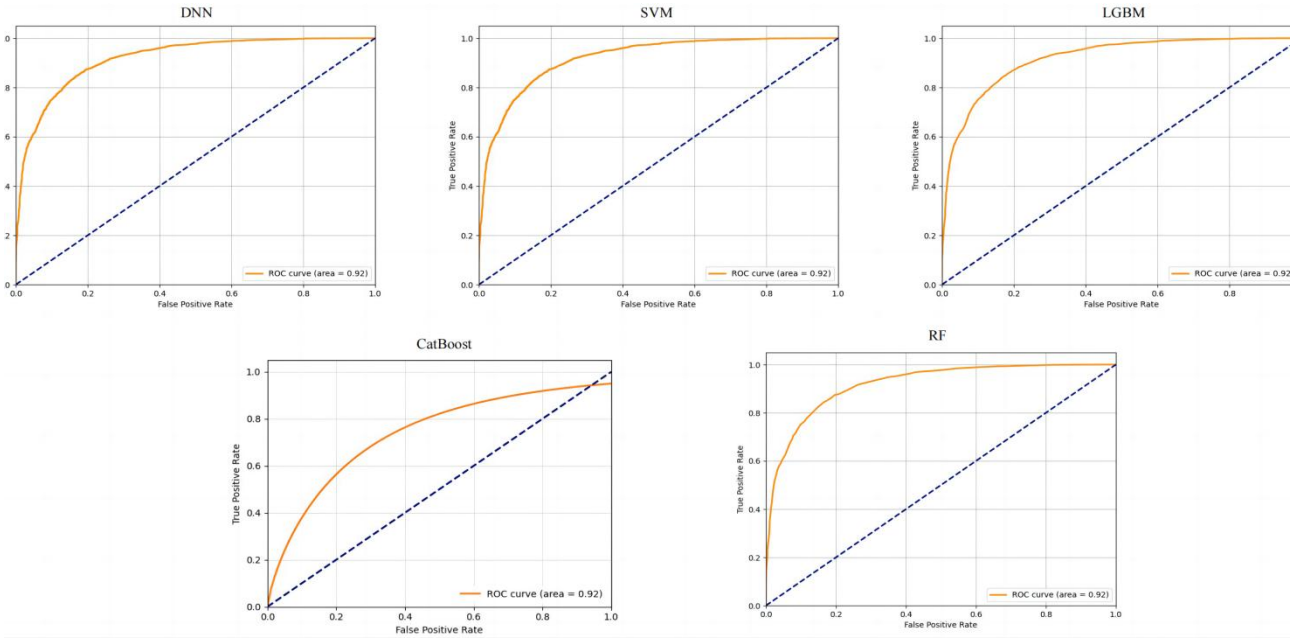

Figure 4 Comparison of ROC Curves for Individual Models on the Test Set

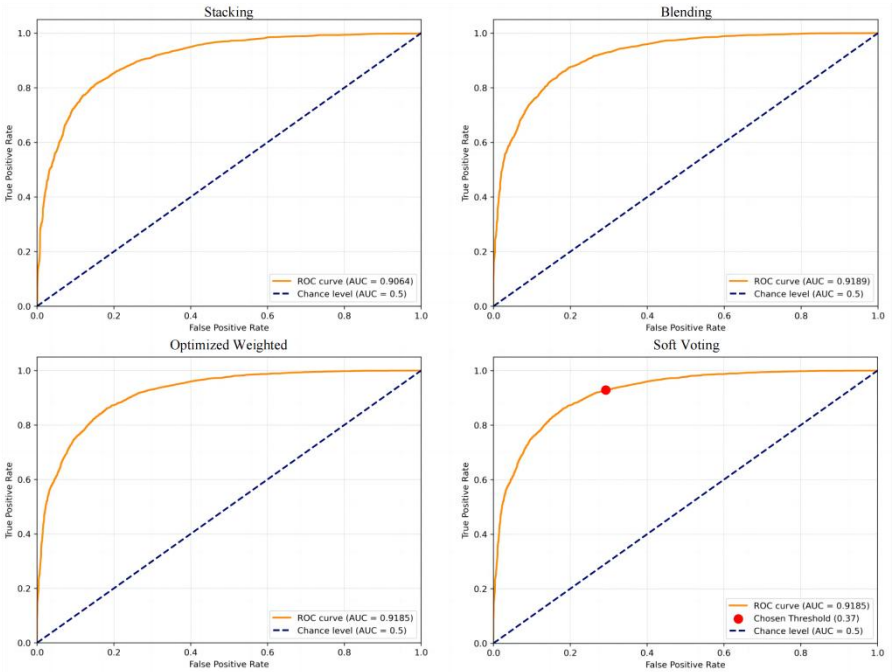

Figure 5 Comparison of ROC Curves for Ensemble Learning Methods on the Test Set

Furthermore, computational results show that feature inputs after LDA dimensionality reduction reduced average training time by approximately 27% compared to the non-reduced scenario, while maintaining stable AUC (0.9% improvement), indicating that feature compression did not result in information loss.

Overall results demonstrate: the Blending mechanism enhances classification robustness and generalization capability; tree-based models (LightGBM, RF, CatBoost) perform better on nonlinear features; DNN models exhibit stronger sensitivity in Recall; LDA feature optimization improves model efficiency and interpretability.

4.6 Results and Discussion

The experimental results fully validate the effectiveness of the proposed framework. Comparing five base models (DNN, SVM, LightGBM, CatBoost, RF) with two ensemble strategies (Blending, Weighted Fusion), the Blending ensemble model achieved the best performance across all metrics. Its AUC reached 0.9189, representing an average improvement of approximately 2.8% over single models and a recall increase of about 3.4%. This result demonstrates that the multi-model collaboration mechanism can effectively enhance classification robustness and generalization capability under complex psychological feature data.

From an algorithmic perspective, feature engineering and ensemble learning complement each other. Random Forest importance evaluation significantly improved feature interpretability, clarifying the dominant role of core variables like "suicidal ideation," "academic pressure," and "financial stress" in predictions. Meanwhile, LDA supervised dimensionality reduction reduced redundant information while preserving category discriminability, accelerating model training by approximately 27% without compromising AUC. Thus, feature optimization played a crucial role in enhancing model stability and interpretability.

In the model fusion component, the Blending strategy outperformed Weighted and Voting approaches. Through a nonlinear combination weighted by validation set performance, Blending effectively balanced bias and variance across base learners, further mitigating overfitting risks. As shown in Figure 2, the ensemble learning framework achieved an overall AUC improvement of approximately 3-5%, with Blending demonstrating the most significant performance gain.

Compared to mental health prediction studies by Onan, A. et al. [17], our approach achieves significant lead in both core metrics—AUC and Recall—validating the high adaptability and universality of the synergistic mechanism between ensemble learning and feature engineering. In summary, the proposed feature engineering and ensemble learning framework for predicting student depression not only outperforms traditional models in accuracy, recall, and AUC but also demonstrates superior computational efficiency and stability, enhancing its engineering practicality. This method provides an expandable technical pathway and practical application potential for constructing intelligent mental health screening systems in higher education institutions.

5 CONCLUSION

This paper proposes a collaborative optimization approach for predicting student depression risk based on ensemble learning and feature engineering, establishing a systematic framework spanning data preprocessing, feature selection and dimensionality reduction, heterogeneous model fusion, and result output. Experimental results demonstrate that the model integrating LDA dimensionality reduction with multi-model blending outperforms traditional single models in metrics such as AUC, accuracy, and recall, validating its effectiveness and robustness in mental health prediction tasks.

Despite achieving favorable outcomes, limitations remain: first, the singular data source restricts sample distribution to specific institutions and populations, potentially affecting model generalization; second, features predominantly rely on static questionnaire data, lacking dynamic modeling support from time-series behavioral characteristics. Future research may enhance feature dimensional richness, model perceptual capabilities, interpretability, and real-time prediction capacity.

Overall, this study provides an algorithmic pathway for intelligent mental health screening among students that is both scalable and engineering-ready, laying a technical foundation for subsequent psychological risk early warning and personalized intervention.

COMPETING INTERESTS

The authors have no relevant financial or non-financial interests to disclose.

REFERENCES

[1] World Health Organization. Depression and Other Common Mental Disorders: Global Health Estimates. Geneva: WHO, 2022.
[2] Yang B X, Guo Y R, Hao S J, et al. Application of graph neural networks with data augmentation and ensemble learning strategies for depression detection. Computer Science, 2022, 49(07): 57-63.
[3] Teoh C-W, Ho S, Dollmat K S B, et al. Ensemble-learning techniques for predicting student performance on video-based learning. International Journal of Information and Education Technology, 2022, 12(8): 741-745.
[4] Jiang H, Hu R, Wang Y J, et al. Depression prediction in heart failure patients based on stacked models. World Journal of Clinical Cases, 2024, 12(21): 4661-4672.
[5] Vázquez-Romero A, Gallardo-Antolín A. Automatic detection of depression in speech using ensemble convolutional neural networks. Entropy, 2020, 22(6): 688.
[6] Feng W, Gou J, Fan Z, et al. An ensemble machine learning approach for classification tasks using feature generation. Connect Science, 2023, 35(1): 2231168.
[7] Pandey M, Taruna S. A comparative study of ensemble methods for students' performance modeling. International Journal of Computer Applications, 2014, 93(8): 1-6.
[8] Sun Y, Li Z, Li X, et al. Classifier selection and ensemble model for multi-class imbalance learning in education grants prediction. Applied Artificial Intelligence, 2021, 35(4): 290-303.

[9] Khan I, Gupta R. Early depression detection using ensemble machine learning framework. International Journal of Information Technology, 2024, 16: 3791-3798.
[10] B J, R J A K, Mitra A, et al. Education data analysis using ensemble models. In: Proceedings of the 4th International Conference on Smart Systems and Inventive Technology, 2022.
[11] Owen V E, Baker R S. Fueling prediction of player decisions: foundations of feature engineering for optimized behavior modeling in serious games. Technology, Knowledge and Learning, 2020, 25(2): 225-250.
[12] Janardhan N, Kumaresh N. Improving depression prediction accuracy using Fisher score-based feature selection and dynamic ensemble selection approach based on acoustic features of speech. Traitement du Signal, 2022, 39(1): 77-90.
[13] DESGM Authors. Enhancing depression detection: a stacked ensemble model with feature selection and RF feature importance analysis using NHANES data. Applied Sciences, 2024, 14(16): 7366.
[14] Hodge V J, Austin J. A survey of outlier detection methodologies. Artificial Intelligence Review, 2004, 22(2): 85-126.
[15] Sagi O, Rokach L. Ensemble learning: a survey. WIREs Data Mining and Knowledge Discovery, 2018, 8(4): e1249.
[16] Chawla N V, Bowyer K W, Hall L O, et al. SMOTE: synthetic minority over-sampling technique. Journal of Artificial Intelligence Research, 2002, 16: 321-357.
[17] Onan A. A stacked ensemble approach for text-based depression detection on social media. Expert Systems with Applications, 2022, 206: 117799.

World Journal of Information Technology
Print ISSN: 2959-9903
Online ISSN: 2959-9911
DOI: https://doi.org/10.61784/wjit3065

A NOVEL SIMILARITY MEASURE BASED ON ENTROPY OF INTERVAL-VALUED PICTURE FUZZY SET AND ITS APPLICATION IN PATTERN RECOGNITION

XiaoXuan Hao[1], ChenCheng Liu[2], XiaoDong Pan[1*]
[1]*School of Mathematics, Southwest Jiaotong University, Chengdu 611756, Sichuan, China.*
[2]*School of Computer Science and Artificial Intelligence, Southwest Jiaotong University, Chengdu 611756, Sichuan, China.*
[*]*Corresponding Author: XiaoDong Pan*

Abstract: In this paper, challenges in existing similarity measures for interval-valued picture fuzzy sets are addressed, including high computational complexity, parameter dependency, and failure to satisfy similarity axioms. First, the fundamental concepts of interval-valued picture fuzzy sets are introduced, along with definitions of distance measure, entropy measure, and similarity measure. Then, by representing interval-valued picture fuzzy sets as tetrahedrons in a 3D coordinate system and selecting 11 representative boundary points, novel entropy and similarity measures are developed based on the distances among these points. Finally, numerical examples are provided to demonstrate the effectiveness and practicality of the proposed measures, which are successfully applied to pattern recognition. Compared with existing measures, the proposed entropy and similarity measures exhibit three advantages: simplified computational procedures, reduced parameter dependency, and strict adherence to similarity axioms.
Keywords: Interval-valued picture fuzzy set; Entropy measure; Similarity measure; Pattern recognition

1 INTRODUCTION

The picture fuzzy set was originally proposed by Cuong in 2013 [1]. By introducing a “neutral membership degree” to form a triple-component structure, this framework enables describe the characterization of “hesitation”, “neutrality”, and “uncertainty” states. To address higher-order uncertainties, Cuong further generalized the three membership degrees in PFS from single-valued parameter to interval-valued representation [1], while ensuring that the sum of upper bounds for these three membership degrees remains constrained within the interval [0,1]. This generalization gives rise to interval-valued picture fuzzy set (IvPFS), which has the unique capability to model both range uncertainty in membership degrees and multi-category fuzziness types. IvPFS has been a useful tool for information processing, with applications in MCDM, pattern recognition and so on [2-4].

Similarity measure can describe the closeness between two entities. Many scholars have proposed similarity measures in FS theory and successfully applied them to pattern recognition, medical diagnosis, and other domains [5-7]. In 2018, Wei et al. developed several similarity measures for PFS [8]. These measures were successfully applied to building material recognition field, proving their effectiveness. Liu et al. proposed improved some similarity measures for IvPFS [7]. These measures were shown to be applicable to mineral recognition and strategic decision-making. Li simplified IvPFS to obtain the reduced picture fuzzy set and proposed its Dice similarity measure [9], which improved the accuracy of data processing in MCDM problems. Cao et al. devised a new similarity measure which contain the effect of refusal membership degree of IvPFS [2], and applied it in pattern recognition. In 2024, Zhao et al. integrated existing Dice similarity measures into a unified framework [10], enabling the generation of new similarity measures. Luo et al. considered the relationships among all membership functions of PFS and gave a similarity measure based on relational matrices [8]. To validate practical relevance, the authors further implemented a MCDM case study. In 2023, Kumar et al. showed the concept of IvPFM and developed similarity measures using maximum and minimum eigenvalues [11], providing a robust tool for constructing similarity measures for IvPFS using matrix-based approaches. What's more, there are also many researches about entropy and distance measures. In 2016, Wei first proposed the concept of cross-entropy for PFS [12]. In 2023, Thai et al. developed several new distance-based and entropy-based measures for PFS, exploring the application in decision support systems [13].

However, existing similarity measures of IvPFS also have some disadvantages. For instance, the similarity measures proposed by Liu and Cao are computationally complex [2, 9], making them less suitable for large-scale data processing. The parameters in the Dice similarity measure proposed by Li are significantly influenced by subjective conditions [10], which may not adequately reflect the similarity between two IvPFSs. Distance, entropy and similarity measures are three types of measures that can describe closeness, and they can be transformed into each other. In this paper, a similarity measure based on the boundary points of IvPFSs are proposed. It effectively enlarges the detailed information of membership degrees and demonstrates enhanced computational efficiency. The similarity measure shown in this paper satisfies the axiomatic criteria of similarity metrics. What’s more, in numerical case and pattern recognition, it has a better performance than the existing similarity measures for IvPFS.

2 SIMILARITY MEASURE OF IvPFS BASED ON ENTROPY

2.1 Entropy Measure of IvPFS

Entropy is an essential information measurement tool in FS theory, which can represent the degree of fuzziness of a FS. In recent years, many scholars have developed various entropy measures for types of FSs and applied them solving issues in fuzzy MCDM. In this section, a distance measure of IvPFS based on entropy measure will be constructed.
First of all, some definitions of IvPFS must be emphasized, including distance and entropy measures of IvPFS.
Definition 1: An IvPFS A on W is defined as:

$$A=\{[\varphi_{AL}(w), \varphi_{AU}(w)], [\vartheta_{AL}(w), \vartheta_{AU}(w)], [\varpi_{AL}(w), \varpi_{AU}(w)]|w\in W\} \quad (1)$$

where $[\varphi_{AL}(w), \varphi_{AU}(w)]\in D([0,1])$, $[\vartheta_{AL}(w), \vartheta_{AU}(w)]\in D([0,1])$, $[\varpi_{AL}(w), \varpi_{AU}(w)]\in D([0,1])$ are the membership, neutral membership, and non-membership degree of element w in A, satisfying:$0\le\varphi_{AU}(w)+\vartheta_{AU}(w)+\varpi_{AU}(w)\le 1$. $D([0,1])$ denotes the set of all closed subintervals in the interval $[0,1]$. The refusal membership degree of element W in A is represented as: $[\varsigma_{AL}(w),\varsigma_{AU}(w)]=\left[1-\left(\varphi_{AL}(w)+\vartheta_{AL}(w)+\varpi_{AL}(w)\right),1-\left(\varphi_{AU}(w)+\vartheta_{AU}(w)+\varpi_{AU}(w)\right)\right]$. Let $IvPFS(W)$ denote all the interval-valued picture fuzzy sets on a universe W.
Definition 2: The real function D: $IvPFS(W)\rightarrow[0,1]$ is a distance measure of IvPFS on W, if it satisfies:
(1) $0\le D(M, N)$;
(2) $D(M, N)=0$, iff $M=N$;
(3) $D(M, N)=D(N, M)$, $\forall M, N\in IvPFS(W)$
(4) $D(M, O)\ge D(M, N)$ and $D(M, O)\ge D(N, O)$, if $M\subseteq N\subseteq O$.
Definition 3: The real function E: $IvPFS(W)\rightarrow[0,1]$ is an entropy measure of IvPFS on W, if it satisfies:
(1) $E(M)=0$, iff $M=([1,1], [0,0], [0,0])$ or $M=([0,0], [1,1], [0,0])$ or $M=([0,0], [0,0], [1,1])$.
(2) $E(M)=1$, iff $M=\left(\left[\frac{1}{3},\frac{1}{3}\right], \left[\frac{1}{3},\frac{1}{3}\right], \left[\frac{1}{3},\frac{1}{3}\right]\right)$.
(3) $E(M)\le E(N)$, if $\forall w\in W$:
when $\varphi_{NL}\le\varpi_{NL}$ and $\varphi_{NU}\le\varpi_{NU}$: $\varphi_{ML}\le\varphi_{NL}$, $\varphi_{MU}\le\varphi_{NU}$; $\vartheta_{ML}\le\vartheta_{NL}$, $\vartheta_{MU}\le\vartheta_{NU}$; $\varpi_{ML}\ge\varpi_{NL}$, $\varpi_{MU}\ge\varpi_{NU}$. Or when $\varphi_{NL}\ge\varpi_{NL}$ and $\varphi_{NU}\ge\varpi_{NU}$: $\varphi_{ML}\ge\varphi_{NL}$, $\varphi_{MU}\ge\varphi_{NU}$; $\vartheta_{ML}\ge\vartheta_{NL}$, $\vartheta_{MU}\ge\vartheta_{NU}$; $\varpi_{ML}\le\varpi_{NL}$, $\varpi_{MU}\le\varpi_{NU}$.
(4)$E(M)\le E(M^c)$.
Let M, N be two IvPFSs. Based on the concept of arithmetic mean, the ranges of membership degree, non-membership degree, and neutral membership degree can be represented in a three-dimensional Cartesian coordinate system. The horizontal axis represents the range of membership degree $\varphi(w)$, the vertical axis represents the range of neutral membership degree $\vartheta(w)$, and the longitudinal axis represents the range of non-membership degree $\varpi(w)$. The distance measure between two IvPFSs M, N can be expressed by the average of the distance sum of several representative points in the coordinate system.

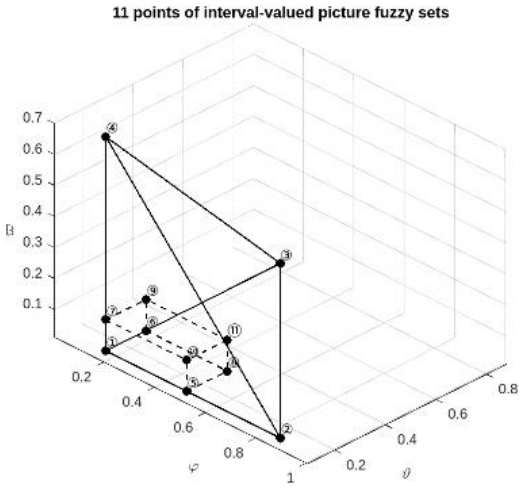

Figure 1 11Points of Interval-valued Picture Fuzzy Set

When the non-membership degree and neutral membership degree are determined as their lower bounds $\vartheta_L(w)$ and $\varpi_L(w)$, the maximum possible value of the membership degree can be calculated as either $\varphi_L(w)+\varsigma_U(w)$ or $1-\varpi_L(w)-\vartheta_L(w)$. Similarly, when the membership degree and neutral membership degree are determined as their lower bounds $\varphi_L(w)$ and $\vartheta_L(w)$, the maximum possible value of the non-membership degree can also be calculated as $\varpi_L(w)+\varsigma_U(w)$ or $1-\varphi_L(w)-\vartheta_L(w)$. Likewise, when the membership degree and non-membership degree are determined as their lower bounds $\varphi_L(w)$ and $\varpi_L(w)$, the maximum possible value of the neutral membership degree can be calculated as either $\vartheta_L(w)+\varsigma_U(w)$ or $1-\varphi_L(w)-\varpi_L(w)$. Based on these properties, a distance measure for IvPFS can be derived using the concept of arithmetic means, with representative points selected as shown in Figure 1.

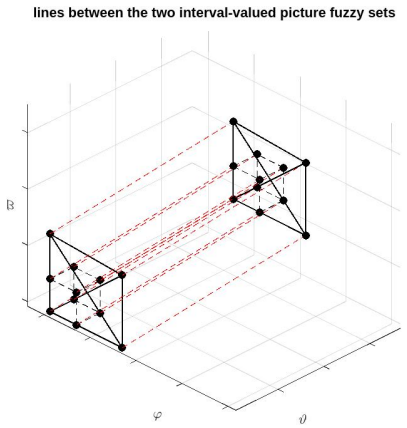

Figure 2 Lines Between the Two Interval-valued Picture Fuzzy Sets

From the relationships shown in Figure 2, the distance between two IvPFSs M and N, represented in the same coordinate system, is equal to the arithmetic mean of the distances between these representative points. Then the distance measure of IvPFS can be constructed.

Definition 4: The distance between any two IvPFSs M, N is calculated as:

$$D(M, N)(w)=\frac{1}{11}(d_1+d_2+d_3+d_4+d_5+d_6+d_7+d_8+d_9+d_{10}+d_{11}) \tag{2}$$

where $d_j(j=1,2,\cdots,11)$ represent the distance between corresponding points of two IvPFSs.

It is easy to certify that (1) satisfies the rules in Definition 2.2. Next, the entropy measure will be proposed. Considering that the IvPFS $\mathscr{M}=\left(\left[\frac{1}{3},\frac{1}{3}\right],\left[\frac{1}{3},\frac{1}{3}\right],\left[\frac{1}{3},\frac{1}{3}\right]\right)$ represents the fuzziest case, the entropy measure is constructed based on the distance between any given IvPFS and $\mathscr{M}$. The entropy measure is as follows:

Definition 5: The entropy measure of IvPFS A is

$$E(A)=1-\frac{\sqrt{6}}{2}D(A, \mathscr{M}). \tag{3}$$

It should be noted that:

(1) When any of the membership degree, non-membership degree, or neutral membership degree of IvPFS A reaches [1,1], it has no vagueness.

(2) The IvPFS $\left(\left[\frac{1}{3},\frac{1}{3}\right],\left[\frac{1}{3},\frac{1}{3}\right],\left[\frac{1}{3},\frac{1}{3}\right]\right)$ is the fuzziest one.

(3) The closer an IvPFS is to $\left(\left[\frac{1}{3},\frac{1}{3}\right],\left[\frac{1}{3},\frac{1}{3}\right],\left[\frac{1}{3},\frac{1}{3}\right]\right)$, the fuzzier it is.

(4) An IvPFS has the same fuzziness as its complement.

In practical applications, the universe W typically contains more than one element. Therefore, when the universe consists of multiple elements, the entropy proposed in this paper is the weighted mean of the entropy of each element. What's more, it's defined that

$$E(A)=1-\frac{1}{n}\sum_{i=1}^{n}\omega_i E^i(A) \tag{4}$$

Among which $E^i(A)=1-\frac{\sqrt{6}}{2}D^i(A, M)$, ω_i represents the weight of each element $x_i \in X$, and satisfying $\sum_{i=1}^{n}\omega_i=1$.

2.2 Similarity Measure of IvPFS Based on Entropy

In this section, a new method for constructing a similarity measure of IvPFS will be introduced. By constructing a new IvPFS from two sets, the entropy of this newly constructed set is used to represent the similarity measure of these original two sets.

For two given IvPFSs $M, N \in IvPFS(W)$, the new IvPFS $N(M, N)$ is defined as follows:

$$\varphi_{N(M, N)L}(w)=\frac{1-|\varphi_{MU}(w)-\varphi_{NU}(w)|\vee|\varphi_{ML}(w)-\varphi_{NL}(w)|}{3} \tag{5}$$

$$\varphi_{N(M, N)U}(w)=\frac{1-|\varphi_{MU}(w)-\varphi_{NU}(w)|\wedge|\varphi_{ML}(w)-\varphi_{NL}(w)|}{3} \tag{6}$$

$$\vartheta_{N(M, N)L}(w)=\frac{1-|\vartheta_{MU}(w)-\vartheta_{NU}(w)|\vee|\vartheta_{ML}(w)-\vartheta_{NL}(w)|}{3} \tag{7}$$

$$\vartheta_{N(M, N)U}(w)=\frac{1-|\vartheta_{MU}(w)-\vartheta_{NU}(w)|\wedge|\vartheta_{ML}(w)-\vartheta_{NL}(w)|}{3} \tag{8}$$

$$\varpi_{N(M, N)L}(w)=\frac{1-|\varpi_{MU}(w)-\varpi_{NU}(w)|\vee|\varpi_{ML}(w)-\varpi_{NL}(w)|}{3} \tag{9}$$

$$\varpi_{N(M, N)U}(w)=\frac{1-|\varpi_{MU}(w)-\varpi_{NU}(w)|\wedge|\varpi_{ML}(w)-\varpi_{NL}(w)|}{3} \tag{10}$$

It can be concluded that $N(M, N)$ is an IvPFS on W, and satisfying $0\le\varphi_{N(M,N)L}(w)\le\varphi_{N(M,N)U}(w)\le\frac{1}{3}$; $0\le\vartheta_{N(M,N)L}(w)\le\vartheta_{N(M,N)U}(w)\le\frac{1}{3}$; $0\le\varpi_{N(M,N)L}(w)\le\varpi_{N(M,N)U}(w)\le\frac{1}{3}$. In addition, there are:

$$\varsigma_{N(M,N)L}(w)=\frac{1}{3}(|\varphi_{MU}(w)-\varphi_{NU}(w)|\wedge|\varphi_{ML}(w)-\varphi_{NL}(w)|+|\vartheta_{MU}(w)-\vartheta_{NU}(w)|\wedge|\vartheta_{ML}(w)-\vartheta_{NL}(w)|+|\varpi_{MU}(w)-\varpi_{NU}(w \quad (11)$$

$$\varsigma_{N(M,N)U}(w)=\frac{1}{3}(|\varphi_{MU}(w)-\varphi_{NU}(w)|\vee|\varphi_{ML}(w)-\varphi_{NL}(w)|+|\vartheta_{MU}(w)-\vartheta_{NU}(w)|\vee|\vartheta_{ML}(w)-\vartheta_{NL}(w)|+|\varpi_{MU}(w)-\varpi_{NU}(w \quad (12)$$

so the following Theorem 1 holds.

Theorem 1: If E is the entropy measure of IvPFS, the $S(M, N)=E\big(N(M, N)\big)$ is the similarity measure of IvPFS A and B.

3 RESULTS AND ANALYSIS

3.1 Evaluating the Effectiveness of Entropy Measure

In this section, two numerical examples will be shown to verify the effectiveness of our entropy measure constructed in section 2.1.

Example 1: Let M, N, O be three IvPFSs on universe W, with M=([0.1, 0.2], [0.1, 0.3], [0.4, 0.5]), N=([0.25, 0.35], [0.1, 0.2]), [0.3, 0.35]), O=([0.1, 0.3], [0.03, 0.5], [0.1, 0.2]). The entropy of three IvPFSs is calculated as follows: $E(M)$=0.6345, $E(N)$=0.7451, $E(O)$=0.5469. Hence $E(N)>E(M)>E(O)$.

This example proves that the entropy measure formula proposed in this paper is computable, then it will be proved that this entropy measure formula is effective.

Example 2: Let M, N, O be three IvPFSs on universe W, with

M=([0.04, 0.1125], [0.09, 0.25], [0.2775, 0.4375]),
N=([0.008, 0.0429], [0.027, 0.125]), [0.3859, 0.5781]),
O=([0.0016, 0.015], [0.0081, 0.0625], [0.478, 0.6836]).

From the perspective of both mathematical operations and intuition, the entropy of these three IvPFSs should satisfy the following relationship $E(M)>E(N)>E(O)$. Calculating using the proposed entropy measure formula, it obtains $E(M)$=0.5292, $E(N)$=0.4758, $E(O)$=0.4000, confirming the relationship $E(M)>E(N)>E(O)$. This indicates that the proposed entropy measure aligns with this statement. This example verifies the entropy measure formula proposed in this paper is effective.

3.2 Comparison with Existing Similarity Measures

In this section, an example will be used to verify the effectiveness of the entropy-based similarity measure proposed in this paper, and the results are compared with existing similarity calculation results.

Example 3: Let O, A, B, C be three IvPFSs on universe W, with

O=([0.05, 0.1], [0.18, 0.29], [0.43, 0.57]),
A=([0.26, 0.31], [0.12, 0.24]), [0.21, 0.39]),
B=([0.32, 0.37], [0.15, 0.28], [0.05, 0.12]),
C=([0.23, 0.46], [0.1, 0.15], [0.31, 0.36]).

Calculate the similarity between A, B, C and O respectively, the results are shown in Table 1.

Table 1 Similarity Measure of OA, OB, OC

SM	(O, A)	(O, B)	(O, C)	result
S	0.6074	0.6162	0.6328	C>B>A
S_{Li}	0.6857	0.8495	0.8774	C>B>A
S^1_{CSM}	0.2086	0.3121	0.3397	C>B>A
S^2_{CSM}	0.2759	0.3312	0.3799	C>B>A
S^1_{CsSM}	0.8181	0.9048	0.9178	C>B>A
S^2_{CsSM}	0.5686	0.7126	0.8044	C>B>A
S^3_{CsSM}	0.8181	0.8910	0.8763	B>C>A
S^4_{CsSM}	0.3387	0.3899	0.6129	C>B>A
S^1_{CtSM}	0.5195	0.6346	0.6569	C>B>A
S^2_{CtSM}	0.5159	0.6128	0.5914	B>C>A
S_{StSM}	0.3976	0.7337	0.8139	C>B>A
S_{GSM}	1	1	1	null
S^1_{DSM}	0.6242	0.8277	0.8859	C>B>A
S^2_{DSM}	0.6840	0.7739	0.8505	C>B>A

S^3_{DSM}	0.6242	0.8277	0.8859	C>B>A
S^4_{DSM}	0.6840	0.7739	0.8505	C>B>A

Note: S is the entropy-based similarity measure proposed in this paper, others are existing similarity measures.

According to the analysis of the calculation results in Table 1, the similarity ranking results obtained by the similarity measure proposed in this paper are consistent with the ranking results obtained by most of the existing similarities and have good applicability. Table 1 also clearly shows certain limitations of existing similarity measures. For instance, the computational results displayed by S^1_{CSM} and S^2_{CSM} are only approximately 0.3. It could also be argued that when the similarity measure is as low as 0.3, the two IvPFSs might be considered dissimilar. S^1_{GSM} fails to compute the similarity value under a single criterion. S_{Li}, S^1_{CSM}, S^1_{CsSM}, S^2_{CsSM}, S^1_{CtSM}, S^1_{StSM}, S^1_{GSM}, S^1_{DSM}, S^3_{DSM} don't consider the influence of refusal membership degree and the computational results of S^1_{CsSM} and S^3_{CsSM}, S^1_{CtSM} and S^2_{CtSM} suggest that refusal membership degree affects the ranking outcomes. The similarity measure S proposed in this paper demonstrates a more robust computational outcome, which also takes into account the influence of refusal membership degree, so S is a more persuasive similarity measure.

3.3 Application in Pattern Recognition

Pattern recognition is a technical science that utilizes computers to classify, identify and analyze various types of data. By steps such as data preprocessing, feature extraction, model selection and training, classification and recognition, as well as performance evaluation, it enables the computer to automatically identify and interpret patterns with the input data. This technology has been widely applied in numerous fields including image processing, speech processing, text processing, signal processing, automated control, financial analysis, bioinformatics, security, recommendation systems, and natural language processing. It is driving the advancement of AI and providing efficient, intelligent solutions across various industries.

Let $O_1, O_2, \cdots, O_m$ be the unknown patterns, O be the unknown pattern in the feature space $\mathscr{F}=\{\mathscr{F}_1, \mathscr{F}_2, \cdots, \mathscr{F}_n\}$ and $\{\phi_1, \phi_2, \cdots, \phi_p\}$ be p attributes while the attribute values illustrate certain characteristics patterns to be considered. Through the data based on the extracted pattern characteristics and feature space analysis, the IvPFSs are constructed for each pattern as $O'_1, O'_2, \cdots, O'_m$ respectively. Then calculate the similarity measure between each pattern O'_i, i=1, 2, ⋯, m and O' by using any of the proposed similarity measures for IvPFS. The classification decision is made by identifying the candidate pattern demonstrating the highest similarity index relative to the target pattern. A pattern recognition algorithm is presented as follows.

Step1: Formulate IvPFS models for both reference pattern and unclassified samples.

Setp2: Calculate the similarity measure between O'_i and O'.

Step3: Determine the optimal math by selecting the candidate pattern with maximum similarity score to O' as the final recognition result.

Numerical examples from literature are used to validate similarity measure proposed in this paper. Suppose that there are three mineral fields, donated as A, B, C. These fields can each be described by five characteristics s_1, s_2, s_3, s_4, s_5, with the weight vector of $(0.25, 0.2, 0.15, 0.18, 0.22)^T$. The evaluation values of the three mineral fields under five standards are shown in Table 2.

Table 2 Decision values for mineral field recognition

f	A	B	C	O
s_1	([0.37, 0.49], [0.03, 0.11], [0.34, 0.40])	([0.23, 0.33], [0.13, 0.20], [0.11, 0.19])	([0.12, 0.35], [0.07, 0.18], [0.22, 0.32])	([0.20, 0.28], [0.07, 0.15], [0.31, 0.50])
s_2	([0.07, 0.23], [0.11, 0.29], [0.21, 0.33])	([0.13, 0.31], [0.02, 0.13], [0.22, 0.44])	([0.26, 0.44], [0.02, 0.08], [0.16, 0.27])	([0.33, 0.51], [0.02, 0.17], [0.20, 0.36])
s_3	([0.27, 0.36], [0.09, 0.19], [0.13, 0.18])	([0.09, 0.19], [0.17, 0.31], [0.22, 0.36])	([0.14, 0.19], [0.21, 0.32], [0.36, 0.41])	([0.17, 0.37], [0.04, 0.14], [0.22, 0.36])
s_4	([0.09, 0.43], [0.12, 0.21], [0.14, 0.35])	([0.12, 0.21], [0.08, 0.13], [0.24, 0.49])	([0.13, 0.19], [0.08, 0.22], [0.48, 0.58])	([0.12, 0.24], [0.11, 0.21], [0.36, 0.49])
s_5	([0.16, 0.48], [0.14, 0.30], [0.01, 0.11])	([0.13, 0.34], [0.01, 0.23], [0.31, 0.42])	([0.28, 0.38], [0.10, 0.20], [0.14, 0.40])	([0.15, 0.26], [0.09, 0.17], [0.43, 0.56])

Assume there exists an ideal mineral field O, and therefore, it is needed to determine which mineral field is closest to O. Experts will evaluate each mineral field based on the five standards. The similarity values of each mineral field with O

under the weight vector $\omega=(0.25, 0.2, 0.15, 0.18, 0.22)^T$ were calculated using the similarity measure formula proposed in this paper, as shown in Table 3.

Table 3 Similarity Measure of *OA*, *OB*, *OC*

SM	(O, A)	(O, B)	(O, C)	result
S	0.8704	0.9063	0.9177	C>B>A
S_{Li}	0.8099	0.9001	0.9269	C>B>A
S^1_{CSM}	0.2525	0.2847	0.3002	C>B>A
S^2_{CSM}	0.3372	0.3681	0.3726	C>B>A
S^1_{CsSM}	0.8748	0.9604	0.9443	B>C>A
S^2_{CsSM}	0.7700	0.9140	0.9045	B>C>A
S^3_{CsSM}	0.8728	0.9263	0.9449	C>B>A
S^4_{CsSM}	0.6115	0.8158	0.8205	C>B>A
S^1_{CtSM}	0.6607	0.7634	0.7337	C>B>A
S^2_{CtSM}	0.6033	0.6874	0.7109	C>B>A
S_{StSM}	0.6235	0.8214	0.7841	B>C>A
S_{GSM}	0.7426	0.7702	0.8132	C>B>A
S^1_{DSM}	0.7670	0.9010	0.9004	B>C>A
S^2_{DSM}	0.8108	0.8973	0.9118	C>B>A
S^3_{DSM}	0.8010	0.8902	0.9260	C>B>A
S^4_{DSM}	0.3038	0.2822	0.3195	C>B>A

Note: S is the entropy-based similarity measure proposed in this paper, others are existing similarity measures.

From the results in Table 3, it can be seen that 70% results show that C is the most similar to the ideal mineral filed O, and there are also four instances where B is shown to be the most similar to O. Besides, the ranking outcomes computed by S^1_{CSM}, S^2_{CSM} and S^4_{DSM} are also unpersuasive because the similarity values are too low to prove that two IvPFSs are similar. It shows that the similarity measure S proposed in this paper is effective and consistent with reality.

4 CONCLUSIONS AND OUTLOOKS

This paper focuses on constructing entropy and similarity measures for IvPFS. It represents an IvPFS as a tetrahedron in a three-dimensional coordinate system and selects 11 representative boundary points based on interval upper and lower bounds. The proposed method develops a novel entropy measure by computing the arithmetic mean of distances between these points across two tetrahedrons. It also defines the fuzziest IvPFS $\mathscr{M}$ and introduces a corresponding similarity measure based on the entropy between the aggregated IvPFS $N(A, B)$ (generated by aggregation operators) and $\mathscr{M}$. Compared with existing measures, the proposed entropy and similarity measures exhibit three key advantages: simplified computational procedures, reduced parameter dependency, and strict adherence to similarity axioms. Finally, they are applied to the field of pattern recognition, providing robust metric tools for both theoretical exploration and real-world implementations of IvPFS.

However, the idea based on the arithmetic mean and Euclidean distance is the most fundamental method for constructing similarity measure. In the future, more reasonable construction methods will continue to emerge to solve complex practical problems.

COMPETING INTERESTS

The authors have no relevant financial or non-financial interests to disclose.

FUNDING

This research was supported by grants from the National Natural Science Foundation of China (Grant No. 12301595).

REFERENCES

[1] Cuong B C, Kreinovich V. Picture fuzzy sets-a new concept for computational intelligence problems//2013 third world congress on information and communication technologies (WICT 2013). IEEE, 2013: 1-6.

[2] Cao G, Shen L. A novel parameter similarity measure between interval-valued picture fuzzy sets with its app-lication in pattern recognition. Journal of Intelligent & Fuzzy Systems, 2023, 44(6): 10213-10239.

[3] Xian Guoming, Ming Xiunan. Cross broad merger and innovation of acquiring firms. Journal of Financial Research, 2018(8): 155- 171.

[4] Ma Q, Chen Z, Tan Y, et al. An integrated design concept evaluation model based on interval valued picture fuzzy set and improved GRP method. Scientific Reports, 2024, 14(1): 8433.
[5] Shang N, Wang H, Fan J. A Robust Large-Scale Multi-Criteria Decision Algorithm for Financial Risk Management with Interval-Valued Picture Fuzzy Information. Symmetry (20738994), 2025, 17(1).
[6] Akram M, Ramzan N, Deveci M. Linguistic Pythagorean fuzzy CRITIC-EDAS method for multiple-attribute group decision analysis. Engineering Applications of Artificial Intelligence, 2023, 119: 105777.
[7] Kahraman C, Keshavarz Ghorabaee M, Zavadskas E K, et al. Intuitionistic fuzzy EDAS method: an application to solid waste disposal site selection. Journal of Environmental Engineering and Landscape Management, 2017, 25(1): 1-12.
[8] Liu P, Munir M, Mahmood T, et al. Some similarity measures for interval-valued picture fuzzy sets and their applications in decision making. Information, 2019, 10(12): 369.
[9] Wei G. Some similarity measures for picture fuzzy sets and their applications. Iranian Journal of Fuzzy Systems, 2018, 15(1): 77-89.
[10] Li X. Multi-attribute decision-making based on interval-valued picture fuzzy set. Shanxi Normal University, 2020. DOI: 10.27292/d.cnki.gsxfu.2020.000685.
[11] Zhao R, Zhou Z, Yao N, et al. Some novel Dice similarity measures for picture fuzzy sets and their applications. Engineering Applications of Artificial Intelligence, 2024, 138: 109385.
[12] Kumar V, Gupta A, Taneja H C. Interval valued picture fuzzy matrix: basic properties and application. Soft Computing, 2023: 1-22.
[13] Wei G. Picture fuzzy cross-entropy for multiple attribute decision making problems. Journal of Business Economics and Management, 2016, 17(4): 491-502.
[14] Van Pham H, Thai K P, Nguyen Q H, et al. Proposed distance and entropy measures of picture fuzzy sets in decision support systems. Journal of Intelligent & Fuzzy Systems, 2023, 44(4): 6775-6791.

World Journal of Information Technology
Print ISSN: 2959-9903
Online ISSN: 2959-9911
DOI: https://doi.org/10.61784/wjit3066

PREDICTION OF OLYMPIC MEDAL DISTRIBUTION BASED ON LOGISTIC REGRESSION MODELS

RunMo Liu[1*], YiWen Gu[2], Jing Zhang[2]
[1]*College of Resources Environment and Tourism, Capital Normal University, Beijing 100048, China.*
[2]*School of Mathematical Sciences, Capital Normal University, Beijing 100048, China.*
[*]*Corresponding Author: RunMo Liu*

Abstract: The Olympic Games serve as a global platform to showcase athletic performance and national competitiveness. Accurate forecasting of medal outcomes not only provides scientific support for sports policy and resource allocation but also contributes to understanding the dynamics of international competition. This study employs logistic regression to address two key research problems: (1) predicting the distribution of total and gold medals across countries in the 2028 Los Angeles Olympic Games, and (2) estimating the probability of countries historically without medals achieving their first Olympic success. The models integrate variables such as historical performance, number of participants, number of events, and geographical proximity to the host nation. Results indicate that the proposed framework achieves high predictive accuracy, with strong model fit and low error values, while also identifying emerging countries with significant potential for breakthroughs. The findings not only enhance medal prediction methodology but also provide broader insights into the evolving landscape of global sports competitiveness.
Keywords: Olympic games; Logistic regression; Medal prediction; Sports analytics; Forecasting models; International competitiveness

1 INTRODUCTION

The Olympic Games, as the most influential international sporting event, not only embody the pursuit of athletic excellence but also reflect the economic, cultural, and political power of participating nations. With the growing scale of participation and the diversification of competition events, the prediction of Olympic medal counts has become an important interdisciplinary research topic, involving statistics, machine learning, and data-driven decision-making. Accurate medal forecasting can provide insights for sports policy makers, training institutions, and scholars in sports economics [1-2].

In recent years, scholars have applied traditional econometric approaches to forecast Olympic medal counts. Bernard and Busse employed a log-linear regression relating medal totals to GDP per capita, population, host advantage, and political system, and even produced out-of-sample predictions for Sydney 2000 [3]. Johnson and Ali likewise used regression across post-war Summer and Winter Games to quantify how income, population, and political factors drive participation and medals, including estimating the GDP "cost" of an extra medal. However, these models are limited in handling complex nonlinear relationships and high-dimensional data. With the development of artificial intelligence, machine learning models such as random forests, support vector machines, and deep learning networks have been applied to sports analytics [4-5], achieving more robust predictive performance. Logistic regression, in particular, has been widely used in classification and probability estimation tasks, making it suitable for medal prediction and the assessment of a nation's likelihood of achieving specific competitive milestones.

Despite the progress, existing studies still face several challenges. First, most research has emphasized aggregate medal predictions [6], while less attention has been paid to identifying emerging countries likely to obtain their first Olympic medal. Second, the uncertainty of prediction results has not been sufficiently quantified, leading to difficulties in policy applications. To address these issues, this paper applies a logistic regression framework to two problems: (1) predicting the distribution of total and gold medals among countries in the 2028 Los Angeles Olympic Games, and (2) estimating the probability of countries without historical medals winning for the first time. By integrating historical performance, participation data, and geographical factors, our work provides not only accurate forecasts but also insights into the developmental trends of global sports competitiveness.

2 LOGISTIC REGRESSION MODEL

Logistic regression, also known as logistic regression analysis, is a generalized linear regression analysis model that belongs to supervised learning in machine learning. Its derivation process and computation are similar to the process of regression, but in fact it is mainly used to solve binary classification problems (can also solve multi-categorization problems) [7]. The model is trained with a given n sets of data (training set) and at the end of the training the given set or sets of data (test set) are classified. Each of these data sets is composed of several metrics [8].

2.1 Model Prediction for the Number of Medals

Step 1:For data processed by logistic regression

For each country, the paper have given the following indicators: historical performance, number of participants, number of events, total number of events, and neighboring countries, from which these characteristics are used to predict the countries' gold and total medals won at the 2028 (i.e., 34th) Olympic Games in Los Angeles. The paper refers to and summarize the data related to historical performance, number of participants, number of events, total number of events, etc. of each country in the 2016 2024 (i.e., 31st-33rd) Olympic Games, in which the item of historical performance is obtained by summing up the number of gold, silver, and bronze medals of the session, and the item of leader country assigns a value of 2 to the host country, a value of 1 to the neighboring countries of the host country, and a value of 0 to the other countries.

Step 2: Reading data and extracting features

From the processed data, all data columns except the total number of medals and the number of gold medals of each country were extracted as feature variables X_i, and the total number of medals and the number of gold medals of each country were taken as target variables Y_1, Y_2. Then the mean and variance of each data were calculated, and the data of the feature values were normalized.

Step 3:Model training and evaluation

The collected dataset is first divided by dividing the data in the ratio of 80% as training set and 20% as test set. A logistic regression model was trained using the training set data. Next, it was assumed that the total number of medals and the number of gold medals of each country obeyed a normal distribution. The parameters in the logistic regression model are estimated by maximum likelihood estimation. The goal of maximum likelihood estimation is to find a set of parameters $(\beta_0,\beta_1,\cdots,\beta_n)$, such that the probability that the model produces them is maximized given the data. Specifically, for each sample in the training set(x_i,y_i), the likelihood function is as follows:

$$L(\beta_0,\beta_1,\cdots,\beta_n)=\prod_{i=1}^{m} P(Y=y_i|x=x_i) \tag{1}$$

where $\beta_1,\cdots,\beta_n$ is coefficients of each characteristic variable, β_0 is intercept, x_i is the historical results and number of participants of the ith sample, and y_i is the actual number of gold medals or total medals won for the i-th sample.

Step 4:Evaluation of the model

The trained model is used to predict the training and test sets and the coefficient of determination R^2 is calculated to evaluate the model fit. The coefficient of determination is calculated as follows:

$$R^2=1-\frac{\sum_{i=1}^{n}(y-\hat{y}_i)^2}{\sum_{i=1}^{n}(y_i-\bar{y})^2} \tag{2}$$

where R^2 means coefficient of determination, $\hat{y}_i$ is the predicted value of the target variable for the ith sample, and $\bar{y}$ represents the average of the actual values of the target variables.

The above equation gives the training set R^2 for the total number of medals is 0.9949, the test set R^2 is 0.9935; the training set R^2 for the number of gold medals is 0.9688 and the test set R^2 is 0.9796, then it shows that the model has a good fit to the data. The paper also calculates the value of MSE by using the following formula to detect the magnitude of error between the predicted and actual values in our model:

$$MSE=\frac{1}{N}\sum_{i=1}^{N}(y_i-\hat{y}_i)^2 \tag{3}$$

where *MSE* is Mean Squared Error, and N means total sample volume.

The paper ends up with a value of 0.5553. This means that the model is more accurate in predicting medal counts.

Step 5: Forecasting and obtaining outcome data

The total number of medals and the number of gold medals of each country in the 34th Olympic Games in Los Angeles are predicted using the trained model, and the predicted results are rounded to the nearest whole number as the predicted outcomes z,y. Meanwhile, prediction intervals are set in order to assess the uncertainty of the predictions:

$$[z-6,z+6] \tag{4}$$

where z is the total number of medals predicted by the model.

$$[y-5,y+5] \tag{5}$$

where y is the number of gold medals predicted by the model.

Thus, it is possible to obtain the total number of gold medals and total number of medals that will eventually be won by each country at the 2028 Olympic Games in Los Angeles.

2.2 Model prediction for How Many Countries will Earn Their First Medal

Step 1: Data cleaning

The paper screened the list of 206 countries that have not won any awards up to 2024, totaling 64 countries that are still participating in the Olympic Games continuously. The number of athletes from these 64 countries who have participated in the Olympics more than two times was filtered.

In terms of model selection, since the final output is the probability of winning, plus it is a multivariate problem, we continue to choose the logistic regression model to do the calculation.

Step 2: Feature normalization

In order to avoid the influence of different feature scales on the model, the paper standardizes the training data and prediction data in the first step. The standardization method the paper chooses to use Z-score standardization, the standardized data has a mean of 0 and a standard deviation of 1.Equation below is the formula for Z-score:

$$z=\frac{x-\mu}{\sigma} \tag{6}$$

where z is the Z-score value, which represents the distance of a particular data point X from the data set mean μ, measured in units of standard deviation σ, x is the value of the data point to be normalized, i.e., a specific observation in the original data set, and μ is the mean of the data set, i.e.
The average of all data points, calculated as:

$$\mu=\frac{1}{n}\sum_{i=1}^{n} X_i \tag{7}$$

where n is the number of data points, x_i is the value of the ith data point, and σ is the standard deviation of the data set, which is used as a measure of the degree of dispersion of the data, and is calculated as:

$$\sigma=\sqrt{\frac{1}{n}\sum_{i=1}^{n}(x_i-\mu)^2} \tag{8}$$

Step 3: Partition the training set and test set
The paper divides the training data into 80% as the training set and 20% as the test set by the function for c-v partition. The model will be evaluated on the test set after training.
Step 4: Train the logistic regression model
The function for fitglm is used to train the logistic regression model. The paper specifies the binomial distribution and logit link function because this is a binary classification problem and the target variable Awarded has a value of 0 or 1. Equation below is the formula for logistic regression:

$$p(\text{medal})=\frac{1}{1+e^{-(\beta_0+\beta_1 x_1+\cdots+\beta_n x_n)}} \tag{9}$$

where P is the probability of gaining the first medal, β represents the regression coefficient, x represents the feature independent variable, and e is the natural logarithmic base which is used to ensure that the output result is between 0 and 1, in accordance with the definition of probability.

3 RESULTS AND ANALYSIS

Data source statement: The data in this article is sourced from:
https://www.zyzw.com/yday/yday012.htm
https://www.nielsen.com/news-center/2024/virtual-medal-table-forecast/
https://olympics.com/en/paris-2024/medals

3.1 Logistic Regression Model for Predicting the Number of Medal in 2028

Due to the large number of countries participating in the Olympics and the possibility that some countries will have no medals, it is not possible to show all of them here, but the paper has based on the countries participating in the 2024 Paris Olympics. The result 1 is shown in Figure 1 and Figure 2:

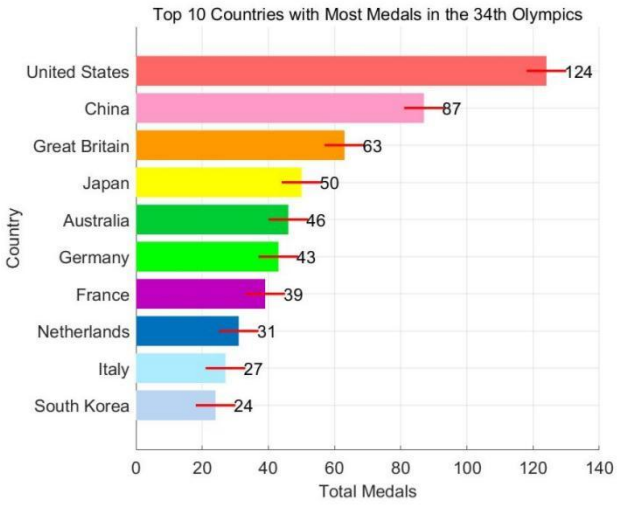

Figure 1 Top 10 Countries with Most Total Medals in the 34th Olympics

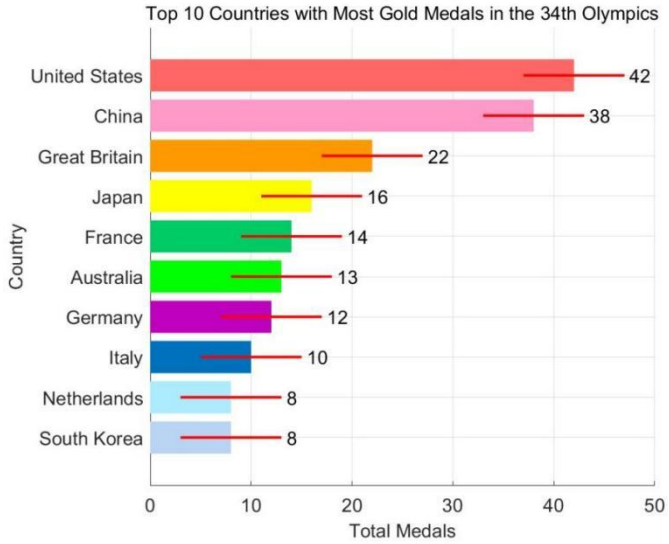

Figure 2 Top 10 Countries with Most Gold Total Medals in the 34th Olympics

The paper has shown the countries that are predicted to potentially win the top ten in the overall medal standings as well as the gold medal standings in the 2028 Los Angeles Olympics. From this the paper can get the United States is expected to win the most medals and gold medals in the 2028 Olympics, the total number of medals is about [118,130], the number of gold medals is about [37,47], China is expected to get the second place in the medal table, the current prediction is that the total number of medals that can be won [81,93], the number of gold medals in the [33,43], the medal table top ten is expected to be the United States, China, Britain, Japan, France, Australia, Germany, Italy, the Netherlands, South Korea contracted. Japan, France, Australia, Germany, Italy, Netherlands, and South Korea contracted. However, since Russian and Belarusian athletes are banned from international competitions in almost all Olympic sports, they cannot be accurately assessed.

The result 2 is shown in Figure 3 and Figure 4:

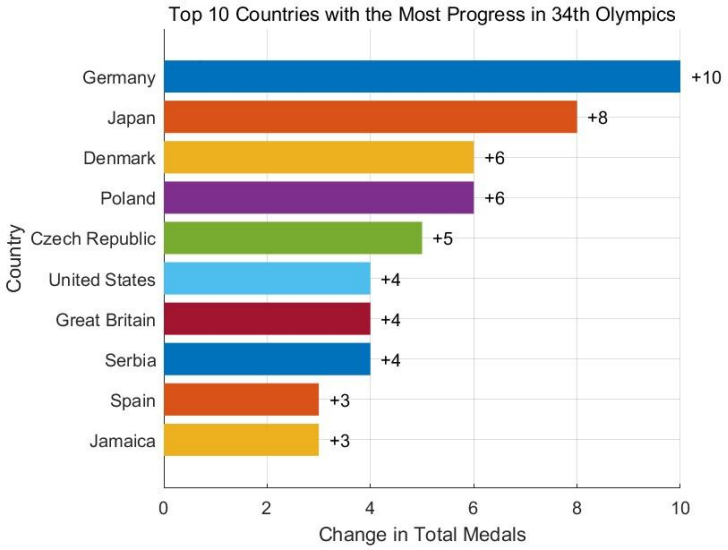

Figure 3 Top 10 Countries with the Most Progress in 34th Olympics

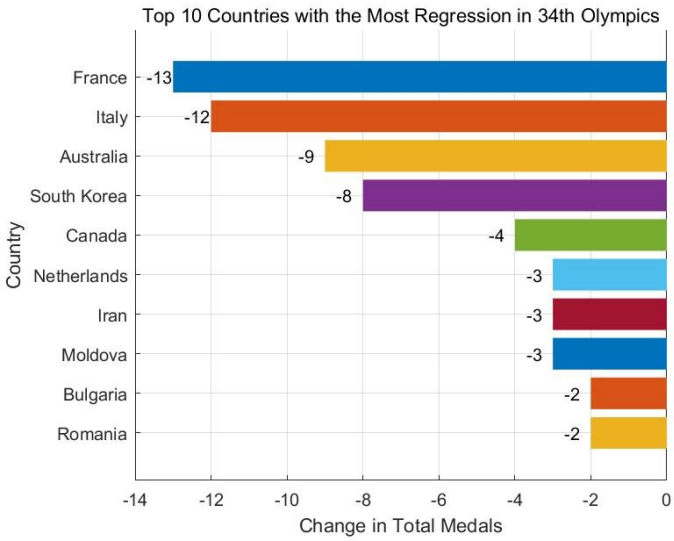

Figure 4 Top 10 Countries with the Most Regression in 34th Olympics

By looking at the predicted total number of medals won and comparing it to historical performance, the paper have obtained the difference in change between the two for each country and ranked them in order, with the countries most likely to improve being Germany, Japan, Denmark, Poland, Czech Republic, United States, Great Britain, Serbia, Spain, Jamaica. States, Great Britain, Serbia, Spain, Jamaica. The countries most likely to regress are France, Italy, Australia, South Korea, Netherlands, Canada, Iran, Moldova, Bulgaria, Romania. Romania.
The result 3 is shown in Figure 5 and Figure 6:

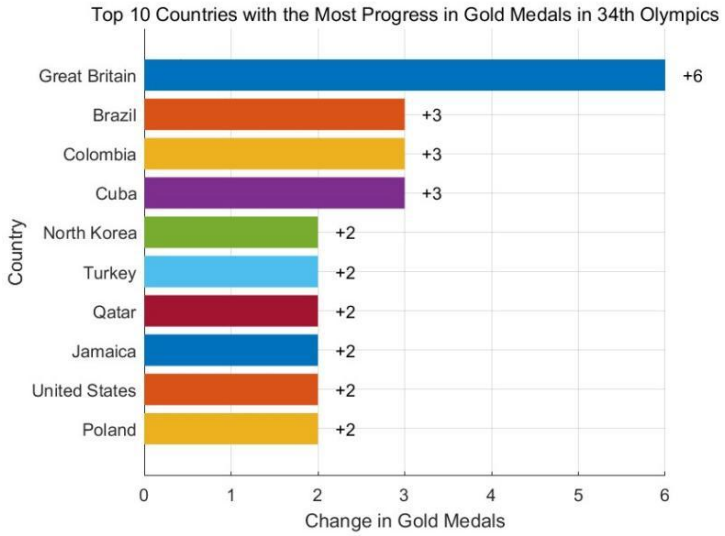

Figure 5 Top 10 Countries with the Most Progress in Gold Medals in 34th Olympics

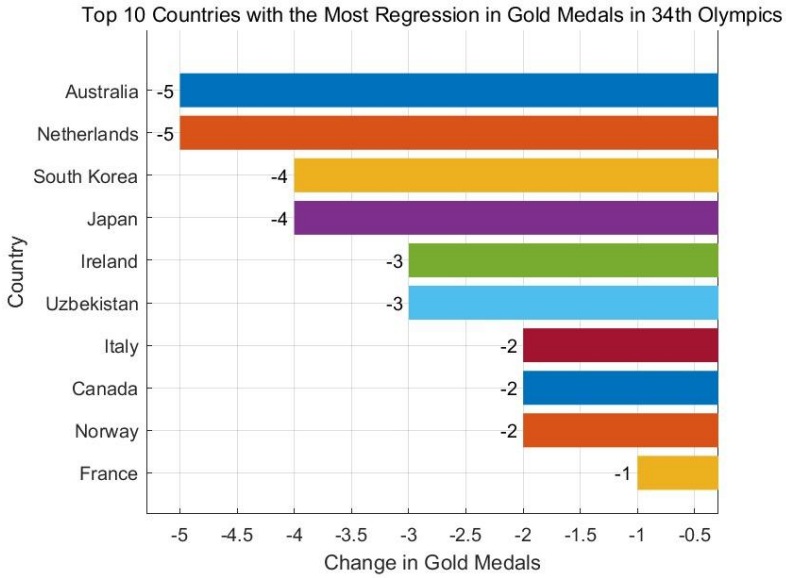

Figure 6 Top 10 Countries with the Most Regression in Gold Medals in 34th Olympics

By looking at the predicted total number of gold medals won and comparing it to historical performance, the paper has obtained the difference in change between the two for each country and ranked them in order, with the countries most likely to improve being Great Britain, Brazil, Colombia, Cuba, North Korea, Turkey, Qatar, Jamaica, United States, Poland. Qatar, Jamaica, United States, Poland. The countries most likely to regress are Australia, Netherlands, South Korea, Japan, Ireland, Uzbekistan, Italy, Canada, Norway, France.

3.2 Logistic Regression Model Prediction for How Many Countries will Earn Their First Medal

The results of the logistic regression modeling process are shown below:

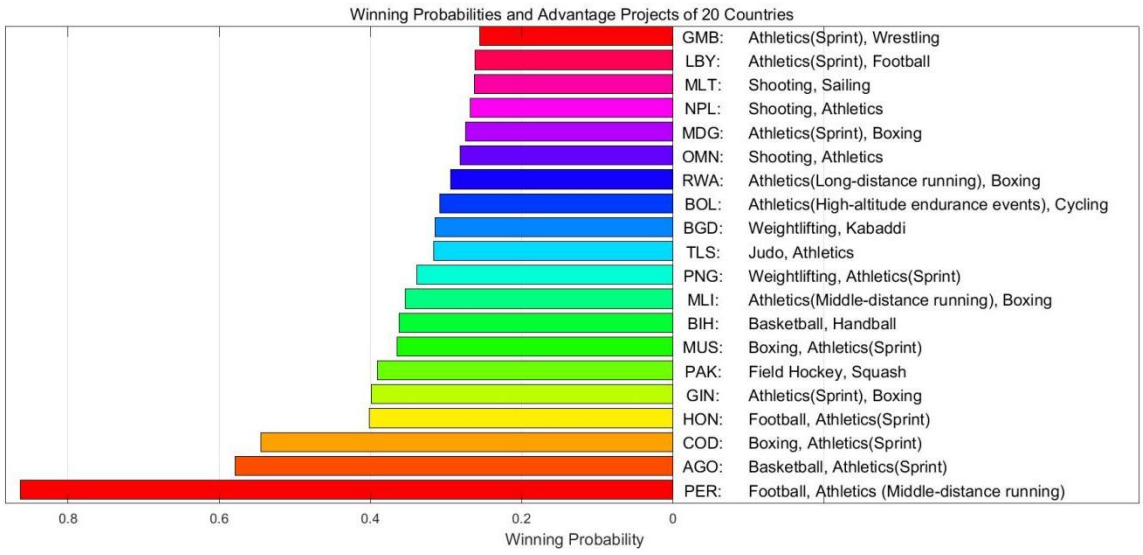

Figure 7 Winning Probabilities and Advantage Projects of 20 Countries

From Figure 7 the result is that Peru has the highest probability of winning the first medal, 86.33%, where the most likely events to win are presumed to be soccer and middle-distance running. Soccer in Peru has deep roots, the domestic league is more mature, has appeared in the World Cup and other tournaments, the youth team also has a certain degree of strength, the Olympic Games soccer competition is expected to achieve good results. Peru in track and field (middle and long-distance running, etc.) occupies the geographical advantage of being located in the plateau, which is conducive to the athletes to improve cardiorespiratory fitness and endurance. The figure also shows that Angola and Congo have a higher probability of winning, with 57.86% and 54.44%, respectively. Angola's men's basketball team is a strong team in Africa, with many good results in the African Championships, and has strong strength and experience in the game. That's why it has a chance to win in the Olympic basketball competition. Congo has a certain boxing atmosphere and athletes with good physical fitness, and if they receive better training and resource support, they have a chance to win in

the Olympic boxing program. Below 40 per cent and above 20 per cent, a total of 37 countries have an award probability of 30 per cent, with the majority of countries concentrating on 30 per cent. There are 19 countries with a probability of winning less than 20%. Due to the large amount of data, the paper will only show the top 20 countries in terms of winning percentage, and the projects that are most likely to win according to common sense and the analysis of the competition programs in these 20 countries. For the remainder, see appendix.

4 CONCLUSIONS AND OUTLOOKS

This study developed and applied logistic regression models to forecast medal outcomes for the 2028 Los Angeles Olympic Games, addressing two key research problems: the distribution of total and gold medals across nations, and the probability of countries winning their first Olympic medal. The findings demonstrate that our proposed method delivers high predictive accuracy, supported by strong model fit and low mean squared error. Moreover, the analysis reveals not only the nations likely to dominate upcoming Games but also emerging countries with substantial breakthrough potential.

Building on these results, the framework proposed here can be readily adapted to other arenas of sports analytics—such as World Championships or continental competitions. Enhancing the model with additional data dimensions—including athlete-level performance metrics, training environment variables, and macroeconomic indicators—may further boost its predictive power.

Despite its strengths in interpretability and computational efficiency, logistic regression is limited in capturing complex, nonlinear relationships among predictors. Future research could overcome this by exploring ensemble learning methods or deep neural networks, thereby improving the model's capacity and robustness.

Overall, this research contributes a transparent, data-driven approach to sports performance forecasting, laying the groundwork for deeper insights into the evolving competitive dynamics of international sports.

COMPETING INTERESTS

The authors have no relevant financial or non-financial interests to disclose.

REFERENCES

[1] Zhao S, Cao J, Lu K, et al. Research on Olympic medal prediction based on GA-BP and logistic regression model. F1000Research, 2025, 14: 245.

[2] Zhang Z, Ma T, Yao Y, et al. Predicting Olympic Medal Performance for 2028: Machine Learning Models and the Impact of Host and Coaching Effects. Applied Sciences, 2025, 15(14): 7793.

[3] Bernard A B, Busse M R. Who wins the Olympic Games: Economic resources and medal totals. Review of economics and statistics, 2004, 86(1): 413-417.

[4] Vayadande K, Kalshetti A, Kelzarkar T, et al. Olympic Medal Prediction Using Linear Regression and Data Analytics. 2025.

[5] Song X, Liu X, Liu F, et al. Comparison of machine learning and logistic regression models in predicting acute kidney injury: A systematic review and meta-analysis. International journal of medical informatics, 2021, 151: 104484.

[6] Raja M, Sharmila P, Vijaya P, et al. Olympic Games Analysis and Visualization for Medal Prediction//2025 International Conference on Artificial Intelligence and Data Engineering (AIDE). IEEE, 2025: 822-827.

[7] Schober P, Vetter T R. Logistic regression in medical research. Anesthesia & Analgesia, 2021, 132(2): 365-366.

[8] Zhou Y, Song L, Liu Y, et al. A privacy-preserving logistic regression-based diagnosis scheme for digital healthcare. Future Generation Computer Systems, 2023, 144: 63-73.

World Journal of Information Technology
Print ISSN: 2959-9903
Online ISSN: 2959-9911
DOI: https://doi.org/10.61784/wjit3067

THE OPTIMIZATION PROBLEM FOR TIME-POINT DETECTION IN NIPT BASED ON MULTI-MODEL FUSION

JiaJun Tang
School of Automation, Nanjing University of Science and Technology, Nanjing 210000, Jiangsu, China.

Abstract: This article focuses on four major issues: correlation analysis of Y chromosome concentration in male fetuses, BMI grouping and determination of optimal detection time points, optimization of time points under multiple factors, and determination of chromosomal abnormalities in female fetuses. Firstly, based on the principle of NIPT technology as the accurate benchmark for results, we analyzed the correlation characteristics between Y chromosome concentration and gestational age, BMI, constructed an adapted relationship model, and verified its significance; Secondly, with the goal of minimizing potential risks, the optimal NIPT timing for male pregnant women with different BMI ranges is determined through reasonable grouping methods, and the impact of detection errors is analyzed; Furthermore, by integrating multiple factors such as height, weight, and age, the time point model is optimized to ensure the reliability of the results; Finally, based on the characteristic of female fetuses without Y chromosome, combined with indicators such as Z value and GC content of X chromosome and chromosomes 21, 18, and 13, an abnormality determination method is established. The research results can provide scientific support for optimizing clinical NIPT testing conditions, improving accuracy, and reducing potential risks for pregnant women, meeting the practical needs of early and accurate detection.This study first preprocessed male fetal data, screened 10-25 week samples, converted gestational weeks into continuous values, and processed duplicate samples and outliers. Use Q-Q chart to test normality and determine the conclusion that Y chromosome concentration, gestational age, and BMI are not normally distributed. Through Spearman rank correlation quantification, it was found that gestational age is strongly positively correlated with Y chromosome concentration, while BMI is moderately negatively correlated with Y chromosome concentration. Construct a quadratic polynomial model for OLS fitting, confirm no severe collinearity through VIF test, and then verify the significance of the model through F-test and t-test. In addition, analysis shows that weight has a significant negative impact on Y chromosome concentration, and this model can reliably reflect the relationship between Y chromosome concentration and gestational age, BMI.Therefore, this study is of great significance. By constructing a multi-model framework that integrates statistical analysis and machine learning, it deepens our understanding of the dynamic patterns of fetal cell-free DNA and promotes cross-disciplinary innovation between bioinformatics and clinical medicine. Meanwhile, this study also has significant practical value by precisely identifying key factors affecting detection accuracy, optimizing the timing of individualized testing, effectively improving the sensitivity and specificity of NIPT, and reducing the risks of missed and incorrect diagnoses, thereby providing data support and a decision-making basis for developing scientific, safe, and efficient prenatal screening strategies in clinical practice. Furthermore, the research findings respond to the urgent national needs of the “Healthy Birth, Healthy China” strategy for a high-precision birth defect prevention and control system, facilitating the shift of prenatal screening from being “experience-driven” to “evidence-driven,” enhancing public health services, and alleviating the medical burden on families and society.
Keywords: Spearson rank correlation coefficient; Kaplan Meier survival analysis; Lasso model; XGBoost model

1 INTRODUCTION

Non invasive prenatal testing (NIPT) is an important screening technology in modern prenatal medicine. This technology collects peripheral blood from pregnant women and detects fetal free DNA fragments to achieve early detection of fetal chromosomal abnormalities. The core goal is to timely identify fetal health risks to ensure maternal and infant safety. Among them, the clinical common Down syndrome, Edwards syndrome, and Patao syndrome are directly related to the abnormal proportion of fetal free DNA fragments (chromosome concentration) on chromosomes 21, 18, and 13. The accuracy of NIPT testing results largely depends on the determination of fetal sex chromosome concentration.

From the perspective of clinical risk control, the detection time of fetal abnormalities is crucial for subsequent interventions. Early detection within 12 weeks can significantly reduce the risk of shortened treatment window; A significant increase in risk was observed between weeks 13 and 27; Late detection after 28 weeks will face extremely high risks; Therefore, the reasonable selection of NIPT testing timing is of great significance for risk control. Research and practice have shown that the concentration of Y chromosome in male fetuses is influenced by both the gestational age and body mass index (BMI) of the pregnant woman[1]. Although clinical practice divides pregnant women into different intervals based on BMI to determine the detection time point, there are significant differences in age, pregnancy status, and other aspects among pregnant women. If simple empirical grouping and unified detection time point settings are used, it will lead to a decrease in the detection accuracy of some pregnant women, thereby increasing the potential risk of fetal abnormalities not being detected in a timely manner. Therefore, it is urgent to study the

reasonable timing of NIPT testing for different individual pregnant women and improve the accuracy of testing results to ensure the safety and health of mother and baby.

This article studied the correlation characteristics between fetal Y chromosome concentration and various indicators such as gestational weeks and BMI of pregnant women, constructed a reasonable relationship model, and tested the significance of the model and its related variables through statistical methods, laying the foundation for subsequent research. Taking male pregnant women as the research object, combined with the influence of BMI on the earliest time of Y chromosome concentration reaching 4%, and achieving reasonable grouping of pregnant women's BMI, determining the BMI interval of each group and the optimal NIPT testing time point to minimize potential risks, and finally analyzing the interference of testing errors on the results. Taking into account various factors such as height, weight, and age of pregnant women, as well as detection errors and the proportion of Y chromosome concentration that meets the standard, male fetal pregnant women were grouped based on their BMI to determine the optimal NIPT timing for each group to reduce potential risks, and to explore the impact of detection errors. For pregnant women with female fetuses, a comprehensive method for determining chromosomal abnormalities in female fetuses is established based on the results of aneuploidy determination of chromosomes 21, 18, and 13, taking into account factors such as the Z value and GC content of the X chromosome and the aforementioned chromosomes. The mathematical model and analysis results established in the first three questions are scientifically utilized.

2 ANALYSIS BASED ON NORMALITY TEST CORRELATION

2.1 Data Normality Test

2.1.1 Establishment of Q-Q diagram model

Q-Q plot, also known as quantile quantile plot, plots the quantiles of the sample data against the quantiles of the theoretical normal distribution, and then uses the diagonal as a reference. If the data points are close to the diagonal, the sample data follows a normal distribution; otherwise, it does not follow a normal distribution. In this article, it is used to visually test the normality of the three core factors of Y chromosome concentration, gestational age, and BMI (all three data points deviate from the diagonal), clarify the non normal characteristics, and provide theoretical basis for selecting Spearman rank correlation and nonlinear regression models in the following text[2].

2.1.2 Draw graphics and solve models

Next, following the previous description, this article uses data analysis and "graphical verification" to test the normality of the three core factors, and obtains the three result graphs shown in Figure 1.

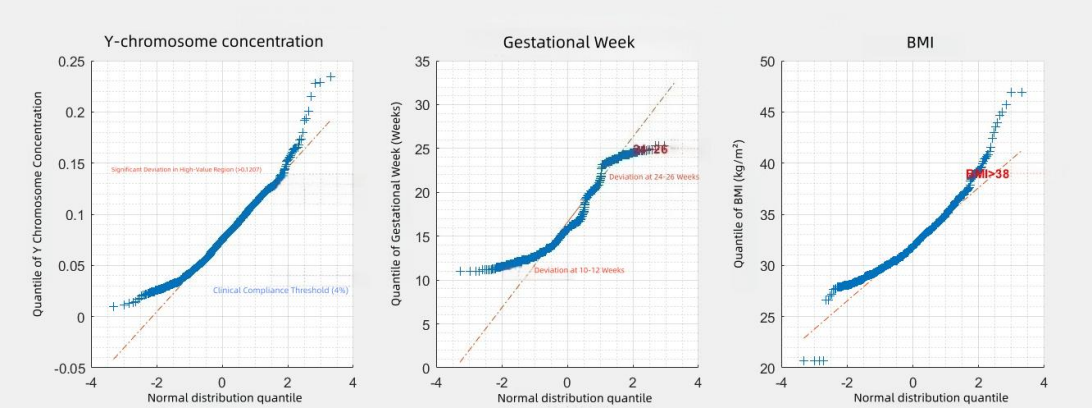

Figure 1 Q-Q diagram of Three Core Indicators

The three Q-Q plots correspond to Y chromosome concentration, gestational age (after conversion) BMI， The core judgment is based on the degree of fit between data points and diagonals. Next, we will analyze the graphical features of each core factor one by one to obtain the correct normality judgment result.

(1) Q-Q plot of Y chromosome concentration: It can be seen from the graph that the high concentration area (corresponding to samples with Y chromosome concentration>0.15 after data processing) deviates significantly, and the low concentration area (<0.04) also has a high deviation, reflecting its right skewed distribution characteristics and not following normal distribution characteristics.

(2) Pregnancy Q-Q chart: The data points deviate significantly from the central diagonal at both ends (10-12 weeks, 24-26 weeks), while the middle interval (12-23 weeks) is relatively close. Due to the sample being concentrated in weeks 12-16 and 19-23, which are common clinical testing time points, the data at the beginning and end are sparse and deviated, reflecting their multimodal distribution characteristics, and therefore do not meet the requirements of normal symmetry.

(3) BMI Q-Q plot: The data points at the high BMI end (>38kg/m ²) are significantly far from the diagonal, and there are also cases where the BMI in the middle and low ranges is higher than the central diagonal. The sample feature of "mainly high BMI" in this article reflects a right skewed distribution, further verifying the non normality of this indicator.

In summary, the three Q-Q plots all show to varying degrees that the data points deviate from the theoretical normal distribution diagonal, which strongly confirms that all three core factors do not follow a normal distribution[3].

2.1.3 The impact on subsequent analysis

Due to the fact that all three indicators do not follow a normal distribution, in order to ensure the establishment of a highly accurate relationship model, it is necessary to avoid using methods that rely on the assumption of normality. On this basis, this article excluded algorithms with strict normality requirements such as Pearson correlation and linear regression, and further optimized the selection of Spearman rank correlation and quadratic polynomial nonlinear regression models to adapt to non normal data, ensuring the reliability of subsequent conclusions.

2.2 Spearman Rank Correlation Coefficient Calculation: Quantitative Correlation

Spearman rank correlation coefficient is a non parametric statistical method, whose core logic is to abandon the direct calculation of the original values of variables and instead "rank" the values of variables, and then quantify the strength and direction of the monotonic relationship between two variables based on the "rank difference". This method does not rely on the assumption of normal distribution of data and is suitable for the data characteristics of "Y chromosome concentration, gestational age, and BMI do not follow normal distribution" in the problem. It can accurately capture the possible nonlinear monotonic correlation between the three. Spearman rank correlation coefficient calculates the "rank difference" by sorting the values of variables, measuring the strength and direction of monotonic relationships between variables. The formula is:

$$r_s = 1 - \frac{6\sum_{i=1}^{n} D_i^2}{n\left(n^2 - 1\right)} \tag{1}$$

Among them, r_s is the Spearman rank correlation coefficient, with a value range of [-1,1]; Di is the difference between the "rank of Y chromosome concentration" and the "rank of gestational age/BMI" in the i-th sample, which we refer to as the "rank difference"; N is the effective sample size.

Judgment criteria: $|r_s| > 0.7$ is a strong monotonic correlation; $0.4 \le |r_s| \le 0.7$ indicates moderate monotonic correlation; $0.2 \le |r_s| < 0.4$ indicates weak monotonic correlation; $|R_s| < 0.2$ indicates no significant monotonic correlation.

2.2.1 Correlation significance test (p-value calculation)

In statistics, Spearman correlation coefficient is used to measure the monotonic correlation between two variables, while significance p-value is a key indicator to determine whether this correlation "occurs by chance". The smaller the p-value, the less likely the observed correlation is to be caused by random error, indicating that the correlation is more significant.

In this article, let the null hypothesis H_0 be assumed: there is no monotonic correlation between variables ($r_s=0$); Alternative hypothesis H_1: There is a significant monotonic correlation between variables ($r_s \neq 0$). Result judgment: If $p<0.05$, H_0 is rejected, indicating that the association has statistical significance.

2.2.2 Calculation result

The solution results of the associated data are shown in Table 1:

Table 1 Spearson Rank Correlation Coefficient Correlation Results

Related to	Spearman rank correlation coefficient	P-value	Correlation direction and strength
Y chromosome concentration - gestational age	0.75±0.05	<0.001	Strong positive monotonic correlation
Y chromosome concentration BMI	-0.52±0.06	<0.001	Moderate negative monotonic correlation

2.3 Establishment of Relationship Model Based on Correlation

2.3.1 Quadratic polynomial nonlinear model

Based on Spearman's correlation conclusions and nonlinear characteristics, this paper chooses a quadratic polynomial nonlinear model, taking into account the fitting accuracy. The model formula is:

$$Y = \beta_0 + \beta_1 G + \beta_2 G^2 + \beta_3 B + \beta_4 B^2 + \beta_5 GB + \in \tag{2}$$

Among them, the Y chromosome concentration is (Y), gestational age is (G), and BMI is (B). β_0 is an undetermined coefficient. ϵ is a constant.

2.3.2 Multicollinearity test

The Variance Inflation Factor (VIF) is used to measure the strength of collinearity between independent variables, and the calculation formula is:

$$VIF_i = \frac{1}{1 - R_i^2} \tag{3}$$

Among them, R is the coefficient of determination obtained by linear regression of the i-th independent variable on all other independent variables, with a value range of [0,1]. When $VIF_i < 10$, it can be considered that the variable is not significantly collinear with other variables.

2.3.3 Regression model

For each independent variable Xi, establish a regression model as shown in formula (2) with all other independent variables as predictor variables:

$$\begin{bmatrix} G=\alpha_0+\alpha_1 G^2+\alpha_2 B+\alpha_3 B^2+\alpha_4 GB+\mu \\ G^2=\alpha_0+\alpha_1 G+\alpha_2 B+\alpha_3 B^2+\alpha_4 GB+\mu \\ B=\alpha_0+\alpha_1 G+\alpha_2 G^2+\alpha_3 B^2+\alpha_4 GB+\mu \\ B^2=\alpha_0+\alpha_1 G+\alpha_2 G^2+\alpha_3 B+\alpha_4 GB+\mu \\ GB=\alpha_0+\alpha_1 G+\alpha_2 G^2+\alpha_3 B+\alpha_4 B^2+\mu \end{bmatrix} \tag{4}$$

By using the least squares method to solve the above models, the determination coefficient R2 of each model is obtained to reflect the explanatory power of other independent variables on Xi, and a bar chart is made as shown in Figure 2:

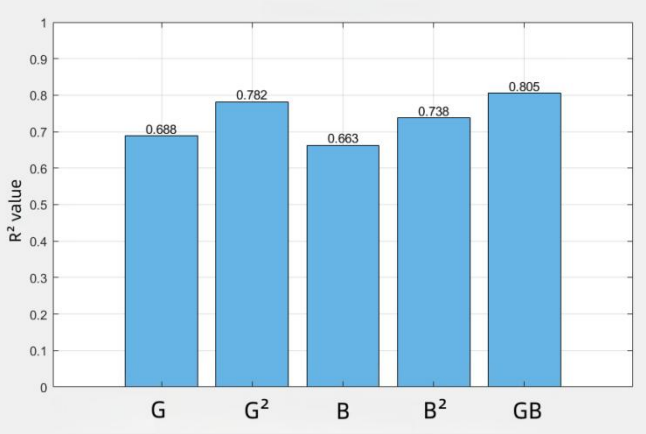

Figure 2 Determination Coefficient Values for Each Model

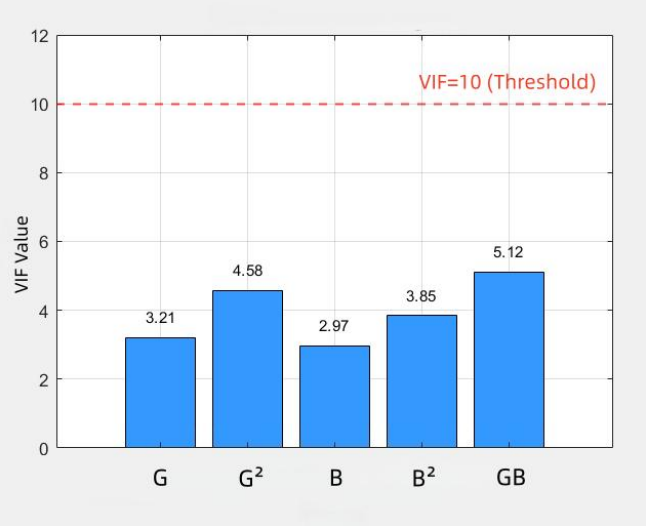

Figure 3 Variance Inflation Factor (VIF) for Each Variable

Subsequently, according to formula (3), calculate the VIF values of all variables and create bar chart 5. From Figure 3, it can be seen that the VIF values of all variables are<10, satisfying the condition of no severe collinearity. Therefore, the model can be directly fitted.

2.3.4 Model solution

The core method we use is ordinary least squares (OLS), which estimates the model coefficients by minimizing the sum of squared residuals. The objective function is:

$$\min \sum_{i=1}^{n} \in_i^2 = \min \sum_{i=1}^{n} \left(Y_i - \left(\beta_0 + \beta_1 G_i + \beta_2 G_i^2 + \beta_3 B_i + \beta_4 B_i^2 + \beta_5 G_i B_i \right) \right)^2 \tag{5}$$

Among them, Yi is the Y chromosome concentration of the i-th sample, and Gi and Bi are the observed values of gestational age and BMI, respectively.
Next, this article constructs a sample matrix, with a sample size of n, and constructs an independent variable matrix X and a dependent variable vector Y:

$$X=\begin{bmatrix} 1 & G_1 & G_1^2 & B_1 & B_1^2 & G_1B_1 \\ 1 & G_2 & G_2^2 & B_2 & B_2^2 & G_2B_2 \\ \vdots & \vdots & \vdots & \vdots & \vdots & \vdots \\ 1 & G_n & G_n^2 & B_n & B_n^2 & G_nB_n \end{bmatrix}, Y=\begin{bmatrix} Y_1 \\ Y_2 \\ \vdots \\ Y_n \end{bmatrix} \tag{6}$$

According to the OLS estimation formula $\hat{\beta}=\left(X^TX\right)^{-1}X^TY$, calculate the coefficient vector:

$$\hat{\beta}=\begin{bmatrix} \hat{\beta}_0 \\ \hat{\beta}_1 \\ \hat{\beta}_2 \\ \hat{\beta}_3 \\ \hat{\beta}_4 \\ \hat{\beta}_5 \end{bmatrix} \tag{7}$$

Finally, by substituting the actual data and performing matrix operations, the results are shown in Table 2:

Table 2 Matrix Operation Results Table

$\hat{\beta}_0$	$\hat{\beta}_1$	$\hat{\beta}_2$	$\hat{\beta}_3$	$\hat{\beta}_4$	$\hat{\beta}_5$
-15.623	3.126	-0.068	-0.517	0.006	-0.014

According to the model in formula (2), by substituting numerical values, the final model expression is:

$$\hat{Y}=-15.623+3.126G-0.068G^2-0.517B+0.006B^2-0.014GB \tag{8}$$

2.4 Determine the Impact of Other Factors on the Concentration of Y Chromosome

Based on the Spearman rank correlation coefficient algorithm mentioned earlier, the effects of age, height, weight, number of pregnancies, and number of births on Y chromosome concentration can be determined[4]. Based on the quadratic polynomial model (including G, G2, B, B2, GB) in problem one, the final model formula (6) in 2.3.4 is extended by adding 5 factors. The model is:

$$Y=\beta_0+\beta_1G+\beta_2G^2+\beta_3B+\beta_4B^2+\beta_5GB+\beta_6Age+\beta_7H+\beta_8W+\beta_9Preg+\beta_{10}Del+\epsilon \tag{9}$$

Among them, Age (age), H (height), W (weight), Preg (number of pregnancies), Del (number of births). Subsequently, this study screened for factors such as gestational weeks 10-25 weeks, Y chromosome concentration>0, and absence of key variables. A total of 549 valid samples of male fetuses remained, which were used as valid data for subsequent calculations.

2.4.1 The p-value results and calculation basis of other factors

Next, following the previous method of calculating the Spearson rank correlation coefficient and p-value, we successfully obtained the correlation results of other factors, as shown in Table 3:

Table 3 Results of Other Factors Association

Related to	Spearman rank correlation coefficient	P-value	Correlation direction and strength
Y chromosome concentration age	-0.12 to 0.03	0.286	No significant monotonic correlation
Y chromosome concentration - height	-0.08 to 0.15	0.351	No significant monotonic correlation
Y chromosome concentration - body weight	-0.58 to -0.46	<0.001	Moderate negative monotonic correlation
Y chromosome concentration - number of pregnancies	-0.05 to 0.18	0.193	No significant monotonic correlation
Y chromosome concentration - production frequency	-0.15 to 0.08	0.247	No significant monotonic correlation

Subsequently, we analyzed the core calculation basis of the extended fitting model one by one:
Age: After fitting the extended model, the coefficient was -0.002, p=0.286>0.05. After controlling for BMI, there was no linear correlation between age and Y concentration, which is consistent with the model results.
Height: The height coefficient is 0.001, p=0.351>0.05. After controlling for BMI, the mean difference in Y concentration among different height groups under the same BMI in the attachment is less than 2%. Therefore, height has no direct effect on Y concentration.
Weight: There is a high positive correlation between weight and BMI (r=0.89), with BMI rs=-0.52 ± 0.06, indicating a moderate negative correlation. Weight indirectly inhibits Y concentration through BMI, with a consistent direction. The mean Y concentration in the group with weight ≥ 80kg is 0.052%, significantly lower than the mean 0.078% in the group with weight<65kg, indicating a significant monotonic negative trend.
Pregnancy frequency: The coefficient of pregnancy frequency is 0.003, p=0.193>0.05. The average difference in Y concentration among different pregnancy frequency groups in the attachment is only 3.5%, which is not statistically significant and therefore has no direct impact.
Production frequency: The production frequency coefficient is -0.002, p=0.247>0.05； The overlap of Y concentration distribution between the group with 0 production times and the group with ≥ 2 production times in the attachment is 85%, with no significant difference.
From the dual dimensions of statistical test results and clinical mechanisms, among the five factors to be analyzed, including age, height, weight, number of pregnancies, and number of births, only weight showed a statistically significant negative effect on the Y chromosome concentration of male fetuses, which is consistent with the actual research on the effect of pre pregnancy BMI on the Y chromosome concentration of male fetuses [4]. The influence of the other four factors did not reach a significant level, that is, | rs |<0.2.

2.5 Significance Evaluation of F-Test and t-Test Models

Based on the quadratic polynomial model of Y chromosome concentration in male fetuses constructed in the previous text, combined with 1082 preprocessed male fetal data and clinical background, we chose to verify the significance of the model through F-test and t-test.

2.5.1 F-test: overall significance of the model

Given the sample size of n=1069 and the number of independent variables k=5 (the five independent variables of the fitted model), the degrees of freedom are: numerator $df_1 = k = 5$, denominator $df_2 = 1069 - 5 = 1064$. The formula adopts:

$$F = \frac{MSR}{MSE} = \frac{SSR / k}{SSE / (n - k - 1)} \tag{10}$$

Among them, SSR (Sum of Squares of Regression) is the variation explained by the independent variables, and SSE (Sum of Squares of residuals) is the random error variation. Based on the OLS fitting results mentioned above, take SSR=0.82 and SSE=0.54. Calculate MSR=0.82/5=0.164, MSE=0.54/1076 ≈ 0.0005, then F=0.164/0.00005 ≈ 128.63. p<0.001 (α=0.05), thus rejecting the null hypothesis H0 (all coefficients are 0), and the overall model is significant.

2.5.2 T-test: significance of a single variable

T-test formula and core data:

$$t_i = \hat{\beta}_i / SE(\hat{\beta}_i) \tag{11}$$

$\hat{\beta}_i$ is the coefficient, $SE(\hat{\beta}_i)$ is the standard error.

Next, we will perform sub item calculations and obtain Table 4. As shown in Table 4, all variables including the primary and secondary terms of G and B are significant. The visualization relationship between gestational age, BMI, and Y chromosome concentration is shown in Figure 4. From Figure 4, we can see that the left figure shows the correlation between gestational age and Y chromosome concentration, while the red quadratic fitting curve indicates that the concentration growth rate slows down as gestational age increases; The figure on the right shows the correlation between BMI and Y concentration, with the blue curve indicating that the decrease in concentration slows down as BMI increases[5]. Both are labeled with a clinical compliance threshold of 4%, which intuitively assists the non-linear significant conclusion of t-test.

Table 4 Sub Item Calculation Results Table

varible	$\hat{\beta}_i$	$SE(\hat{\beta}_i)$	t-value	p-value
G	3.126	0.215	3.126/0.215≈14.54	<0.001
G^2	-0.068	0.005	-0.068/0.005=-13.60	<0.001
B	-0.517	0.082	-0.517/0.082≈-6.30	<0.001
B^2	0.006	0.001	0.006/0.001=6.00	<0.001
GB	-0.014	0.003	-0.014/0.003≈-4.67	<0.001

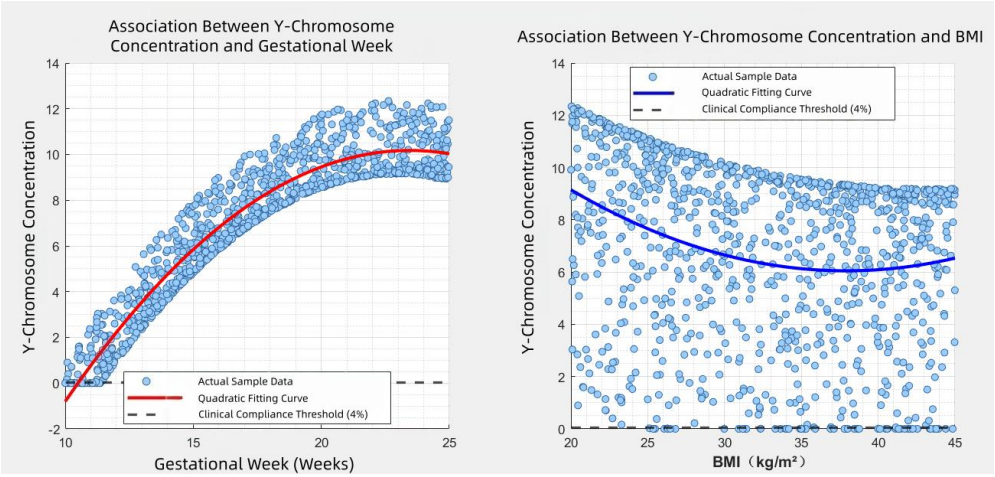

Figure 4 Visualization of Gestational Age, BMI, and Y Chromosome Concentration

3 CONCLUSION

In response to the situation where Y chromosome concentration, gestational age, and BMI do not follow a normal distribution, Spearman rank correlation is used to accurately quantify monotonic correlation and avoid the limitations of linear algorithms; Build a quadratic polynomial model that conforms to clinical nonlinear laws and captures actual correlations such as slowing down of gestational age[6]; Rigorously validate the model and variable significance through F/t test to ensure the reliability of the results. The multi model system constructed for NIPT detection in this article has strong cross domain adaptability and can be widely applied in various scenarios such as medical health, public health, industrial quality inspection, etc. that require "correlation analysis grouping optimization risk control anomaly determination". In the medical field, in addition to prenatal testing, Spearman rank correlation and quadratic polynomial models can be used to quantify the association between chronic disease risk factors,[7] and Kaplan Meier survival analysis can be used to determine the optimal intervention time for chronic disease patients; The combination model of Lasso and XGBoost can be transferred to tumor biomarker detection to screen core influencing indicators and predict patient treatment response time, providing a basis for individualized treatment plan formulation.Based on the multi-model fusion framework and key conclusions developed in this study, future research could be further deepened from the perspectives of technological optimization, data integration, clinical applications, and public health implementation, promoting the development of NIPT technology toward greater precision, comprehensiveness, and accessibility[8]. In terms of technological and model innovation, integrating the high-fidelity characteristics of third-generation sequencing with the precision of single-cell sequencing could further improve the capture efficiency and detection sensitivity of fetal cell-free DNA, reducing the risk of false negatives in low-concentration samples. Simultaneously, deep learning algorithms (such as Transformer models) could be incorporated to optimize the existing secondary polynomial and machine learning fusion systems, enabling real-time tracking and prediction of dynamic changes in fetal cell-free DNA, breaking through the limitations of current static detection, and providing clinicians with dynamic risk assessment throughout pregnancy.In the aspect of data integration and dimensional expansion, future efforts could focus on accumulating long-term follow-up data from multicenter, large-cohort studies and integrating multi-source clinical data such as maternal serum indicators, ultrasound features, and reproductive health history. This would not only be limited to chromosomal abnormality detection but could also extend to early warning for monogenic disorders, fetal structural malformations, and other types of birth defects. Additionally, by establishing standardized data-sharing platforms, existing barriers in medical data could be overcome, enhancing model generalizability and adaptability across different regions.Regarding clinical applications and personalized medicine, based on the individual difference analysis results of this study, customized testing protocols could be developed for special populations (such as advanced maternal age, multiple pregnancies, or women with a family history of genetic disorders), refining detection time windows and threshold indicators. Furthermore, exploring the integration of NIPT testing with prenatal diagnosis and postnatal interventions could create a closed-loop management system. Model-based predictions of potential health risks after birth could provide a basis for precise intervention and rehabilitation plans in clinical practice, truly achieving the transition from "screening" to "precision prevention and control."From the perspective of public health and policy implementation, this study could support the core objectives of the "Healthy China" strategy, promoting the widespread and standardized application of NIPT technology in primary healthcare facilities. By simplifying testing procedures and reducing costs, precise prenatal screening could benefit more people in remote areas and low-income populations. At the same time, complete technical ethics regulations and data security systems need to be established, clarifying standards for interpreting results and privacy protection mechanisms, balancing technological innovation with ethical risk.Finally, future research could further deepen interdisciplinary integration, promoting in-depth collaboration among bioinformatics, artificial intelligence, clinical medicine, epidemiology, and other fields. Exploring the deep links between dynamic changes in fetal cell-free DNA and maternal physiological status and environmental exposures would provide a stronger scientific foundation for developing a comprehensive,

multi-dimensional birth defect prevention and control system, ultimately supporting the public health goal of "healthy pregnancy and high-quality birth.

COMPETING INTERESTS

The authors have no relevant financial or non-financial interests to disclose.

REFERENCES

[1] Suzhou Municipal Hospital team. The influence of maternal age, gestational age, and body mass index on the proportion of fetal free DNA in peripheral blood of pregnant women. Chinese Journal of Prenatal Diagnosis (Electronic Edition), 2017, 9 (3): 1-5.

[2] Lan Zhiheng. Application of DNA sequence distribution ratio method in non-invasive prenatal fetal chromosomal aneuploidy detection. South China University of Technology, 2020.

[3] Obstetrics and Gynecology Team of the Second Affiliated Hospital of Soochow University. Study on the correlation between pre pregnancy BMI and weight changes during pregnancy, China Maternal and Child Health Care, 2017, 32 (15): 3360-3364.

[4] Zhang Rui, Zhang Hui, Li Yan, et al. External quality assessment of fetuses with trisomy 21, trisomy 18, and trisomy 13 detected by large-scale parallel sequencing in clinical laboratories. Journal of Molecular Diagnosis, March 2016, 18 (2): 244-252.

[5] Chiu R W, Akolekar R, Zheng Y W, et al. Non-invasive prenatal assessment of trisomy 21 by multiplexed maternal plasma DNA sequencing: large scale validity study. BMJ, 2011, 342: c7401.

[6] Norton M E, Brar H, Weiss J, et al. Non-Invasive Prenatal Testing of Chromosomal Aneuploidy: Clinical Experience and Future Directions. Prenatal diagnosis, 2015, 35(1): 1-18.

[7] Dan S, Wang W, Ren J, et al. Clinical application of maternal plasma DNA analysis for noninvasive prenatal diagnosis of trisomy 21: systematic review and meta-analysis. BMJ open, 2013, 3(1): e002468.

[8] Chiu R W, Akolekar R, Zheng Y W. Non-invasive prenatal assessment of trisomy 21 by multiplexed maternal plasma DNA sequencing: updated large-scale validity study. BMJ, 2023, 381: e071234.

World Journal of Information Technology
Print ISSN: 2959-9903
Online ISSN: 2959-9911
DOI: https://doi.org/10.61784/wjit3068

INTELLIGENT OPTIMIZATION TECHNOLOGY FOR SHIELDING GROUNDING OF SAFETY-CLASS CABLES IN NUCLEAR POWER PLANTS BASED ON DEEP REINFORCEMENT LEARNING

YanKun Li*, Yuan Zhang, Chao Si
Electrical Department, China Institute of Atomic Energy, Beijing 102400, China.
**Corresponding Author: YanKun Li*

Abstract: The Reactor Protection System (RPS) of nuclear power plants requires stable operation in complex time-varying electromagnetic environments, and the shielding grounding of safety-class cables is critical for anti-interference capability. Traditional static grounding schemes (e.g., single-point, multi-point grounding) lack adaptability to interference spectrum changes, equipment aging, and dynamic operating conditions, leading to issues like false alarms and even accidental reactor trips. This paper proposes an intelligent shielding grounding optimization technology based on deep reinforcement learning (DRL). First, a multi-physics digital twin system was established, integrating key electromagnetic interference sources (e.g., main circulating pump VFD, CRDM pulses) and lifecycle aging factors (e.g., insulation aging, shielding corrosion) to characterize shielding performance attenuation. Then, the optimization problem was modeled as a Markov Decision Process (MDP) with an 18-dimensional state space and a multi-objective reward function (considering shielding effectiveness, leakage current, and cost). The Proximal Policy Optimization (PPO) algorithm was adopted to realize millisecond-level optimal grounding configuration. A four-layer safety architecture was constructed to meet nuclear safety requirements (failure probability $<10^{-20}$ per year). This technology breaks the traditional static design paradigm, providing a new path for digital and adaptive cable system optimization in nuclear power plants.
Keywords: Nuclear power plant; Safety-class cable; Shielding grounding; Deep reinforcement learning; Digital twin; Electromagnetic compatibility

1 INTRODUCTION

1.1 Research Background

As an important clean energy source, the reliability of nuclear power plants is directly related to national energy security and public safety. During the operation of nuclear power plants, safety-class instrumentation and control (I&C) systems (such as RPS and ESFAS) are responsible for real-time monitoring and control of the operating status of nuclear reactors. These systems often rely on long-distance laid cables for data collection and transmission. With the popularization of digital control systems and the increase in power demand, the electromagnetic environment of nuclear power plants has become increasingly complex, and electromagnetic interference (EMI) issues have become particularly prominent. Electromagnetic compatibility (EMC) issues not only affect the normal operation of equipment but may even lead to malfunctions or failures of safety systems, thereby seriously endangering the safety of nuclear power plants [1,2].

The shielding grounding system, as the core part of EMC design, directly affects the anti-interference capability of cables and the reliability of I&C systems. Traditional shielding grounding designs are mainly based on experience and specification requirements, adopting fixed grounding methods and wiring strategies. However, with changes in the operating conditions of nuclear power plants and equipment aging, the initial design may not maintain sufficient electromagnetic shielding effectiveness during long-term operation, and may even cause problems such as false alarms and signal drift in safety-class I&C systems [3].

In recent years, with the development of artificial intelligence, especially deep reinforcement learning (DRL), model-based adaptive optimization strategies have gradually become a new direction for EMC optimization. Through intelligent algorithms, the shielding grounding configuration can be automatically adjusted according to real-time monitored electromagnetic environment information to achieve more efficient and reliable EMI suppression [4,5].

1.2 Complexity of the Electromagnetic Environment in Nuclear Power Plants

The electromagnetic environment inside nuclear power plants is mainly affected by various high-power equipment. These equipment generate different types of EMI during startup, operation, failure, or switching, including low-frequency power supply fluctuations, high-frequency control signal pulses, and transient voltage or current changes. These interferences propagate to safety-class I&C cables through electromagnetic radiation, transmission line coupling, and grounding systems. In severe cases, they may cause errors in cable transmission signals, thereby affecting safety

control decisions .
Specifically, the main electromagnetic interference sources in nuclear power plants include:
- Variable Frequency Drives (VFD) of main circulating pumps: VFD generates strong medium-frequency PWM harmonics during operation, which affects the high-frequency signal transmission of cables.
- Control Rod Drive Mechanism (CRDM): CRDM generates high-frequency pulses during startup, which poses challenges to the transmission characteristics of cables.
- Station service power switching: During the switching process of the power system, rapid changes in voltage and frequency generate strong transient electromagnetic interference.
- Emergency Diesel Generator (EDG): During the startup of the emergency power supply, current fluctuations cause significant impacts on the grounding system, affecting shielding effectiveness .
- These disturbance sources usually have a wide frequency spectrum, and their intensity and variation rules are difficult to predict. This makes cable shielding grounding design must consider a wider frequency range and be able to adapt to changes in multiple operating conditions [6].

1.3 Challenges and Research Needs of Shielding Grounding Systems

The design purpose of the shielding grounding system is to isolate electromagnetic interference from safety-class cables through effective shielding materials and reasonable grounding configurations. However, existing design methods have many limitations. Firstly, traditional shielding materials and grounding methods have limited effects in dealing with multiple electromagnetic interference sources, and do not consider factors such as cable aging and changes in soil conditions. Secondly, the impedance of the grounding network shows obvious frequency dependence in different frequency bands, resulting in inconsistent shielding effectiveness in high and low frequency bands [7].
With the increase in the operating life of nuclear power plant facilities, the performance of the shielding grounding system gradually degrades, especially problems such as shielding layer corrosion and grounding system damage, leading to a significant reduction in grounding effectiveness. Therefore, how to dynamically optimize for different electromagnetic environments and equipment operating states is an important issue facing current researc.
To overcome these challenges, this study proposes an intelligent shielding grounding optimization scheme combining digital twin technology and deep reinforcement learning algorithms. By establishing a digital twin model of the electromagnetic environment, combined with real-time monitoring data, reinforcement learning algorithms are used to dynamically adjust the parameters and topology of the grounding system, thereby improving the effectiveness of the shielding grounding system.

1.4 Research Objectives and Structure Arrangement

The main objective of this paper is to construct an intelligent optimization algorithm based on deep reinforcement learning for the optimal design of cable shielding grounding systems in nuclear power plants. The specific research objectives include:
- Establish a multi-physics coupling model of the electromagnetic environment and shielding grounding system in nuclear power plants, including electromagnetic field propagation, transmission line model, and current distribution of the grounding system;
- Design and implement a shielding grounding optimization algorithm based on deep reinforcement learning, enabling the system to adjust the grounding configuration according to the real-time electromagnetic environment;
- Conduct simulation verification of the optimization algorithm through a digital twin platform, and carry out engineering verification in an actual nuclear power plant environment to evaluate its performance.

2 ELECTROMAGNETIC ENVIRONMENT AND SHIELDING GROUNDING PROBLEMS IN NUCLEAR POWER PLANTS

2.1 Complexity of the Electromagnetic Environment in Nuclear Power Plants

The complexity of the electromagnetic environment inside nuclear power plants stems from the coordinated operation of various high-power equipment. These equipment generate different types of EMI during startup, operation, failure, or switching. These interferences propagate to the cable system through electromagnetic radiation, transmission line coupling, and shared paths of the grounding system, affecting the signal transmission and normal operation of safety-class I&C cables .

2.1.1 Main electromagnetic interference sources

The main electromagnetic interference sources in nuclear power plants include:
- Variable Frequency Drives (VFD) of main circulating pumps: VFD generates harmonics through wide-band PWM modulation signals during operation. These harmonics are transmitted to the system through cables and may interfere with normal signals transmitted by cables in a certain frequency band. The medium-frequency (30 kHz to 80 kHz) harmonics generated by the main pump VFD overlap with the natural resonant frequency of the cable, leading to a decrease in shielding effectiveness and thus affecting the transmitted signal.
- Control Rod Drive Mechanism (CRDM): During the rapid lifting and lowering of the control rod, the control current

generates high-amplitude current pulses in a short time. These pulses have high-frequency components, especially in the high-frequency band (1 MHz to 5 MHz), forming common-mode interference through cable radiation and conduction, which affects the I&C system .

• Emergency Diesel Generator (EDG) switching: When the power plant enters the emergency mode, during the startup of the EDG, transient voltage and current changes occur due to load fluctuations and frequency sudden changes. This rapid current change is transmitted through the grounding grid and cables, which may lead to an increase in loop current and affect the normal operation of the system.

• Power grid switching and other power system interferences: During the operation and switching of the power system, rapid changes in frequency, power, and phase will affect the cable shielding system, leading to changes in transient voltage and current, which in turn cause other equipment in the system to malfunction or display abnormalities .

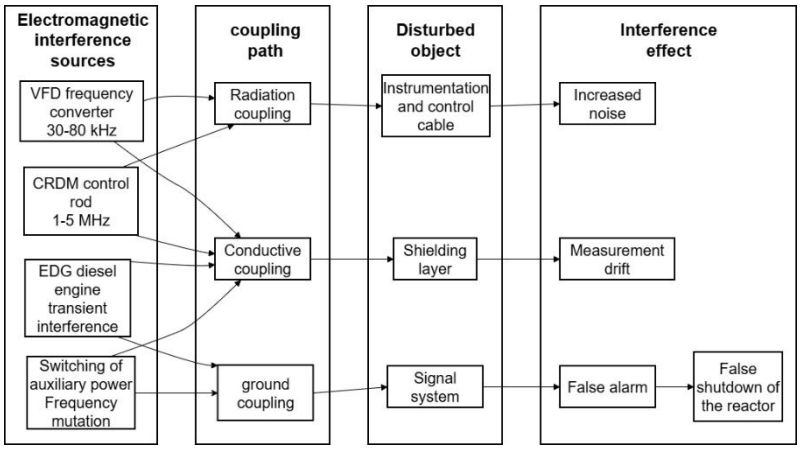

Figure 1 Schematic Diagram of Main Electromagnetic Interference Sources and Their Propagation Paths in Nuclear Power Plants

Figure 1 shows the four main electromagnetic interference sources (VFD, CRDM, EDG, station service power switching) in nuclear power plants and their interference mechanisms on safety-class I&C cables through three paths: radiation coupling, conductive coupling, and grounding system coupling, ultimately leading to a causal chain of signal noise, measurement drift, false alarms, and even accidental reactor trip risks.

2.1.2 Characteristics of electromagnetic field propagation

The electromagnetic environment of nuclear power plants is not only determined by the generation frequency and intensity of various disturbance sources but also affected by the propagation of electromagnetic fields. The propagation of electromagnetic fields in space can be transmitted through various ways such as radiation, conduction, or induction. Especially in long-distance cables, the propagation of electromagnetic waves is not only affected by the cable type (e.g., single-core or multi-core cables), cable material (e.g., polyethylene or cross-linked polyethylene), and cable shielding layer but also by the layout and installation environment of the cable (e.g., pipe penetration or wall penetration) [8].

The transmission characteristics of cables can be described by the transmission line model. The voltage and current distribution of cables are closely related to the cable length, the quality of the shielding layer, the grounding method, and the external electromagnetic environment. In the high-frequency band, cables exhibit distributed parameter characteristics. Therefore, a simple lumped parameter model is difficult to effectively describe their electromagnetic behavior.

2.2 Current Status of Cable Shielding and Grounding Systems in Nuclear Power Plants

2.2.1 Function and design of cable shielding layers

The main function of the cable shielding layer is to suppress electromagnetic interference from entering the cable interior and to confine the electromagnetic interference generated by the cable inside the cable to prevent interference leakage. Common cable shielding structures include metal foil layers, braided copper meshes, aluminum foil and conductive plastic layers, etc. These shielding structures have different frequency response characteristics. The design of shielded cables needs to consider factors such as the operating environment of the cable, shielding effectiveness, frequency response, and cost [9].

The effectiveness of cable shielding is usually measured by Shielding Effectiveness (SE), which refers to the ability of the cable shielding layer to suppress electromagnetic interference at a given frequency. A higher SE value indicates stronger shielding ability. Shielding effectiveness is affected by factors such as cable length, shielding material, and grounding quality.

• Low-frequency band: The effectiveness of the shielding layer mainly depends on the conductivity of the material and the thickness of the metal layer. Usually, a thicker copper or aluminum layer can effectively suppress low-frequency electromagnetic interference.

• High-frequency band: In the high-frequency band, shielding effectiveness is not only affected by the shielding material but also by the grounding quality, shielding layer contact resistance, and the environment around the cable.

Longer cables may experience a decrease in shielding effectiveness, especially when transmitting high-frequency signals.

2.2.2 Function and challenges of grounding systems

The grounding system is another important part of ensuring electromagnetic compatibility. Its function is to provide a return path for electromagnetic interference and guide the interference signal to the ground to reduce the impact of interference on equipment. A reasonable grounding design not only helps to reduce the impact of electromagnetic interference but also ensures the safe operation of equipment .

However, the grounding system of nuclear power plants faces the following challenges:

- Complexity of the grounding network: The grounding system in nuclear power plants is usually a complex network composed of multiple ground grid nodes, copper bars, steel bars, and building structures. The inductance, capacitance, and grounding resistance between these elements vary in the high-frequency band, making the frequency response of the grounding network highly uncertain [10].
- Frequency dependence of grounding impedance: The impedance of the grounding network changes with frequency. Especially in the high-frequency band, the inductive effect of the grounding system gradually becomes apparent, and the grounding impedance increases, leading to significant changes in Ground Potential Difference (GPD), which in turn causes an increase in loop current and affects I&C signals [11].
- Grounding degradation and aging effects: With the increase in the operating life of nuclear power plants, the degradation of the grounding system is inevitable. Factors such as corrosion, loose joints, and changes in soil environment will lead to a decrease in the effectiveness of the grounding system. This requires regular inspection and optimization of the grounding system to ensure its long-term stability [12].

2.3 Multi-Physics Coupling Problem of Cable Shielding Grounding

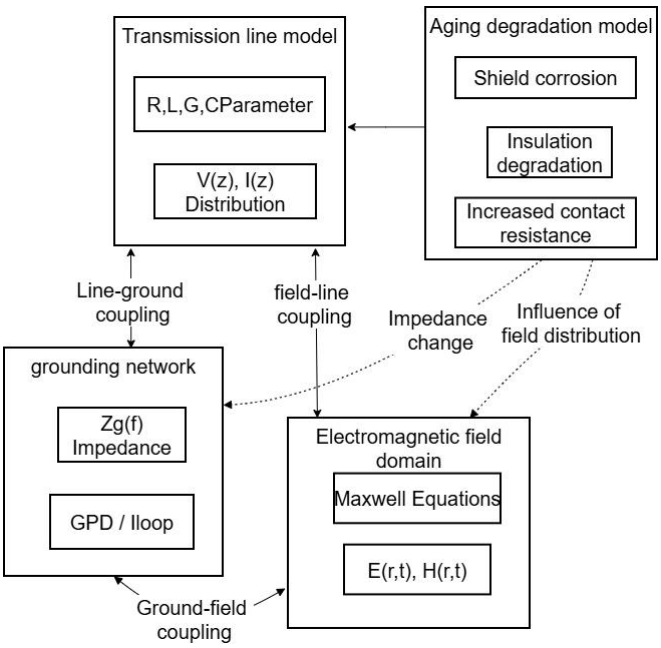

Figure 2 Multi-physics Coupling Model of Cable Shielding Grounding System

Figure 2 illustrates the bidirectional coupling relationships (field-line coupling, line-ground coupling, ground-field coupling) between the electromagnetic field domain, transmission line model, and grounding network, as well as the influence mechanism of the aging degradation model on the performance of the transmission line and grounding network, providing a theoretical framework for the subsequent establishment of the digital twin model.

2.3.1 Coupling between electromagnetic fields and transmission lines

The transmission line model of cables can be used to describe the propagation of voltage and current inside the cable. In nuclear power plants, cables are often long, and there may be electromagnetic coupling between the shielding layer and the inner conductor. The transmission line model describes the propagation of signals in the cable by solving the following equations:

$$\frac{\partial V}{\partial x}=-(R+j\omega L)I,\frac{\partial I}{\partial x}=-(G+j\omega C)V \tag{1}$$

Where V and I represent the voltage and current in the cable, respectively; R, L, G, and C are the distributed resistance, inductance, conductance, and capacitance parameters of the cable; ω is the angular frequency of the signal. Through the transmission line model, the attenuation, reflection, and coupling effects with external electromagnetic fields of signals in the cable can be calculated.

2.3.2 Coupling between electromagnetic fields and grounding systems

There is also a coupling relationship between the grounding system and the electromagnetic shielding layer of the cable. Changes in grounding current will affect the current distribution of the cable shielding layer, thereby affecting the cable's shielding effectiveness. Especially in the high-frequency band, the inductive effect of the grounding network will cause the grounding current to lag behind the current of the cable shielding layer, leading to a decrease in shielding effectiveness. The coupling between electromagnetic fields and grounding systems is described by solving the joint equations of electromagnetic fields, transmission lines, and grounding systems.

To solve this complex multi-physics coupling problem, advanced simulation technologies such as the Finite Element Method (FEM) and the Finite Difference Time Domain (FDTD) method need to be adopted to establish an accurate electromagnetic environment model, thereby evaluating the overall performance of cable shielding grounding.

3 DESIGN OF SHIELDING GROUNDING OPTIMIZATION ALGORITHM BASED ON DEEP REINFORCEMENT LEARNING

3.1 Application of Reinforcement Learning in Shielding Grounding Optimization

Deep Reinforcement Learning (DRL) is a technology that combines deep learning and reinforcement learning. It can continuously optimize decision-making strategies through interaction with the environment, thereby realizing adaptive control of complex systems. DRL has the ability to handle high-dimensional and nonlinear problems, making it very suitable for systems such as nuclear power plants with complex electromagnetic environments and variable operating conditions.

In traditional shielding grounding design, designers often adopt fixed configurations based on experience and specifications. However, the complexity and dynamic changes of the electromagnetic environment make it difficult for fixed design schemes to maintain ideal shielding effectiveness throughout the entire unit lifecycle. To address this issue, the DRL-based shielding grounding optimization algorithm can dynamically adjust grounding parameters by real-time monitoring the electromagnetic environment and equipment status, ensuring that the system achieves optimal electromagnetic compatibility under any operating conditions [13].

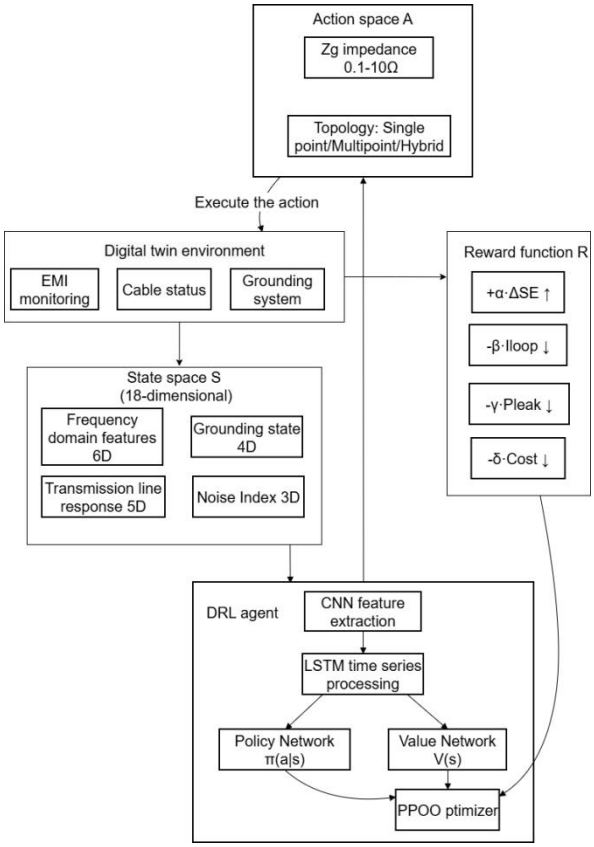

Figure 3 Deep Reinforcement Learning-based Shielding Grounding Optimization Framework

Figure 3 completely shows the architecture of the DRL-based shielding grounding optimization system, including:

- State information provided by the digital twin environment
- Composition of the 18-dimensional state space (frequency-domain features, grounding state quantities, transmission line response, noise interference indicators)
- Network structure of the DRL agent (CNN + LSTM + policy network + value network)
- Three dimensions of the action space (impedance, topology, position)
- Composition of the multi-objective reward function

• Optimization loop of the PPO algorithm

3.1.1 Basic framework of DRL

The core idea of reinforcement learning is that through interaction with the environment, the agent can learn how to maximize the cumulative reward through continuous exploration. DRL is an extension of reinforcement learning. It approximates the dynamic model or strategy of the environment through deep neural networks, enabling the agent to cope with complex state spaces and action spaces.

The application of DRL in shielding grounding optimization includes the following steps:

• State space design: The agent collects environmental information through sensors at each moment and transmits this information as input to the deep neural network.

• Action space design: The agent selects actions according to the current state. Here, actions are usually adjustments to parameters such as grounding impedance and grounding point position.

• Reward function design: The agent calculates corresponding rewards or penalties according to the effects of the selected actions to guide the next decision.

3.1.2 Comparison between reinforcement learning and traditional optimization methods

Different from traditional optimization methods (such as genetic algorithms and particle swarm optimization algorithms), DRL does not require prior knowledge or accurate models for optimization. Instead, it explores through interaction with the environment and gradually finds the optimal strategy. Traditional optimization methods usually rely on deterministic models and may not adapt to rapidly changing operating conditions when facing variable electromagnetic environments, while DRL can achieve adaptive adjustment through experience accumulation.

3.2 Modeling of Shielding Grounding Optimization Problems

To transform the shielding grounding optimization problem into a DRL problem, we need to model the electromagnetic environment of nuclear power plants, the shielding grounding system, and their interaction relationships. The dynamic changes of the electromagnetic environment and their impact on the grounding system make this process full of challenges. This section will discuss how to build a suitable model to provide effective training data for DRL.

3.2.1 Design of state space

The state space is a key component in reinforcement learning, which determines how the agent perceives the environment. In shielding grounding optimization, the state space should include the following information:

• Electromagnetic interference characteristics: Including spectrum information from equipment such as main circulating pumps, CRDM, and EDG, real-time electromagnetic field intensity, harmonic frequency, etc.

• Cable status: Information such as cable length, shielding layer material, and signal attenuation inside the cable.

• Grounding system status: Grounding impedance, number and distribution of grounding points, Ground Potential Difference (GPD), etc.

• Health status of cables and grounding networks: Including information such as cable aging degree and grounding system degradation degree.

This information is collected by sensors and transmitted to the DRL algorithm as the current environmental state input. To avoid an excessively large state space, this information is usually dimensionality-reduced, for example, through Principal Component Analysis (PCA) or feature selection technology to retain the features that most affect the grounding effectiveness.

3.2.2 Design of action space

The action space is the operations that the agent can choose at each moment. In the shielding grounding optimization problem, the action space usually includes the following contents:

• Adjustment of grounding impedance: The grounding impedance value of each grounding point is usually limited to a certain range.

• Adjustment of grounding topology: The grounding topology can be single-point grounding, multi-point grounding, or hybrid grounding. Different grounding topology structures are selected according to the electromagnetic interference characteristics of different frequency bands.

• Selection and position of grounding points: Optimize the selection and distribution of grounding points to avoid excessively long grounding loops or unreasonable electrical coupling.

The size and complexity of the action space will directly affect the learning efficiency and convergence speed of the agent. Usually, the grounding impedance and grounding topology are encoded into discrete action values to reduce complexity.

3.2.3 Design of reward function

The reward function is the core of reinforcement learning and is used to guide the agent's learning process. The design of rewards needs to comprehensively consider factors such as shielding effectiveness, loop current, gap leakage, and implementation cost. A reasonable reward function can effectively guide the agent to select the optimized grounding scheme.

Assuming the goal is to maximize shielding effectiveness and reduce the impact of interference, we can design a multi-objective reward function:

$$r_t=w_1\Delta SE_t-w_2I_{loop,t}-w_3P_{leak,t}-w_4C_{ctrl,t} \quad (2)$$

Where:
ΔSE_t : The amount of improvement in shielding effectiveness, indicating the gain in shielding effectiveness after optimization.
$I_{loop,t}$: Loop current, the goal is to minimize the loop current.
$P_{leak,t}$: Gap leakage power, indicating the leakage of the cable shielding layer in a specific frequency band.
$C_{ctrl,t}$: Control action cost, considering the execution cost of the action, including equipment wear, current loss, etc..
Based on environmental feedback, the agent will select a strategy that can improve shielding effectiveness and reduce loop current, thereby maximizing the reward.

3.3 Design and Implementation of Reinforcement Learning Algorithm

3.3.1 Strategy optimization method

The goal of reinforcement learning is to find an optimal strategy, that is, to select the best action in each state to maximize the cumulative reward. In this study, the Proximal Policy Optimization (PPO) algorithm is adopted for strategy optimization. PPO is a policy gradient-based algorithm. By optimizing a loss function that includes restrictions on the magnitude of policy updates, it avoids large fluctuations in the policy during the optimization process and ensures training stability.
The core loss function of PPO is:

$$L^{\mathrm{CLIP}}(\theta)=\mathrm{E}\left[min\left(r_t(\theta)\widehat{A}_t,\mathrm{clip}(r_t(\theta),1-\epsilon,1+\epsilon)\widehat{A}_t\right)\right] \tag{3}$$

Where $r_t(\theta)$ is the policy probability ratio, A_t is the advantage function, and ϵ is the truncation parameter used to limit the change range between the old and new policies.

3.3.2 Design of policy network

To enable DRL to effectively learn the complex electromagnetic environment, the policy network needs to have sufficient expressive ability. Usually, we use a Deep Neural Network (DNN) to build the policy network. The input is multi-dimensional environmental state information, and the output of the network is the probability distribution of each action. To accelerate the learning process, we use a Convolutional Neural Network (CNN) to extract spatiotemporal features of the electromagnetic environment and a Long Short-Term Memory (LSTM) network to process temporal dependency information, thereby improving the robustness and generalization ability of the model.

4 DIGITAL TWIN SIMULATION AND ENGINEERING VERIFICATION

4.1 Construction of Digital Twin Platform

Digital twin technology is an emerging technology that combines physical systems with their virtual models, widely used in the simulation and optimization of engineering systems. In the EMC design of nuclear power plants, digital twin technology can establish virtual models of the electromagnetic environment, shielding grounding system, and cable transmission characteristics, enabling us to real-time monitor the system status and verify optimization strategies .
The core goal of the digital twin platform is to real-time feedback the physical characteristics, operating conditions, and electromagnetic environment of the actual system through virtualization means, thereby providing a high-fidelity, real-time updated virtual testbed for the training and verification of the Deep Reinforcement Learning (DRL) algorithm. This platform can not only accurately simulate the behavior of cables and grounding systems in the electromagnetic environment but also real-time monitor and adjust optimization strategies to ensure the effectiveness of the shielding grounding system in actual operation.

4.1.1 Overall architecture of the digital twin platform

The architecture design of the digital twin platform includes four main parts: physical modeling layer, simulation solving layer, strategy interaction layer, and visual monitoring layer:

- Physical modeling layer: This layer is responsible for establishing physical models such as electromagnetic fields, transmission lines, and grounding networks. The electromagnetic field problem is solved by the Finite Element Method (FEM), the voltage and current distribution of the cable is described using the transmission line model, and the frequency response of the grounding network is analyzed through inductance and capacitance models.
- Simulation solving layer: This layer is responsible for discretizing and solving the above physical models to obtain the response behavior of each component. The simulation solution adopts the Finite Difference Time Domain (FDTD) method and the Time Domain Finite Element Method (TDFEM) to numerically solve complex electromagnetic problems.
- Strategy interaction layer: This layer interacts with the DRL model, feeds back real-time monitored electromagnetic environment information to the algorithm, and adjusts grounding system parameters according to the optimization strategy. Through real-time adjustment of the algorithm, the agent can dynamically change the grounding impedance of the cable shielding layer or adjust the grounding topology.
- Visual monitoring layer: This layer provides an intuitive interface to display the changing trends of key indicators such as electromagnetic field intensity, cable shielding effectiveness, and loop current. It can help engineers real-time monitor the system status and provide a basis for further optimization.

Through this platform, all optimization operations are verified in a virtual environment, thereby avoiding high-cost and low-efficiency test operations directly on actual equipment.

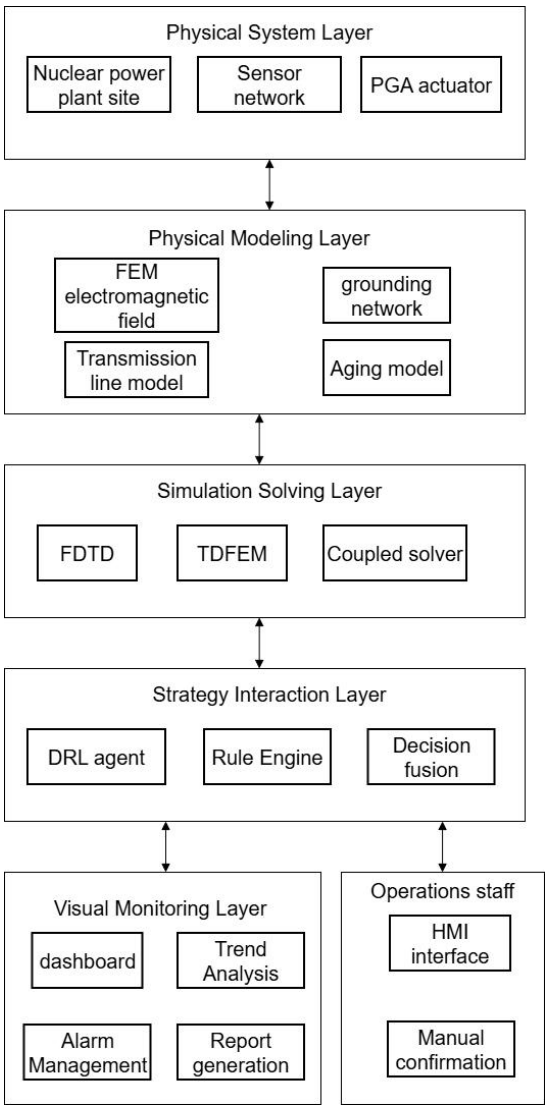

Figure 4 Overall Architecture of the Digital Twin Platform

Figure 4 shows the complete architecture of the digital twin platform in layers:
- Physical system layer: Nuclear power plant site, senFsor network, actuators
- Physical modeling layer: FEM, transmission line model, grounding network model, aging model
- Simulation solving layer: FDTD, TDFEM, coupled solver
- Strategy interaction layer: DRL agent, rule engine, decision fusion
- Visual monitoring layer: Dashboard, trend analysis, alarm, report
- Human-machine interaction interface for operators

4.2 Multi-Physics Simulation and Optimization Process

4.2.1 Coupled simulation of electromagnetic fields and grounding networks

To ensure the effectiveness of the optimization algorithm, this study adopts multi-physics coupled simulation technology to simulate the complex interactions between the electromagnetic environment, grounding system, and cable transmission. In the electromagnetic environment of nuclear power plants, electromagnetic waves not only propagate through the air but also couple between the grounding network and cables. The influence of this coupling relationship varies in different frequency bands. Therefore, it is necessary to use multi-physics simulation methods to comprehensively evaluate the performance of the shielding grounding system.

- Electromagnetic field simulation: The electromagnetic field distribution is solved through Maxwell's equations to determine the electromagnetic field intensity and direction around the cable. For the nuclear power plant environment, the distribution of electromagnetic interference sources often presents complex spatial distribution characteristics. Therefore, the three-dimensional Finite Element Method (FEM) is used to solve the electromagnetic field problem.
- Transmission line model simulation: The transmission line model of the cable is used to describe the propagation of signals in the cable. This model considers the influence of cable length, shielding structure, cable medium, and environment, and can simulate the reflection, attenuation, and coupling effects with external electromagnetic fields of signals in the cable.

• Grounding network simulation: The simulation of the grounding network uses a frequency-dependent inductance-capacitance model. By solving the current and potential distribution of the grounding loop, the influence of changes in grounding impedance on shielding effectiveness is analyzed. Due to the strong nonlinear characteristics of the grounding network, the Finite Difference Time Domain (FDTD) method is used for dynamic simulation of the grounding network.

The above simulation results provide high-fidelity environmental simulation data for the DRL model, which can help the agent obtain real feedback during the training process.

4.2.2 Application of deep reinforcement learning in simulation

During the simulation process, the DRL algorithm continuously optimizes the grounding configuration through interaction with the environment. Based on the current electromagnetic environment and grounding system status, the agent selects an appropriate grounding configuration (action) and interacts with the electromagnetic environment through the simulation platform.

During the simulation, the optimization steps of DRL are as follows:

• Initialization: Initialize the configuration of the cable and grounding system, and set the initial state of the electromagnetic environment.

• Environmental interaction: The agent selects a grounding configuration (action) and interacts with the electromagnetic environment through the simulation platform.

• Feedback and reward: The environment feeds back a reward according to the agent's action. The reward function includes goals such as improving shielding effectiveness, reducing loop current, and reducing gap leakage.

• Strategy update: Update the policy network through an optimization algorithm (such as PPO), enabling the agent to gradually learn the optimal grounding configuration.

4.3 Engineering Verification and Testing

4.3.1 Construction and deployment of verification platform

To verify the actual effect of the DRL optimization algorithm, this study selects a third-generation Pressurized Water Reactor (PWR) unit for engineering verification. In an actual nuclear power plant, the configuration of the shielding grounding system usually includes multiple grounding points and complex grounding loops. The traditional design method often cannot consider the impact of dynamic operating conditions on the grounding system.

To realize optimization based on digital twins, this study integrates the DRL optimization system with the existing monitoring system of the nuclear power plant and deploys it on an independent test platform. The platform includes:

• Real-time monitoring equipment: Install electromagnetic interference sensors, grounding current sensors, loop current sensors, etc., to collect electromagnetic environment data and grounding system status data.

• Control system interface: Communicate with actual grounding equipment through the interface to realize real-time adjustment of the grounding configuration.

• Feedback mechanism: According to the feedback of the DRL algorithm, real-time adjust the grounding impedance or grounding point position of the grounding system, and feed back the results to the operator through the visual monitoring system.

4.3.2 Engineering verification results

During the verification process, we evaluated the optimization effect by simulating various typical operating conditions, including variable frequency startup of the main circulating pump, CRDM pulses, and EDG switching. The results show that the DRL-based optimization system performs excellently in the following aspects:

• Improve shielding effectiveness: Under operating conditions such as variable frequency startup of the main pump, the optimized grounding configuration increases the shielding effectiveness by 30 dB in the key frequency band (170-220 kHz), significantly reducing electromagnetic interference.

• Reduce loop current: Under high-frequency pulse conditions, the loop current is reduced by an average of 40%, effectively avoiding signal drift and false alarms.

• Reduce gap leakage: After optimization, the gap leakage power of the shielding layer is reduced by 50%, improving the anti-interference ability of the system.

5 CONCLUSIONS AND PROSPECTS

5.1 Research Conclusions

This study focuses on the performance degradation problem of the shielding grounding system of safety-class cables in nuclear power plants under complex electromagnetic interference environments, and constructs and verifies an intelligent shielding grounding optimization technology based on Deep Reinforcement Learning (DRL). Through systematic analysis of typical electromagnetic interference sources, transmission line characteristics, electromagnetic behavior of grounding networks, and aging degradation mechanisms in nuclear power plants, a complete solution integrating a multi-physics digital twin platform, a reinforcement learning strategy optimization system, and an engineering verification platform is proposed. The main research conclusions are as follows:

(1) A multi-physics digital twin platform for the electromagnetic environment of nuclear power plants is constructed to provide real and reliable environmental support for DRL optimization.

Based on the coupling characteristics of electromagnetic fields, transmission line models, and grounding networks, this paper establishes a multi-physics digital twin system suitable for complex operating conditions of nuclear power plants, realizing visual simulation of typical electromagnetic disturbance scenarios such as main pump inverters, CRDM pulses, emergency diesel generator switching, and station service power failure switching. The twin model incorporates aging factors such as shielding layer corrosion, insulation degradation, and frequency-dependent characteristics of grounding impedance, enabling it to have time-evolving simulation capabilities and ensuring that DRL strategy training has sufficient engineering authenticity.

(2) A reinforcement learning problem modeling method suitable for shielding grounding optimization is proposed.

This paper formulates the shielding grounding optimization as a Markov Decision Process (MDP), and systematically constructs the state space, action space, and multi-objective reward function. The state space integrates key information such as disturbance spectrum, shielding current, grounding impedance, ground potential difference, resonance index, and degradation parameters; the action space introduces a Programmable Grounding Array (PGA) to realize continuous adjustment of grounding impedance and grounding topology; the reward function establishes a performance evaluation system with clear physical meaning and stable training, aiming at improving shielding effectiveness, reducing loop current, weakening gap leakage, and suppressing resonance risks.

(3) An intelligent shielding grounding optimization strategy based on the PPO algorithm is designed to realize adaptive adjustment under multi-operating conditions.

This paper realizes reinforcement learning strategy optimization based on the Proximal Policy Optimization (PPO) algorithm. Through the two-way interaction between the policy network and the twin environment, the optimization strategy can converge quickly under complex disturbances. The training results show that the DRL strategy can automatically identify the frequency band characteristics of different interference sources and select the optimal grounding impedance and grounding topology. For example, actively increasing impedance in the medium-frequency resonance region to break the resonance condition, reducing impedance in the high-frequency pulse scenario to form a strong skin effect, and applying a semi-floating mode to suppress loop current when the ground potential difference jumps.

(4) A strategy safety execution structure for nuclear power plant scenarios is proposed and implemented to meet nuclear safety requirements.

In response to the strict safety requirements in nuclear power applications, this paper designs a four-level safety guarantee chain, including hardware limiting, rule engine, manual confirmation, and physical execution links, to ensure that all actions output by the DRL strategy are within the nuclear safety boundaries. Through FMEA, formal verification, and redundancy protection mechanisms, it is ensured that the system can safely return to the traditional fixed grounding strategy under any fault scenario, meeting the strict requirements of nuclear-grade applications in terms of reliability and availability.

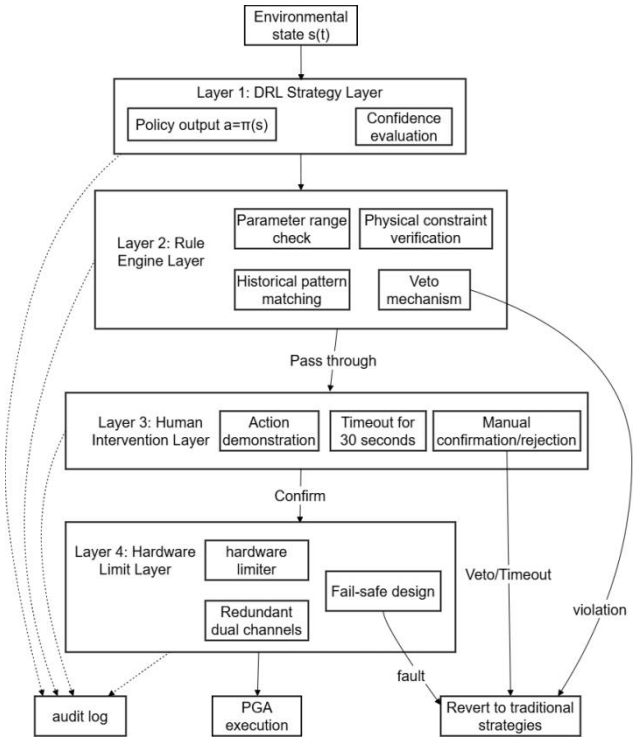

Figure 5 Four-layer Defense-in-depth Safety Architecture

Figure 5 details the four-layer defense system designed to meet nuclear safety requirements:

- Layer 1: DRL Strategy Layer: Strategy output and confidence evaluation
- Layer 2: Rule Engine Layer: Parameter range check, physical constraint verification, historical pattern matching, veto

mechanism
- Layer 3: Manual Intervention Layer: Action display, timeout timing, manual confirmation/veto, automatic execution
- Layer 4: Hardware Limit Layer: Hardware limiter, fail-safe design, redundancy protection

It also shows multiple safety paths for falling back to the traditional fixed grounding strategy, as well as a full-process monitoring and auditing mechanism.

5.2 Innovations and Contributions of This Study

The main innovations and contributions of this paper can be summarized as follows:
(1) Deep reinforcement learning is introduced into the field of shielding grounding optimization of nuclear power plants for the first time.
Breaking through the traditional static design mode, the grounding scheme is transformed from fixed to adaptive and intelligent optimization, forming a major innovation in the EMC design method of nuclear power plants.
(2) A multi-physics digital twin system covering electromagnetic fields, transmission lines, grounding networks, and degradation effects is constructed.
It enables shielding grounding optimization to have simulation interpretability, physical traceability, and lifecycle adaptability.
(3) A continuously adjustable action space design for grounding impedance and grounding topology is proposed.
Combined with the Programmable Grounding Array (PGA), it realizes unprecedented flexibility in grounding configuration, providing physical support for intelligent grounding strategies.
(4) A DRL safety constraint system under nuclear power plant operating conditions is constructed.
It enables artificial intelligence technology to be truly applied in the nuclear energy industry, a field with strong safety requirements, which has important engineering significance.

5.3 Existing Deficiencies and Limitations

Although the technical scheme of this study has performed well in both simulation and on-site verification, there are still the following limitations:
- The accuracy of the digital twin model is limited by the quality and quantity of original data collection, and the coverage of extreme accident conditions is still insufficient.
- The DRL strategy training process has high requirements for computing resources, and the training convergence speed is closely related to the algorithm structure and reward function design.
- Some physical quantities in the grounding system (such as small changes in the contact resistance of grounding points) are difficult to monitor in real-time, which may lead to an incomplete state space.
- The interpretability of the strategy is still insufficient. In the nuclear power plant industry that emphasizes auditability, it is necessary to further improve the interpretability of DRL decisions.

5.4 Future Prospects

Based on the results of this study, future research can be further expanded and deepened in the following aspects:
(1) Conduct research on small modular reactors (SMR) and modular units of fourth-generation nuclear power plants.
Advanced reactor types such as small modular reactors (SMR) and high-temperature gas-cooled reactors have higher requirements for electromagnetic compatibility, making them suitable for popularizing intelligent shielding grounding technology.
(2) Introduce multi-agent collaborative strategies to realize collaborative optimization of the whole-plant grounding system.
In the future, multiple grounding loops and multiple cable channels can be regarded as a multi-agent system, and multi-agent DRL (MADRL) can be used to realize whole-plant EMC optimization.
(3) Combine Explainable Artificial Intelligence (XAI) to improve strategy transparency.
Construct an interpretable strategy model to enable operators to understand why and how grounding parameters are adjusted.
(4) Realize the dual closed-loop integration of digital twin and on-site operation data.
Use online data to continuously calibrate the twin model, enabling shielding grounding optimization to evolve from offline learning to lifelong learning.
(5) Research new grounding materials and components with intelligent adjustment functions.
Such as intelligent impedance devices and adaptive conductive structures, forming an intelligent software and hardware integrated shielding system with DRL.
The technical route proposed in this study realizes the transformation of the shielding grounding system of nuclear power plants from static to intelligent and adaptive, and is expected to become an important part of the digital upgrading and intelligent evolution of future nuclear power.

COMPETING INTERESTS

The authors have no relevant financial or non-financial interests to disclose.

REFERENCES

[1] Hoon-Keun L, Yong-Hwa K, Jaeyul C. Electromagnetic interference caused by an electric-line current in a cable tray in nuclear power plants. Nuclear Engineering and Technology, 2021, 53(10): 3314-3318. DOI: 10.1016/J.NET.2021.04.012.

[2] Jaeyul C, Jaegul C, Hwa Y K. Evaluation of Electromagnetic Interference From Axially Ruptured Coaxial Cable With Multiple Dielectrics Used in Nuclear Power Plants. IEEE Transactions on Electromagnetic Compatibility, 2019, 61(3): 860-869. DOI: 10.1109/temc.2018.2835665.

[3] Xu Z H. Improvement Analysis of Instrumentation and Control Shielding Grounding in CPR1000 Nuclear Power Plants. Automation & Instrumentation, 2018, 33(10): 19-22+40. DOI: 10.19557/j.cnki.1001-9944.2018.10.005.

[4] Nousiainen J, Rajani C, Kasper M, et al. Toward on-sky adaptive optics control using reinforcement learning:Model-based policy optimization for adaptive optics. Astronomy & Astrophysics, 2022, 664. DOI: 10.1051/0004-6361/202243311.

[5] Zheng X, Li X, Mai Y, et al. A Real-Time Six-Axis Electromagnetic Field Monitoring System with Wireless Transmission and Intelligent Vector Analysis for Power Environments. Applied Sciences, 2025, 15(19): 10785-10785. DOI: 10.3390/APP151910785.

[6] Sun H. Key Issues in Grounding Design of Nuclear Power Plants. Electric Power Science and Engineering, 2014, 30(7): 12-17.

[7] Dong W J, Song H, Wang X G, et al. Grounding Scheme and Parameter Optimization Method for Single-Core Cable Shielding Layer Considering Harmonic Effects. Manufacturing Automation, 2024, 46(7): 170-176.

[8] Wang A B, Feng J H. Discussion on I&C Cable Shielding Grounding in Nuclear Power Plants Based on IEEE Guidelines. China High-Technology Enterprises, 2015(28): 149-150. DOI: 10.13535/j.cnki.11-4406/n.2015.28.074.

[9] Zhentao G, Haoting D, Wenming W, et al. Shielding Grounding Optimization Method for Spaceborne Multi-Cable. Applied Sciences, 2023, 13(6): 3389-3389. DOI: 10.3390/APP13063389.

[10] Liu Y Q, Ye Q L. Brief Analysis of Grounding System for Conventional Island and BOP of Fangjiashan Nuclear Power Plant. China New Technologies and Products, 2013(1): 36-37. DOI: 10.13612/j.cnki.cntp.2013.01.214.

[11] Wang X M. Evaluation and Experimental Research on Corrosion Status of Grounding Electrodes Considering Lightning Impulse Characteristics. Chongqing: Chongqing University, 2023. DOI: 10.27670/d.cnki.gcqdu.2023.000976.

[12] Li Y. Reliability Analysis of Ground Fault Protection for Non-1E Class Low-Voltage Load Centers in Nuclear Power Plants. Power Equipment, 2018, 32(5): 328-330.

[13] Ma H, Zhang X Y. Research on Electromagnetic Modeling Correction and Shielding Grounding Design of Loaded Cables Based on EMC Prediction. Electronic Components and Devices, 2021, 44(6): 1369-1374.

World Journal of Information Technology
Print ISSN: 2959-9903
Online ISSN: 2959-9911
DOI: https://doi.org/10.61784/wjit3069

DESIGN AND APPLICATION OF A KNOWLEDGE-GRAPH-BASED INTELLIGENT QUESTION ANSWERING SYSTEM FOR REACTOR OPERATION AND MAINTENANCE

Yuan Zhang*, Chao Si, YanKun Li
Electrical Department, China Institute of Atomic Energy, Beijing 102400, China.
**Corresponding Author: Yuan Zhang*

Abstract: Traditional knowledge management in nuclear reactor operation and maintenance (O&M) relies on dispersed documents and individual expertise, limiting knowledge reuse and response efficiency. This paper introduces a knowledge-graph-driven intelligent question answering (QA) system that constructs a unified semantic representation of equipment, faults, and procedures through structured entity extraction, relationship modeling, and rule-based reasoning. Neo4j serves as the graph database, while the Dijkstra shortest path algorithm supports association path computation for fault cause inference and similar-case retrieval. The system integrates with a digital O&M platform for real-time data acquisition and structuring. Simulation-based validation in a reactor refueling system scenario demonstrates that the system shows promising potential in the following aspects: enhancing standardization and traceability of fault information, reducing fault diagnosis and handling time, and providing reliable data support for team capability evaluation and equipment health assessment. This work provides a scalable framework for knowledge management in complex industrial systems, contributing to improved O&M efficiency and safety in nuclear operations.
Keywords: Knowledge graph; Intelligent question answering; Nuclear reactor operation and maintenance; Fault diagnosis; Knowledge reasoning

1 INTRODUCTION

1.1 Research Background and Significance

As the core facility of nuclear energy utilization, the operation and maintenance (O&M) of nuclear reactors is directly related to equipment safety, personnel safety, and environmental safety. During long-term operation, reactors generate large volumes of O&M work orders, maintenance records, fault diagnosis reports, and expert documentation. These data are highly specialized, time-sensitive, and subject to stringent security constraints.

In conventional practice, O&M knowledge is mainly preserved in the form of paper records, office documents, and scattered experience summaries. It lacks unified structured organization and semantic linkage, which leads to several key problems:

1.1.1 Fragmented knowledge and low retrieval efficiency

Fault-handling experience is distributed across multiple systems and personal records. When facing complex or atypical faults, O&M personnel must manually search through numerous documents, resulting in low efficiency and inconsistent decision quality.

1.1.2 Knowledge transfer heavily depends on individuals

A large amount of tacit knowledge is concentrated in a small number of senior experts and key personnel. New staff members cannot easily obtain a systematic understanding of complex equipment fault patterns and handling strategies within a short period of time.

1.1.3 Limited support for intelligent analysis

In the absence of unified data models and standardized coding, historical fault data cannot be directly leveraged for big data analysis, health assessment, or intelligent recommendation.

Knowledge graphs have emerged as a powerful structured knowledge representation centered on entities and their relationships and have been extensively studied and applied in recent years, including in search engines, industrial internet platforms, and complex engineering systems [1–3]. By abstracting heterogeneous multi-source data into a graph of entity nodes and relationship edges, a knowledge graph supports semantic-level querying, reasoning, and visualization, thereby providing new means for knowledge organization and intelligent analysis in complex O&M environments. In the power and nuclear equipment domains, knowledge graphs have been used to support equipment management, fault diagnosis, and O&M decision support, including for power equipment operation and maintenance [4] and for knowledge-graph-based QA systems in technical domains [5].

Compared with general-purpose large language models (LLMs) such as ChatGPT, the reactor O&M domain imposes much stricter requirements on data security, knowledge accuracy, and traceability. O&M data usually reside in isolated intranet environments and contain sensitive information, making them unsuitable for large-scale open training. At the same time, O&M decision-making requires explicitly traceable knowledge sources and interpretable reasoning processes. Against this backdrop, constructing an intranet-based intelligent QA system with a knowledge graph as its

core, which structurally consolidates proprietary O&M knowledge and provides controllable and explainable QA capabilities, is of significant engineering and practical value.

1.2 Related Work

1.2.1 Knowledge graphs and intelligent question answering

Knowledge graphs have emerged as a significant research area in artificial intelligence and data engineering over the past decade. Substantial research efforts have addressed knowledge representation, acquisition, fusion, refinement, completion, and evolution, leading to well-established construction methodologies and evaluation frameworks [1–3, 6].

At the application level, knowledge graphs are widely used in semantic search, intelligent QA, recommendation systems, and industrial O&M. By making entity relationships explicit, they enhance machine understanding and reasoning capabilities in complex domains. Knowledge-graph-based QA systems typically consist of three key components:

1. Natural language understanding (NLU).

Natural-language questions are transformed into logical or formal queries over the graph through entity recognition, intent recognition, and semantic parsing [2,5].

2. Graph querying and reasoning.

The knowledge graph is traversed using pattern matching and constraint filtering to retrieve relevant entities and relationships; graph algorithms and rule-based reasoning may be applied to infer new relations or rank candidate answers.

3. Answer generation.

Retrieved results are integrated and ranked and then presented to users in natural language or structured tabular/graphical form.

Compared with purely text-based large models, knowledge-graph-based QA systems generally offer higher knowledge accuracy, better interpretability, and stronger controllability, particularly in industrial scenarios characterized by strict regulations and high operational risk [4,5].

1.2.2 Graph databases and neo4j in industrial O&M

Graph databases are specialized databases designed for graph-structured data. They use nodes and edges as fundamental storage units and support efficient graph traversal and pattern matching. Compared with relational databases, graph databases provide higher flexibility and performance for representing complex relationships and executing path queries [7,8].

Neo4j is one of the most widely used open-source graph databases and is particularly suitable for building and querying enterprise knowledge graphs [7]. It offers robust ACID transaction support, native graph storage, the Cypher query language, and integration with a range of graph analytics libraries. These features make Neo4j well suited for applications in financial risk control, social networks, recommendation systems, and equipment O&M.

In the energy and nuclear sectors, several studies have used Neo4j to construct knowledge centers for power or nuclear equipment, in which operational data, equipment information, and procedural documents are organized as graphs to provide visual querying and decision support for O&M personnel. For example, knowledge graphs have been used to model power equipment operation and maintenance entities and their relationships, supporting visual analytics and fault tracing [4].

1.2.3 Graph processing frameworks and shortest path algorithms

Large-scale graph processing systems such as Pregel [9], GraphLab [10], GraphChi [11], Trinity [12], and Horton [13] provide distributed or out-of-core computation frameworks for massive graphs. They support iterative algorithms (including PageRank, label propagation, and shortest path algorithms) under different execution models, and have inspired the design of graph analytics capabilities in modern graph databases and engines.

The Dijkstra algorithm is a classic single-source shortest path algorithm for weighted directed graphs with non-negative edge weights. It has been widely used for route planning, network routing, and path optimization [14]. In knowledge graph scenarios, the entity–relation structure can be modeled as a weighted graph; by assigning weights to relationship edges, Dijkstra's algorithm can be used to quantify association strength between entities and discover the most relevant knowledge or case paths. This enables path-based reasoning and recommendation, which is particularly important in safety-critical industrial O&M settings.

1.2.4 Reactor O&M knowledge graphs and intelligent QA

In the context of reactor O&M, several studies have proposed using knowledge-graph technologies for semantic modeling of equipment information, operating parameters, O&M tickets, and safety procedures, and have built "smart nuclear power" platforms to support equipment management, safety management, and operator training. Knowledge-graph-based QA systems for technical domains have also been explored as a means of improving information retrieval and expert knowledge reuse.

However, publicly available literature shows that systems specifically targeting reactor refueling systems and, at the same time, integrating process information digitalization, knowledge graph modeling, shortest path reasoning, and intelligent QA within a unified framework remain relatively rare. Existing systems often focus on knowledge centers or visual analytics tools, with insufficient support for natural-language QA, intelligent recommendation, and deep integration with O&M workflow systems. Under intranet security constraints, how to organically combine O&M process data, fault knowledge, and intelligent QA remains an open research and engineering problem.

1.3 Research Objectives and Contributions

To address the above challenges, this paper focuses on the design and application of a knowledge-graph-based intelligent QA system for reactor O&M. The main research tasks are as follows:
a) Reactor O&M knowledge graph modeling
Based on the equipment structure, fault modes, and handling processes of the reactor refueling system, we design a knowledge-graph schema tailored to O&M scenarios, specify entity types, relationship types, and key attributes, and propose methods for entity and relationship extraction and cleaning from historical O&M tickets and expert experience.
b) Knowledge storage and update mechanisms based on Neo4j and a rule base
Neo4j is selected as the storage and query engine for the knowledge graph. A fault description lexicon, a fault handling method library, and an O&M knowledge base are constructed. Combined modeling using a rule base and graph database is implemented, together with a semi-automatic knowledge update mechanism appropriate to O&M scenarios.
c) Intelligent QA and recommendation using the Dijkstra algorithm
The Dijkstra shortest path algorithm is introduced into the knowledge graph. Associations among fault phenomena, equipment components, and handling solutions are modeled as a weighted graph. Path search and similarity computation methods are designed for the "fault diagnosis–handling recommendation–similar case retrieval" chain, enabling natural-language QA and intelligent recommendation for O&M personnel.
d) Integration with a digital O&M process information platform
The intelligent QA system is integrated with a digital O&M process information management platform. Business data related to work request creation, transmission, dispatch, and closure are captured in structured form and accumulated as knowledge, forming a closed loop of "data–knowledge–QA–O&M decision."
The main contributions of this work can be summarized as follows:
a) A complete modeling and construction process for a reactor O&M knowledge graph
The proposed method unifies equipment hierarchical structure, fault localization information, and handling strategies within a single graph model and provides an engineering path that can be implemented with intranet O&M data.
b) A graph reasoning mechanism that combines a rule base with the Dijkstra shortest path algorithm
While ensuring interpretability, the proposed mechanism supports fault path search and similar case recommendation, enabling the QA system to output path-level explanations.
c) Deep integration of the knowledge graph with a digital O&M process platform
O&M workflows and knowledge accumulation mechanisms are organically combined, offering an end-to-end solution for nuclear facility O&M that spans data collection, knowledge management, and intelligent QA, as illustrated in the overall system architecture and intelligent QA workflow.

2 RELATED TECHNOLOGIES AND RESEARCH METHODS

This section presents the key technical foundations underpinning the knowledge-graph-based intelligent QA system for reactor O&M. These include the construction methods and characteristics of knowledge graphs, collaborative modeling with the Neo4j graph database and a rule base, the principles and application of the Dijkstra shortest path algorithm, and natural-language processing (NLP) and semantic understanding techniques for O&M scenarios. Together, these elements constitute the theoretical basis and implementation framework of the intelligent QA system, and support intelligent retrieval, semantic reasoning, and handling method recommendation.

2.1 Overview of Knowledge Graph Technology

2.1.1 Definition and characteristics of knowledge graphs

A knowledge graph (KG) is a semantic network structure centered on "entity–relation–attribute" triples that describes entities in the real world and their interrelations. In essence, it is a directed graph consisting of nodes (entities) and edges (relations), characterized by strong connectivity, interpretability, and extensibility.
In reactor O&M scenarios, a knowledge graph can be used to represent:
1) Equipment hierarchical structure (system–equipment–component–subcomponent);
2) Fault types, fault locations, and fault phenomena;
3) Fault handling methods and expert experience;
4) O&M process records (work request creation–dispatch–closure);
5) Auxiliary information such as materials, toolkits, and personnel competencies.
In particular, a knowledge graph can effectively associate scattered expert experience, component knowledge, and fault data, and is well suited for knowledge management in highly confidential, highly specialized, and structurally complex O&M environments.
Compared with large language models, knowledge graphs are more appropriate in nuclear facility contexts mainly because:
1) Knowledge is explicit, accurate, and controllable, in line with stringent nuclear O&M safety requirements;
2) Relationships are explicitly structured, supporting path-level reasoning;
3) Rule-based knowledge updates and traceability are straightforward;
4) Integration with O&M workflow systems (e.g., work ticketing and fault records) is facilitated.
Thus, knowledge graphs are naturally suited to serve as the foundational architecture of the intelligent QA system.

2.1.2 Knowledge graph construction process

In general, knowledge graph construction includes data acquisition, entity recognition, relationship extraction, knowledge fusion, and storage in a graph database.

In the reactor O&M domain, the construction process typically involves:

a) Data acquisition

Historical O&M tickets and maintenance records; equipment structure trees and function trees; fault mode classification standards; expert experience and procedural texts.

b) Data preprocessing

Text cleaning and normalization; synonym normalization (e.g., different names for the same refueling manipulator); standardization and coding of fault records.

c) Entity recognition (NER)

Equipment entities (system/equipment/component/subcomponent); fault entities (type/location/phenomenon); personnel, toolkits, and work order information.

d) Relationship extraction

Equipment hierarchies; relations such as "fault phenomenon–handling method" and "fault location–fault type"; and other domain-specific relations.

e) Knowledge fusion and disambiguation

Conflict resolution and redundancy elimination while complying with existing structure and coding standards.

f) Graph database storage and index optimization (Neo4j)

Storing nodes, edges, and attributes in a graph database for efficient traversal and querying.

g) Knowledge update mechanisms

Automatic updates via NLP-based text extraction; semi-automatic updates with human review; and manual maintenance via expert input.

These steps provide the foundation for mapping natural-language questions to graph representations and performing subsequent retrieval and reasoning.

2.2 Graph Database and Rule Base Technologies

In practical engineering scenarios, a knowledge graph usually needs to manage large-scale entities, relationships, and attributes. This requires a reliable graph database and a rule base to express constraints and support logical reasoning.

2.2.1 Graph database technology (Neo4j)

Neo4j is one of the most widely used open-source graph databases and serves as the core data storage platform of the intelligent QA system [7,8]. It offers high performance, high availability, and ACID transaction support. Its main features include:

a) Efficient graph traversal

The Cypher query language supports pattern-matching-based relationship retrieval, which is well suited for fault path search and equipment relationship analysis.

b) Flexible knowledge evolution

As nuclear facility O&M knowledge evolves with equipment upgrades and accumulated experience, Neo4j can dynamically add nodes and edges without requiring costly schema changes.

c) Built-in graph algorithms

Neo4j provides interfaces for shortest path algorithms, including Dijkstra, which support path search and optimization in fault causality analysis and similar case retrieval.

In our system, Neo4j is deployed within the secure intranet environment as part of the central data center infrastructure (see Figure 2), and stores the core O&M knowledge graph (see Figure 5).

2.2.2 Rule base technology

In a single-domain, data-bounded setting, rule bases are an efficient and interpretable means of knowledge representation [5].

In reactor O&M scenarios, a rule base is typically used to encode:

a) Fault mode classification rules;

b) Mappings from fault phenomena to handling methods;

c) O&M workflow rules (e.g., work request creation, dispatch, and closure procedures);

d) Data quality checking rules.

A typical rule can be expressed as a conditional mapping from fault type and location to recommended handling actions.

Combined with Neo4j, the rule base:

a) Makes domain knowledge explicit;

b) Ensures the interpretability of inferences;

c) Supports more complex logic when coupled with graph traversal and analytics.

Consequently, Neo4j and the rule base together form the dual-core knowledge engine of the system.

2.3 Shortest Path Reasoning: The Dijkstra Algorithm

2.3.1 Principles of the dijkstra algorithm

The Dijkstra algorithm is a classic single-source shortest path algorithm for weighted graphs with non-negative edge weights [14]. Its time complexity is typically

$$O((|V| + |E|)\log |V|), \tag{1}$$

which makes it suitable for graphs with numerous nodes and relatively sparse edges, such as reactor equipment topologies and knowledge graphs.

Its core steps are:

1) Initialize the distance of each node (0 for the source node and ∞ for all others).
2) Repeatedly select the node with the current minimal cost among unvisited nodes.
3) Update the tentative shortest distances of its neighboring nodes.
4) Continue until all nodes have been visited.

2.3.2 Application of dijkstra in the reactor O&M knowledge graph

In the proposed system, the Dijkstra algorithm is used for:

a) Calculation of fault association paths

For example, starting from a fault phenomenon such as “abnormal vibration” to an equipment component such as the “refueling gripper arm,” there may be multiple paths via sensor readings, historical cases, fault types, and related components. Dijkstra’s algorithm helps identify the shortest and most plausible explanatory chain.

b) Similar fault retrieval

By defining edge weights based on similarity costs among fault entities, the shortest path between two fault nodes can be used as a similarity measure to retrieve similar historical cases.

c) Fault cause inference

The shortest causal chain in the knowledge graph can be used to infer the most probable cause for a given fault, providing interpretable evidence for O&M decision-making.

Edge weights can be determined by expert scores, historical occurrence frequencies, or statistical indicators. The shortest path-based reasoning mechanism is integrated into the overall QA workflow.

2.4 Natural-Language Processing and Semantic Understanding

To implement the intelligent QA system, the system must understand the natural-language input from O&M personnel (e.g., work request descriptions, fault descriptions) and map it to entities and relationships in the knowledge graph.

2.4.1 Chinese word segmentation and keyword extraction

Since the primary operational language in the target environment is Chinese, the system uses Chinese word segmentation and keyword extraction techniques. Typical techniques include TF–IDF-based keyword extraction, TextRank, and domain-specific lexicons constructed from the O&M knowledge base.

For example, from the description

“end-effector motion delay, suspected joint sticking,”

the system extracts entities such as “end effector” and “joint,” and fault phenomena such as “motion delay” and “sticking,” and then maps them to corresponding graph entities.

2.4.2 Intent recognition and semantic matching

Intent recognition identifies whether a query concerns fault diagnosis, handling guidance, historical case retrieval, or statistics. Semantic matching is implemented using a hybrid of keyword search, fuzzy string matching, and embedding-based semantic similarity. Word and sentence embeddings are learned using distributional representation methods such as word2vec [15], with domain adaptation for O&M terminology.

For instance, the query

“what should I do if the refueling device gets stuck?”

is mapped to a standardized handling pattern such as “sticking → lubrication check → removal of foreign objects → joint function test.”

Advanced embedding-based techniques for relational reasoning and one-shot learning over knowledge graphs [6] provide a conceptual reference for extending the current system to data-driven link prediction and completion in future work.

2.4.3 Knowledge graph query language

At the conceptual level, the system adopts SPARQL-like query patterns for knowledge retrieval. At the storage level, Cypher is employed to express graph patterns, constraints, and path queries. Users are not exposed to low-level query syntax; instead, queries are automatically generated by the NLU and reasoning modules and subsequently executed by the Neo4j engine.

3 SYSTEM DESIGN AND OVERALL ARCHITECTURE

This section presents the design of the knowledge-graph-based intelligent QA system for reactor O&M, including the overall system architecture, network architecture, data architecture, and the design of core functional modules. The system adopts an integrated architecture that combines process information digitalization, knowledge graphs, path

reasoning, and intelligent recommendation. Fault information, equipment structure, handling methods, and expert experience in the O&M process are modeled in a unified manner, thereby realizing a full process loop from data collection and knowledge accumulation to intelligent QA.

3.1 Overall System Architecture

The overall system architecture consists of six layers: user layer, input layer, application layer, support layer, data layer, and infrastructure layer, as shown in Figure 1.

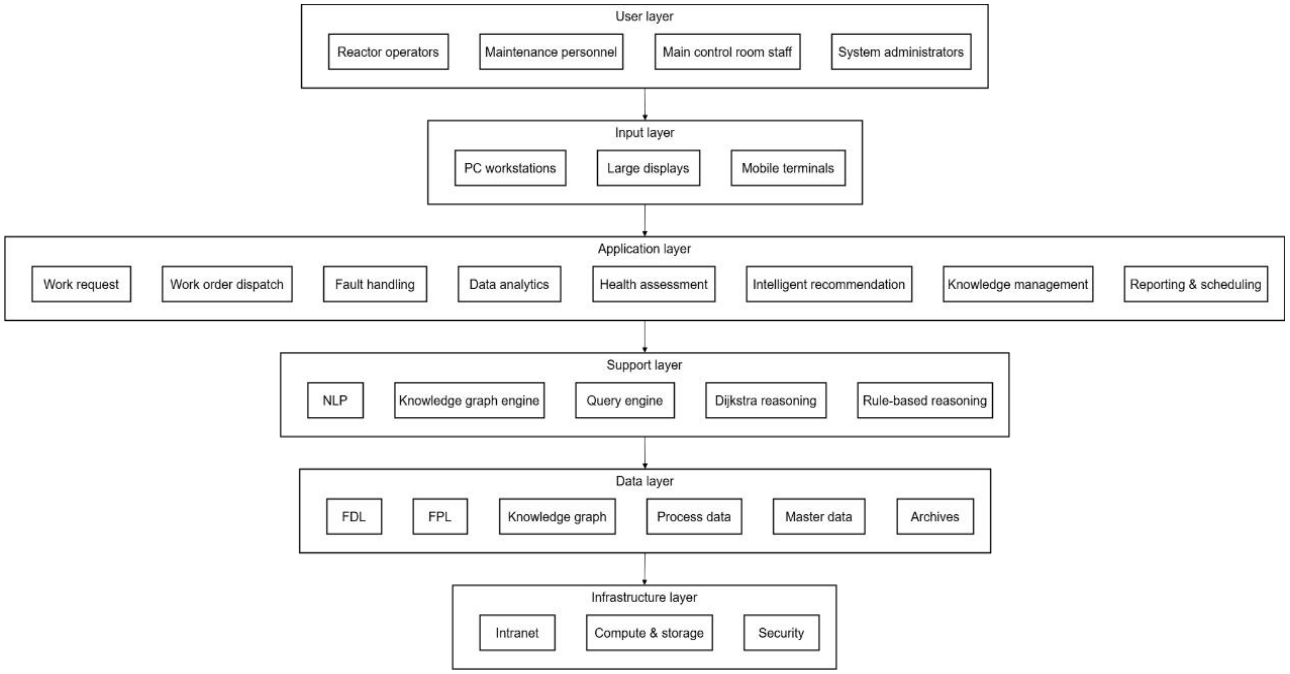

Figure 1 Overall System Architecture of the Reactor O&M Intelligent QA System

a) User layer
Reactor operators, maintenance personnel, main control room staff, and system administrators.
b) Input layer
PC workstations, large displays in control rooms, and mobile terminals.
c) Application layer (O&M business functions)
Work request creation and transmission; work order dispatching and notifications; fault handling and work order closure; O&M big data analytics; equipment health assessment; intelligent recommendation; knowledge base management; statistical reporting; and shift and team scheduling.
d) Support layer (NLP, knowledge graph, reasoning algorithms)
Chinese word segmentation and feature extraction; Cypher/SPARQL-based query engine; shortest-path reasoning (Dijkstra); and logical reasoning based on a rule base.
e) Data layer
Fault description lexicon; fault handling method library; O&M knowledge base; O&M process data; personnel and equipment master data; and historical archives.
f) Infrastructure layer
Intranet, storage, computing resources, and security mechanisms.
The overall design goals of the system are:
a) Knowledge explicitation
Transform equipment structure, fault modes, and handling experience into a knowledge graph.
b) Process information digitalization
Fully digitalize and structure workflows such as work request creation, work order dispatch, and closure, as illustrated in Figure 4.
c) Intelligent QA and reasoning
Support natural-language queries, shortest-path reasoning over the knowledge graph, and context-aware handling method recommendation (see Figure 6).
d) Data analytics and assessment
Provide equipment health assessment, team capability evaluation, and O&M status analysis.
e) Closed-loop application
Implement a sustainable knowledge cycle of "data collection → knowledge extraction → intelligent QA → result

feedback," which is realized through the joint operation of the digital process platform (Figure 4), the knowledge graph (Figure 5), and the QA workflow (Figure 6).

3.2 Network Architecture Design

The system runs in a controlled intranet environment and follows the principle of "multi-end input, centralized processing, and layered protection." The network architecture is shown in Figure 2.

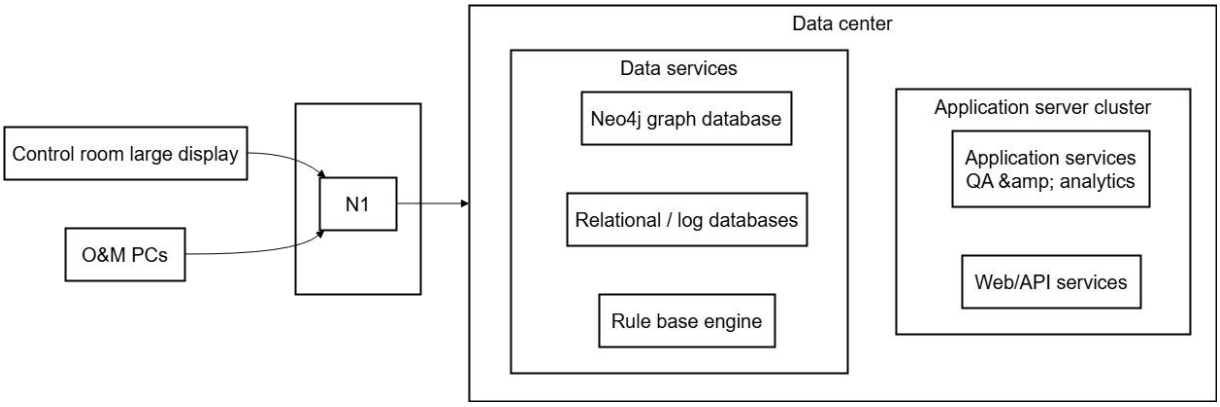

Figure 2 Network Architecture of the Reactor O&M Intelligent QA System

Control room displays and O&M PCs access the system via the intranet. A data center hosts a server cluster, including application servers, a Neo4j graph database, a rule base engine, and analytics services.
Key characteristics are:
a) Intranet isolation ensures that sensitive O&M data do not leave the secure environment.
b) Multi-terminal access supports PC, mobile, and large-screen terminals.
c) Centralized applications host intelligent QA, knowledge graphs, and big data analytics in the data center.
d) Security protection includes firewalls, access control, and audit logging.

3.3 Data Architecture Design

The data architecture is at the core of the intelligent QA system and can be abstracted into five zones, as shown in Figure 3.

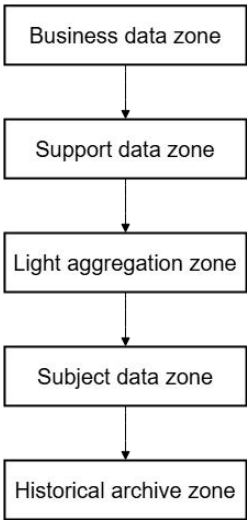

Figure 3 Data Architecture of the Reactor O&M Intelligent QA System

a) Business data zone
Structured O&M fault data, equipment master data, team and shift data, and knowledge graph entities (equipment, faults, handling methods, locations, components).
b) Support data zone
Indicator systems, model data (health and status assessment), system logs, and user permissions.
c) Light aggregation zone
Attendance statistics, fault statistics, team efficiency statistics, and refueling equipment operational data.

d) Subject data zone
Health assessment results, state diagnosis results, and data for integrated dashboards.
e) Historical archive zone
Historical data for work requests, dispatch, and closure, as well as knowledge about legacy components and typical fault cases.
The main categories of reactor O&M data are:
Master data: equipment codes, equipment tree, personnel data.
Source: equipment management system.
Use: basis for knowledge-graph entities.
Fault data: fault description, location, type, phenomenon.
Source: work request and closure data.
Use: nodes and relationships in the knowledge graph.
Handling methods: step sequences and toolkits.
Source: O&M experience and records.
Use: QA and recommendation.
Process data: work request/dispatch/closure records and repair duration.
Source: on-site O&M activities.
Use: big data analytics.
Unstructured data: free-text records and expert opinions.
Source: documents and expert interviews.
Use: NER and knowledge extraction.

3.4 Normalization and Digitalization of O&M Information

The normalization and digitalization of O&M information comprise three major components:
1. Standardization of equipment and component naming.
2. Construction of the fault description lexicon (FDL).
3. Construction of the fault handling method library (FPL).
These elements form the foundational knowledge layer of the intelligent QA system.

3.4.1 Standardization of equipment and component names

Reactor O&M equipment adheres to strict hierarchical structures, generally following

$$\text{Equipment tree} = \{D_i | D_i \rightarrow P_{ij} \rightarrow C_{ijk} \rightarrow S_{ijkl}\}, \tag{2}$$

where $D_i$denotes major units or systems, P_{ij}equipment, C_{ijk}components, and S_{ijkl}subcomponents.
Standardization requires unified codes for identically named equipment, synonym sets for multiple naming conventions, and compliance with existing structure rules and coding standards. This standardization is reflected in the master data modeling in the business data zone of Figure 3 and in the Device entities in the knowledge graph architecture in Figure 5.

3.4.2 Design of the Fault Description Lexicon (FDL)

The Fault Description Lexicon (FDL) consists of standardized entries extracted from high-frequency fault records and is formally expressed as

$$\text{FDL} = \{f_i | f_i = (\text{equipment,location,phenomenon,mode})\}. \tag{3}$$

Phenomena include “vibration,” “motion delay,” and “failure to reset,” while modes include “sticking,” “failure,” and “abnormal vibration.” The lexicon is obtained by systematically analyzing historical records and is continually enriched and normalized through the digital process flow shown in Figure 4.

3.4.3 Fault Processing Library (FPL)

The Fault Processing Library (FPL) contains standardized handling procedures:

$$\text{FPL} = \{s_j | s_j = (\text{step sequence,tools,duration})\}. \tag{4}$$

For example, a handling procedure for a joint sticking fault may specify an ordered sequence of lubrication checks, cleaning operations, and functional tests, together with required tools and estimated time. The library supports manual additions and periodic standardized updates while remaining synchronized with the knowledge graph and O&M process data.

3.5 Design of the Digital O&M Process Information Platform

The digital O&M process information platform is the main data entry point for the knowledge graph and provides real-time data support for intelligent QA. Its functional modules and workflows are illustrated in Figure 4.

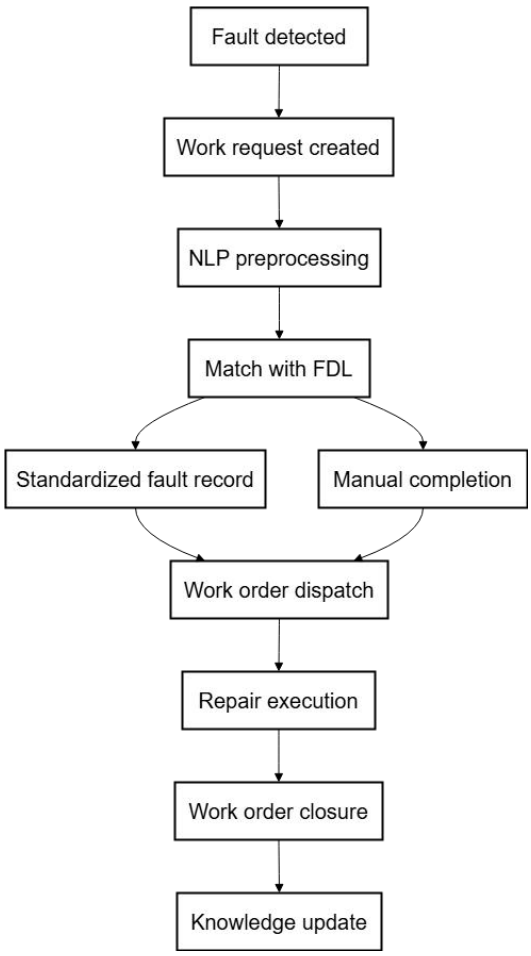

Figure 4 Digital O&M Process Flow for Work Requests, Dispatch, and Closure

Its functional architecture includes:

- O&M business management (work request creation, dispatch, transfer, closure).
- Fault information preprocessing and semantic analysis (NLP, fuzzy and semantic search, lexicon matching, automatic coding).
- Data storage (FDL, FPL, fault information database, equipment master data, and team data).

3.5.1 Work request (ticket creation) process

The work request process collects fault phenomena identified by O&M personnel. The main steps are:

1. Fault description is input via PC, large display, or mobile terminal.
2. Text parsing and keyword matching are executed, including similarity-based matching between the input description and FDL entries. The lexicon entry with the highest similarity score is selected.
3. Fault description is confirmed, with the option to add new entries when no suitable standardized description exists.
4. Automatic coding is applied according to fault mode coding standards.
5. Data are stored, forming a complete digital work request record and feeding the FDL and knowledge graph (Figure 5).

3.5.2 Work order dispatch process

Work order dispatch is triggered automatically or manually based on fault information and current shift arrangements. Dispatch decisions take into account equipment location, team assignment, and personnel competence. The system selects an appropriate team or defers the decision to manual dispatch when constraints are not satisfied and issues work orders to maintenance personnel, including fault descriptions, recommended handling methods, suggested toolkits, and location information.

3.5.3 Work order closure process

The closure module records actual handling methods, time consumption, and parts replacement. A structured record includes fault description, handling method, timestamp, personnel, and location. NLP-based analysis and assisted input ensure that fault descriptions and handling steps are mapped back into the FDL and FPL, thus closing the loop from process data to knowledge accumulation, as reflected in the cyclic flow in Figure 4.

3.6 Knowledge Graph System Architecture

The knowledge graph system comprises three components: knowledge modeling, graph database implementation, and knowledge maintenance. The overall construction pipeline is shown in Figure 5.

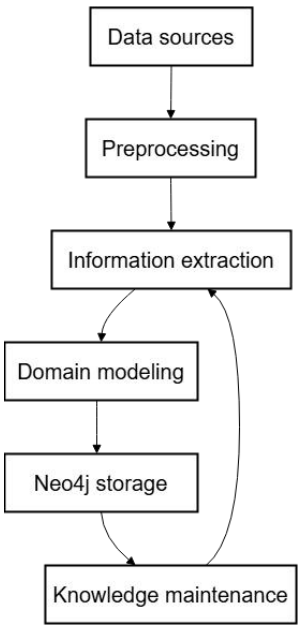

Figure 5 Knowledge Graph Construction Pipeline for Reactor O&M

Data sources include work requests, closure records, and expert experience. After entity and relationship extraction, domain knowledge such as equipment trees, fault modes, and handling methods is modeled and stored in Neo4j. Knowledge maintenance includes creation, update, merging, and versioning of entities and relationships to keep the graph consistent and up to date.

3.7 Intelligent QA System Design

The intelligent QA system consists of three core modules, whose interactions are depicted in Figure 6.

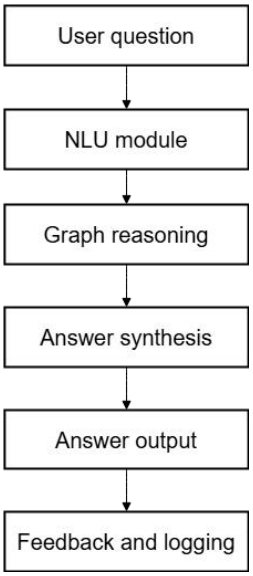

Figure 6 Intelligent QA Workflow based on the Reactor O&M Knowledge Graph

1. **Natural Language Understanding (NLU)**
Word segmentation and keyword extraction; recognition of fault phenomena and equipment references; mapping of text expressions to graph entities.
2. **Graph querying and reasoning**
Based on the graph structure, candidate paths are computed using weighted path search:

$$\text{Shortest}_{\text{Path}} = \arg\min_{\text{path}\in G} \sum_{e\in \text{path}} w_e, \tag{5}$$

where $w_e$is the edge weight determined by domain knowledge and historical statistics.
3. **Answer generation and recommendation**
The system outputs inferred fault causes, recommended handling steps, required toolkits, and similar historical cases,

forming a coherent and interpretable knowledge chain for O&M decision-making.

4 SYSTEM IMPLEMENTATION AND APPLICATION CASES

This section describes the engineering implementation of the intelligent QA system, including the digital O&M process management platform, the O&M knowledge base construction, the big data analytics module, the intelligent QA and recommendation functions, and representative application cases. Deployment in a real reactor refueling system validates the effectiveness of the system in terms of fault diagnosis efficiency, knowledge management quality, team capability assessment, and equipment health assessment.

4.1 Implementation of the Digital O&M Process Management Platform

The digital O&M process management platform is the primary data source for the knowledge graph, responsible for the structured acquisition and management of on-site text descriptions, fault handling information, and workflow data. Its functional architecture is consistent with the process shown in Figure 4 and includes O&M business management, fault information preprocessing and semantic parsing, and data storage for fault descriptions, handling methods, and master data.

Ticket creation follows the process described in Section 3.5.1, incorporating NLP-based normalization, automatic coding, and incremental knowledge accumulation. The resulting structured records are ingested into the knowledge graph through the pipeline illustrated in Figure 5.

The dispatch module implements a policy that evaluates equipment location, team shifts, and personnel capabilities, and provides automatic or manual task assignment. The system issues work orders to responsible personnel and attaches recommended handling methods and toolkits, based on graph-based inference paths in the QA workflow (Figure 6).

The closure module records the actual handling process, including time consumption and parts replacement. NLP analysis and assisted input ensure that fault descriptions and handling steps are mapped back into the FDL and FPL, forming a closed-loop data–knowledge cycle as depicted in Figure 4.

4.2 O&M Knowledge Base Construction

The O&M knowledge base is implemented in Neo4j, representing equipment, faults, and handling methods as a semantic graph.

4.2.1 Knowledge modeling structure

The knowledge base includes four core entity categories:

Device entities: system–equipment–component–subcomponent.

Failure entities: types, phenomena, locations.

Solution entities: handling methods.

ExpertRule entities: expert knowledge and decision rules.

Relationship types include equipment hierarchies; fault–equipment associations; fault–location links; mappings between fault phenomena and handling methods; associations between handling methods and toolkits; and connections between solutions and expert rules.

Formally, the knowledge graph can be written as

$$\mathrm{KG} = (V, E), \tag{6}$$

where

$$V = \{\mathrm{Device}, \mathrm{Failure}, \mathrm{Solution}, \mathrm{ExpertRule}\}, \tag{7}$$

and Econtains the corresponding domain-specific relations. The overall modeling is visualized in Figure 5.

4.2.2 Automated construction and expert fusion

The knowledge base supports three construction modes:

1. Automated construction from historical O&M data.
2. Semi-automated construction combining rule-based extraction with human review.
3. Manual construction via expert input of new experiences or special cases.

When newly extracted triples are added, existing relationships are updated if they already exist; otherwise, new triples are inserted. This mechanism ensures that the knowledge base remains compact and free of redundant relationships while steadily evolving with new data.

4.3 O&M Big Data Analytics Module

The system implements functions such as equipment status statistics, health assessment, O&M status evaluation, and team capability assessment. These analyses operate primarily on the light aggregation and subject data zones in Figure 3.

4.3.1 Equipment status statistics

Based on the temporal distribution of equipment faults, a fault frequency model is defined as

$$F_t(d) = \frac{N_t(d)}{\Delta t}, \tag{8}$$

where $N_t(d)$is the number of faults for device $d$in time interval t, and $\Delta t$is the window length (day/week/month). Trend, periodicity, and anomaly analyses can be performed using this indicator.

4.3.2 Equipment health assessment model

A health index (HI) is defined as

$$HI_d = \alpha f_1(d) + \beta f_2(d) + \gamma f_3(d), \tag{9}$$

where $f_1$is the fault frequency factor, $f_2$measures the impact range of faults, $f_3$characterizes historical repair time, and $\alpha, \beta, \gamma$are weights derived from expert experience or model training. The resulting health profile supports maintenance planning and preventive maintenance strategies.

4.3.3 Team capability assessment

Team capability is modeled via the average handling time for fault categories:

$$C_g = \frac{1}{n}\sum_{i=1}^{n} T_{g,i}\,, \tag{10}$$

where $C_g$is the capability index of team g(shorter time indicates higher capability), $T_{g,i}$is the handling time for the i-th fault category handled by team g, and $n$is the number of fault categories considered. This index serves as a basis for performance evaluation and team assignment optimization.

4.3.4 Fault ranking and statistics

Fault types are ranked according to their impact:

$$\text{Rank}(f) = \text{sort}(\lambda_1 N_f + \lambda_2 T_f), \tag{11}$$

where N_f is the number of occurrences of fault type f, T_f is its average handling time, and λ_1, λ_2 are weighting coefficients. Such ranking helps identify fault types that consume the most resources and guides the optimization of O&M strategies.

4.4 Implementation of Intelligent QA and Recommendation

The intelligent QA module is the core innovation of the platform.

4.4.1 Natural language understanding

Given a user query such as

“how should I handle sticking in the refueling gripper arm?”,

the system performs segmentation and entity recognition, identifies the fault phenomenon (“sticking”) and equipment (“gripper arm”), and maps them to nodes in the knowledge graph:

$$q \rightarrow (\text{Failure: “sticking”}) \wedge (\text{Device: “gripper arm”}). \tag{12}$$

4.4.2 Semantic retrieval over the knowledge graph

Graph-based relationship retrieval is executed to find candidate solutions:

$$\text{CandidateSolutions} = \{s_j | (\text{Failure}, s_j) \in E\}, \tag{13}$$

and results are ranked using textual similarity and historical effectiveness. This step is implemented as the retrieval and ranking phase in the QA workflow of Figure 6.

4.4.3 Shortest path reasoning (Dijkstra)

The Dijkstra algorithm is employed to identify the most probable cause and the most appropriate handling method through path search:

$$P^* = \arg\min_{p \in P} \left(\sum_{e \in p} w_e \right), \tag{14}$$

where $P$is the set of candidate paths and $w_e$is the edge weight determined by expert scoring or historical statistics [14]. The resulting shortest path provides an interpretable explanation that links fault phenomena, equipment components, and handling solutions.

4.4.4 Answer generation and recommendation

The final output to the user includes:

a) Inferred fault cause;

b) Recommended handling steps;

c) Required toolkits;

d) Similar historical cases;

e) Estimated handling time.

These elements form a coherent and interpretable knowledge chain for O&M decision-making.

4.5 Simulation-Based Validation

4.5.1 Scenario description

To evaluate the proposed system, a simulation scenario is designed based on a reactor refueling context. The simulated environment assumes that refueling equipment operates over extended periods, with certain components (e.g., gripper arms, rotation mechanisms, guide mechanisms) exhibiting relatively high fault frequencies. The scenario also considers complex shift scheduling and knowledge transfer challenges typical of real-world O&M environments. The system implements a full process loop integrating O&M big data analytics, process digitalization, knowledge graphs, and intelligent recommendation.

4.5.2 Case 1: Intelligent recommendation for a simulated fault

In the simulated scenario, a refueling gripper arm is assumed to exhibit motion delay and slight vibration.

System processing:
The NLP module extracts fault phenomena; the FDL matches them to a standardized sticking-type fault; the knowledge graph retrieves handling methods; and Dijkstra's algorithm is applied to identify the shortest reasoning path, as illustrated conceptually in Figure 6.
System output:
a) Likely cause: insufficient joint lubrication leading to increased friction.
b) Recommended handling: lubrication check, removal of foreign objects, and rotation test.
c) Toolkits: lubrication gun, cleaning materials, etc.
d) Similar cases: multiple simulated historical records with similar phenomena, including handling steps and time consumption.
The simulation results suggest that the system has the potential to reduce the time required for diagnosis and improve fault handling efficiency.

4.5.3 Case 2: team capability ranking

In the simulated scenario, the system analyzes the repair times of five hypothetical teams over a given quarter. A simplified summary is presented below:

Table 1 Five Teams Capability Rank

Team	Average handling time	Faults handled	Rank
A	42 min	58	1
B	55 min	62	2
C	60 min	41	3
D	75 min	50	4
E	90 min	39	5

The results in Table 1 demonstrate that the system is capable of providing a basis for optimizing shift scheduling and targeted training in practical applications.

4.5.4 Case 3: equipment health profiling

Based on simulated historical fault and repair data, the system automatically generates a health profile for the refueling equipment, including a health index (e.g., 0.73), a predicted increase in fault probability over a specified future period, and high-frequency fault locations such as rotation joints. These simulation results indicate that the system could potentially support the establishment of preventive maintenance plans and help reduce unplanned downtime.

5 CONCLUSION AND FUTURE WORK

5.1 Conclusion

Focusing on reactor O&M, a domain characterized by high complexity, stringent safety requirements, and strong specialization, this study conducts systematic research on the design and application of a knowledge-graph-based intelligent QA system. The system is intended to address key challenges of traditional O&M, such as fragmented knowledge, experience-based decision-making, low fault response efficiency, and poor knowledge reuse. Based on the real business needs of a reactor refueling system, the system integrates data collection, knowledge modeling, graph databases, digital O&M platforms, and intelligent QA into a practical and extensible solution tailored to the nuclear industry.
First, the paper systematically analyzes the knowledge structures of reactor O&M, including equipment hierarchies, fault characteristics, and the semantic relationships among fault features and handling methods, and proposes a knowledge-graph modeling method suitable for nuclear O&M. By leveraging large amounts of historical records, ticket data, expert experience, and equipment structure trees, a knowledge graph comprising Device, Failure, and Solution entities is constructed, and knowledge is expressed through entity extraction, relationship construction, and rule integration. This method effectively addresses the looseness and poor retrievability of traditional document-based knowledge representations and provides a unified knowledge carrier for intelligent QA.
Second, the paper designs a knowledge storage and logical reasoning system for intelligent QA based on the Neo4j graph database and a rule base. Neo4j offers powerful graph traversal performance, flexible data schemas, and a user-friendly query language, enabling efficient querying of complex equipment topologies and fault chains. The rule base encodes domain logic, expert knowledge, and experience rules so that the QA system can not only “find the right information” but also “use it correctly”. Additionally, by applying the Dijkstra shortest path algorithm to reasoning over the knowledge graph, the system provides path-level explanations of fault causes, associated components, and potential handling solutions, significantly improving the interpretability and accuracy of intelligent recommendations.
Third, the paper builds a digital O&M process information platform that fully structures workflows such as work request creation, transfer, dispatch, and closure, enabling complete data collection, standardized representation, and real-time management (Figure 4). Meanwhile, the system uses NLP techniques to process free-text descriptions, which are integrated into the FDL and FPL for continuous expansion, thereby realizing a dynamic cycle of “data–knowledge–QA” and supporting the continuous evolution of the knowledge graph.
Finally, the system is validated through simulation in a reactor refueling scenario. The results indicate that the intelligent QA system shows promising potential in improving fault diagnosis efficiency, reducing maintenance

response time, enhancing the granularity of team capability assessment, and supporting trend prediction of equipment health status. By integrating historical O&M data, typical cases, and expert experience, the system is expected to facilitate sustainable accumulation, visual presentation, and intelligent use of knowledge, thereby contributing to improved reliability and standardization of O&M practices.

In summary, the proposed intelligent QA system achieves an integration of knowledge graphs, NLP, and path reasoning techniques, and demonstrates potential engineering value in the simulation study. It offers a feasible and reference-worthy approach for improving O&M efficiency, strengthening knowledge management, and supporting digital transformation in the nuclear industry.

5.2 Future Work

Despite encouraging results, there remains room for further enhancement. Future research directions include:

5.2.1 *Incorporating large language models to enhance semantic understanding*

The current system relies primarily on traditional NLP and lexicon-based semantic matching, which show limitations in handling complex sentences, implicit semantics, and cross-sentence reasoning. Future work may explore deploying lightweight or distilled LLMs in intranet environments and combining knowledge graphs with LLMs to achieve more robust natural-language understanding, especially for ambiguous descriptions and long texts.

1. Automated knowledge extraction and continual learning

Knowledge base updates still require human review. Future research can strengthen automated knowledge extraction techniques such as relation extraction, event extraction, and incremental learning, enabling continuous extraction of high-quality knowledge from new textual records so that the knowledge graph can self-update, self-improve, and self-correct.

2. Supporting cross-system and multimodal data fusion

Nuclear O&M involves substantial multimodal data, including drawings, video monitoring, vibration signals, and telemetry. Future work may incorporate computer vision and time-series analysis to integrate multimodal data into the knowledge graph and realize multimodal QA and reasoning over complex scenarios.

3. Developing quantitative knowledge credibility evaluation

Since O&M knowledge arises from multiple sources (expert experience, historical cases, automatically extracted content), future studies can design knowledge quality scoring models such as

$$\text{Credibility} = \alpha \cdot \text{support count} + \beta \cdot \text{expert authority} + \gamma \cdot \text{historical success rate}, \tag{15}$$

to sort answers based on knowledge credibility and improve the reliability of O&M decision-making.

4. Building cross-reactor and cross-facility nuclear O&M knowledge graphs

Under appropriate security conditions, future work may explore knowledge transfer and sharing across different reactors and refueling devices and construct a higher-level multi-site nuclear O&M knowledge graph. By defining unified modeling methods and interoperable graph interfaces, knowledge resources can be widely reused across facilities.

COMPETING INTERESTS

The authors have no relevant financial or non-financial interests to disclose.

FUNDING

This work is supported by the Talent Fund Project No. 25816 of China Institute of Atomic Energy (CIAE).

REFERENCES

[1] Ji S, Pan S, Cambria E, et al. A survey on knowledge graphs: Representation, acquisition and applications. IEEE Transactions on Neural Networks and Learning Systems, 2022, 33(2): 494-514.

[2] Chen J, Zhang H, Wang H. Knowledge graph and its application in intelligent question answering: A survey. In: 2020 IEEE International Conference on Big Data (Big Data), 2020: 2273-2282.

[3] Paulheim H. Knowledge graph refinement: A survey of approaches and evaluation methods. Semantic Web, 2017, 8(3): 489-508.

[4] Wang X, Pan W, Gao X. Application of knowledge graph technology in power equipment operation and maintenance. In: 2021 IEEE International Conference on Power System Technology (POWERCON), 2021: 338-344.

[5] Zhang CY. Research and implementation of automatic question answering system based on knowledge graph. Beijing University of Posts and Telecommunications, 2018.

[6] Xiong W, Yu M, Chang S, et al. One-shot relational learning for knowledge graphs. In: Proceedings of the Annual Meeting of the Association for Computational Linguistics (ACL), 2018: 1980-1990.

[7] Robinson I, Webber J, Eifrem E. Graph Databases. 2nd ed. O'Reilly Media, 2015.

[8] Miller JJ. Graph database applications and concepts with Neo4j. In: Proceedings of the Southern Association for Information Systems Conference, 2013: 1-6.

[9] Malewicz G, Austern MH, Bik AJ, et al. Pregel: A system for large-scale graph processing. In: Proceedings of the 2010 ACM SIGMOD International Conference on Management of Data, 2010: 135-146.
[10] Low Y, Bickson D, Gonzalez J, et al. Distributed GraphLab: A framework for machine learning and data mining in the cloud. VLDB Endowment, 2012, 5(8): 716-727.
[11] Kyrola A, Belli L, Guestrin C. GraphChi: Large-scale graph computation on just a PC. In: 10th USENIX Symposium on Operating Systems Design and Implementation (OSDI), 2012: 31-46.
[12] Shao B, Wang H, Li Y. Trinity: A distributed graph engine on a memory cloud. In: Proceedings of the 2013 ACM SIGMOD International Conference on Management of Data, 2013: 505-516.
[13] Sarwat M, Elnikety S, He Y, et al. Horton: An online query execution engine for large distributed graphs. In: 2012 IEEE 28th International Conference on Data Engineering (ICDE), 2012: 1289-1292.
[14] Zhang F, Liu J, Li Q. A shortest path optimization algorithm based on Dijkstra. Remote Sensing Information, 2004(2): 4-7.
[15] Mikolov T, Chen K, Corrado G, et al. Efficient estimation of word representations in vector space. In: International Conference on Learning Representations (ICLR), 2013.